จลนพลศาสตร์ของการดูดซับของสารละลายสององค์ประกอบในน้ำซึ่งประกอบด้วยฟีนอล เรด31 และ/หรือ แบล็ค 5 ด้วยถ่านกัมมันต์ที่ทำจากยางรถยนต์ใช้แล้ว

นางสาวพรรณดา จาบทอง

วิทยานิพนธ์นี้เป็นส่วนหนึ่งของการศึกษาตามหลักสูตรปริญญาวิศวกรรมศาสตรมหาบัณฑิต
สาขาวิชาวิศวกรรมเคมี ภาควิชาวิศวกรรมเคมี
คณะวิศวกรรมศาสตร์ จุฬาลงกรณ์มหาวิทยาลัย
ปีการศึกษา 2547

ISBN 974-17-5974-6

ADSORPTION KINETICS OF AQUEOUS BINARY MIXTURES CONTAINING PHENOL, RED31 AND/ OR BLACK5 ON ACTIVATED CARBON PREPARED FROM WASTE TIRES

Miss Pannada Japthong

A Thesis Submitted in Partial Fulfillment of the Requirements
For the Degree of Master of Engineering in Chemical Engineering
Department of Chemical Engineering
Faculty of Engineering
Chulalongkorn University
Academic Year 2004

ISBN 974-17-5974-6

Thesis Title	ADSORPTION KINETICS OF AQUEOUS BINARY MIXTURES CONTAINING PHENOL, RED31 AND/ OR BLACKS5 ON ACTIVATED CARBON PREPARED FROM WASTE TIRES
By	Miss Pannada Japthong
Field of Study	Chemical Engineering
Thesis Advisor	Professor Wiwut Tanthapanichakoon, Ph.D.

Accepted by the Faculty of Engineering, Chulalongkorn University in Partial Fulfillment of the Requirements for the Master's Degree

……Dean of the Faculty of Engineering
(Professor Direk Lavansiri, Ph.D.)

THESIS COMMITTEE

……Chairman
(Associate Professor Tawatchai Charinpanitkul, D.Eng)

……Thesis Advisor
(Professor Wiwut Tanthapanichakoon, Ph.D.)

……Member
(Associate Professor Prasert Pavasant, Ph.D.)

……Member
(Assistant Professor Tawan Sooknoi, Ph.D.)

นางสาวพรรณดา จาบทอง: จลนพลศาสตร์ของการดูดซับของสารละลายสององค์ประกอบในน้ำซึ่งประกอบด้วยฟีนอล เรด31 และ/หรือ แบล็ค5 ด้วยถ่านกัมมันต์ที่ทำจากยางรถยนต์ใช้แล้ว (ADSORPTION KINETICS OF AQUEOUS BINARY MIXTURES CONTAINING PHENOL, RED31 AND/ OR BLACK5 ON ACTIVATED CARBON PREPARED FROM WASTE TIRES) อ. ที่ปรึกษา : ศ.ดร. วิวัฒน์ ตัณฑะพานิชกุล, 119 หน้า. ISBN 974-17 -5974 -6.

ถ่านกัมมันต์ที่ผลิตจากยางรถยนต์ใช้แล้ว (AC_Tire) และ ถ่านกัมมันต์ที่ใช้ในการค้าขาย (AC_COM) มีสมบัติของรูพรุนแตกต่างกันคือมีขนาดรูพรุนขนาดเมโซพอร์และไมโครพอร์ตามลำดับ งานวิจัยนี้ได้ทำการศึกษาสมดุลและจลนพลศาสตร์การดูดซับของฟีนอลและเรด31 (แบล็ค5) ด้วยถ่านกัมมันต์ทั้งสองประเภทนี้ การศึกษาจลนพลศาสตร์ของการดูดซับที่มีการแข่งขันกันระหว่างตัวถูกดูดซับสองขนาด ได้แบ่งชุดการทดลองออกเป็นดังนี้จลนพลศาสตร์การดูดซับระบบหนึ่งองค์ประกอบ จลนพลศาสตร์การดูดซับระบบสององค์ประกอบพร้อมกัน จลนพลศาสตร์การดูดซับฟีนอลแล้วตามด้วยเรด31 และจลนพลศาสตร์การดูดซับเรด31แล้วตามด้วยฟีนอล จากการทดลองพบว่าสมดุลการดูดซับของฟีนอลและเรด31(แบล็ค5) ด้วย AC_Tire และ AC_COM สามารถอธิบายด้วยสมการของฟรุลด์ลิชและแลงก์เมียร์ตามลำดับ การถ่ายโอนมวลสารภายในถ่านกัมมันต์เป็นแบบการแพร่แบบนัดเสนและขั้นตอนในการควบคุมของกระบวนการดูดซับสามารถอธิบายได้ด้วยแบบจำลองอินทราพาร์ทิเคิล และความแตกต่างของลักษณะโครงสร้างของรูพรุนและการกระจายตัวของขนาดของรูพรุนส่งผลกระทบอย่างมากต่อความสามารถการดูดซับและจลนพลศาสตร์การดูดซับของฟีนอลและเรด31(แบล็ค5)

ภาควิชา.....วิศวกรรมเคมี..... ลายมือชื่อนิสิต.....

สาขาวิชา.....วิศวกรรมเคมี..... ลายมือชื่ออาจารย์ที่ปรึกษา.....

#4570436021 : MAJOR CHEMICAL ENGINEERING

KEY WORD: PHASE ACTIVATED CARBON / ADSORPTION / KINETIC / EQUILIBRIUM

PANNADA JAPTHONG: ADSORPTION KINETICS OF AQUEOUS BINARY MIXTURES CONTAINING PHENOL, RED31 AND/ OR BLACK 5 ON ACTIVATED CARBON PREPARED FROM WASTE TIRES. ADVISOR: PROF. WIWUT TANTHAPANICHAKOON, Ph.D., 119 pp. ISBN 974-17-5974 -6.

Activated carbon produced from waste tires (AC_Tires) and commercial activated carbon (AC_COM) which are highly mesoporous and microporous; respectively, were used to investigate their adsorption equilibrium and kinetics towards phenol and Red31(Black 5). Experimental competitive adsorption kinetics for phenol/Red31 (Black 5) systems consisted of single – solute and binary mixtures, namely, simultaneous adsorption kinetics, phenol adsorption kinetics followed by Red31 and Red31 adsorption kinetics followed by phenol. Adsorption equilibriums of phenol and Red31 (Black 5) adsorbed onto AC_Tires and AC_COM were found to be described well by Freundlich and Langmuir isotherms, respectively. The actual transport mechanism inside the activated carbon particles is shown to be Knudsen diffusion and the adsorption rate controlling step is described well by the intraparticle diffusion model. The porous structure and pore size distribution of the activated carbons has significant effect on the adsorption capacity and kinetics towards phenol and Red31 (Black 5).

Department……Chemical Engineering… Student's signature.....

Field of study....Chemical Engineering….. Advisor's signature.....……..

ACKNOWLEDGMENTS

Firstly, the author sincerely wishes to thank Prof. Wiwut Tanthapanichakoon, thesis advisor, for his invaluable advice and warmest encouragement.

This study has been supported partially by Industry- University Collaborative research Fund and Thailand- Japan Technology Transfer Project.

Next, the author would like to express a special thankful to Prof. Hajime Tamon and Dr. Kyuya Nakagawa for their contributions with kindly and helpful suggestion.

Furthermore, the author is also grateful to the members of thesis committee, Assoc. Prof. Tawatchai Charinpanitkul, Assoc. Prof. Prasert Pavasant, and Asst. Prof. Tawan Sooknoi, for their useful comments.

Moreover, the author would like to thank Union Commercial Development, Co., Ltd. and Asia Dyestuff Industries Co., Ltd. for supplying the waste tires and organic dyes, respectively.

In addition, the author would like to acknowledge the hospitality and encouragement of the teachers, friends, sisters and brothers, especially for Mr. Sittidej Sittipraneed and Dr. Pisit Ariyadejwanich, in Particle Technology and Material Processing Laboratory.

Eventually, the author would like to express deeply and truly thank to her parents and elder brother for their love, supports, understanding and encouragement throughout the course of her life.

CONTENTS

CONTENTS (Continued)

CONTENTS (Continued)

LIST OF TABLES

LIST OF FIGURES

LIST OF FIGURES (Continued)

Page

LIST OF FIGURES (Continued)

Page

LIST OF FIGURES (Continued)

Page

LIST OF FIGURES (Continued)

Page

NOMENCLATURES

a	Specific surface area (area per unit mass of adsorbent) [Eq. 3.27]
$a(b')$	Probability density function of the site distribution [Eq. 3.10]
$a(b')db'$	Fraction of adsorption sites with Langmuir constant between b' and $b' + db'$ [Eq. 3.10]
a_i,	The Langmuir- Freundlich constants [Eq. 5.2.3]
b_j	The Langmuir- Freundlich constants [Eq. 5.2.3]
c_b	Adsorbate concentration in the bulk of fluid [Eq. 3.27]
c_i	Concentration of the ith adsorbate in the solution [Eq. 3.16]
c_s	Adsorbate concentration at the fluid- pellet interface [Eq. 3.27]
d_p	Mean pore diameter [m]
dVp/dlog(Rp)	Pore size distribution [cm^3/g]
k_f	Interphase (or external) mass transfer coefficient [Eq. 3.27]
k_f	The film- diffusion coefficient (cm/s) [Eq. 4.3.2]
k_f	Rate constant of pseudo- first- order model [cm^3/min]
k_i	Rate parameter of intraparticle diffusion model [mg adsorbate/ (g particle $min^{0.5}$)]
k_s	Rate constant of pseudo- second- order model [g particle/ (mg adsorbate min)]
n	Freundlich constants [Eq. 5.2.1]
n_i	The Langmuir- Freundlich constants [Eq. 5.2.3]

NOMENCLATURES (Continued)

p_i^0	Equilibrium pressure of gas phase in the pure- component adsorption of the ith adsorbate [Eq. 3.20]
q	Moles of adsorbate adsorbed per unit mass of adsorbent (or the adsorbed phase concentration) [Eq. 3.1]
$\bar{q}$	Average adsorbed- phase concentration (on mass basis) [Eq. 3.27]
q_{eq}	The amount of adsorbates [Eq. 5.2.1]
q_h	Hypothetical equilibrium solid- phase concentration (mg/g) [Eq. 4.3.4]
q_i^0	Equilibrium adsorbed- phase concentration of the ith adsorbate [Eq. 3.20]
q_m	The maximum adsorbed phase concentration where all the adsorption sites are occupied [Eq. 3.1]
r	The radius of adsorbent at time t [Eq. 4.3.3]
x_i	Mole fraction of the ith adsorbate in the adsorbed- phase [Eq. 3.19]
y_i	Mole fraction of the ith adsorbate in the gas phase [Eq. 3.19]
A	Adsorption surface area per unit mass of adsorbent [Eq. 3.20]
AC_Tire	Activated carbon prepared from waste tires
AC_COM	Commercial activated carbon
C_{eq}	The equilibrium concentration (mg/cm^3)
C_0	The initial concentration (mg/cm^3) [Eq. 4.3.1]

NOMENCLATURES (Continued)

D_{eff}	The effective diffusion coefficient (cm^2/s) [Eq. 4.3.3]
D_i	Molecular diffusion coefficient (cm^2/s)
D_K	Knudsen diffusion coefficient [cm^2/s]
K_F	Freundlich constants [Eq. 5.2.1]
M	The amount of adsorbent (g) [Eq. 4.3.1]
M	The molar mass of the solute
M_i	The molecular weight of the diffusing species
P	Total pressure of gas phase [Eq. 3.19]
P/P_0	Relative pressure [-]
Q	The amount adsorbed of N_2 [cm^3/g]
R	The mean radius of adsorbent (nm) [Eq. 4.3.2]
R_p	Pore radius [nm]
S_{BET}	BET surface area [m^2/g]
T	Temperature [K]
V	The volume of solution (cm^3) [Eq. 4.3.1]
V_m	The molar volume of the solute [$cm^3/g - mole$]
V_{mes}	Mesopore volume [cm^3/g]
V_{mic}	Micropore volume [cm^3/g]
V_p	Pore volume [cm^3/g]

NOMENCLATURES (Continued)

θ	The coverage or for pure- component gas adsorption [Eq. 3.1]
π_i	Spreading pressure equal to that of the multicomponent adsorption case [Eq. 3.19]
ρ_s	Particle density (g/cm^3) [Eq. 4.3.4]
μ	Solvent viscosity [cp]
ϕ	Association factor

CHAPTER I

INTRODUCTION

1.1 Background

Activated carbons can be produced from various carbonaceous materials, for example coal, wood, coconut shell, soy bean, polymer scrap, anthracite and waste tire. In addition, they are widely used in either liquid or gas phase processes, such as air purification, gas separation and purification, wastewater treatment, organic solvent recovery, decolorization of organic substances etc. Activated carbons are used as an adsorbent due to their highly porous texture and large adsorption capacity**.**

Waste tires represent another interesting source for activated carbons because of its high carbon content. As the production of activated carbon from waste tires changes hard- to- dispose waste to pollution- cleaning adsorbents, it is thought to be a very effective method to relieve environmental pollution.

Especially, activated carbon prepared from waste tires has a highly mesoporous. Such activated carbon can be applied in dye adsorption because of its enhanced adsorption capacities. Unfortunately, in the commercial operation of processes based on adsorption technology, an understanding of adsorption equilibrium and adsorption kinetics is required. Gaining a fundamental understanding can be valuable in assisting process prediction and optimization.

An understanding of activated carbon adsorption processes requires knowledge of adsorbate- adsorbent properties, including their respective solution chemistries as well as adsorption capacity, and pore size distribution of the adsorbent. This knowledge is invaluable in selecting a carbon adsorbent for particular treatment application, and applying it in an effective manner. In addition, some important

factors affecting the removal of the organic matters present in waters, the role of pore size distribution in relation between the molecular size distribution of this pollutants and the size distribution of the activated carbons have not been investigated extensively.

Therefore, this research focused on various competitive adsorption kinetics modes of aqueous binary system consisting of phenol and reactive dye onto activated carbon produced from waste tires.

1.2 Objective of study

To study the adsorption kinetics of aqueous binary mixtures containing phenol, red31 and/ or black5 on activated carbon prepared from waste tire

1.3 Scope of the research

1. Activated carbon will be prepared from waste tire
    - Carbonization will be carried out at 500 ^{0}C.
    - Char will be treated by HCl at room temperature.
    - Steam activation will be carried out at 850 ^{0}C.
2. Characterize the porous properties of prepared activated carbon such as surface area, pore volume and pore size distribution of selected samples
3. Study the binary adsorption of phenol, red31 and/ or black5
    - The concentration range of solutions is 100 – 1,000 mg/l.
    - The mass of activated carbon is 1,000 mg with 1,500 ml of solution.
4. Rate of adsorption will be tested.

1.4 Obtained benefits

1. Knowledge of binary adsorption of phenol, red31 and/or black5 will be investigated.
2. Understanding of the rate of adsorption of phenol, red31 and/or black5 will be obtained.

CHAPTER II

LITERATURE REVIEW

2.1 Preparation of activated carbon from waste tires

P. Ariyadejwanich, W. Tanthapanichakoon, K. Nakagawa, S.R. Mukai, and H. Tamon (2003) proposed an activated carbon were produced from waste tires and their characteristics were investigated. Rubber separated from waste tires was first carbonized at 500 ^{o}C in N_2 atmosphere. Next, the obtained chars were activated with steam at 850 ^{o}C. As a result, fairly mesoporous activated carbons with mesopore volumes and BET surface areas up to 109 cm^3/g and 737 m^2/g, respectively, were obtained. To further improve the porous properties of the activated carbons, the char was treated with 1 M HCl at room temperature for 1 day prior to steam activation. This treatment increased mesopore volumes and BET surface areas of the activated carbons up to 1.62 cm^3/g and 1119 m^2/g, respectively. Furthermore, adsorption characteristics of phenol and dye, Black5, on the activated carbon prepared via acid treatment were compared with those of a commercial activated carbon I the liquid phase.

2.2 Adsorption equilibrium

B. Buczek. A. Swiatkowski, J. Goworek (1995) presented an adsorption from binary liquid mixtures of completely miscible components different polarity was studied, in order to characterize the adsorption properties of commercial activated carbons. The excess adsorption isotherms were measured for three binary liquid systems: acetone + n- heptane, acetone + benzene, and benzene + n-heptane on four

activated carbons of various contents. Textural characteristics of the adsorbents were determined on the basis of the adsorption/ desorption isotherms of argon at 77.5 K. The relationship between the extent of adsorption from the liquid phase as well as the shape of the adsorption isotherms and various parameters characterizing the investigated activated carbons are discussed. A good agreement is found as far as the actual surface area of the materials is concerned.

C.F. Lorenzano-Porras, M.J. Annen, M.C. Flickinger, P.W. Carr and A.V. McCormick (1995) studied in the pore structure and diffusion tortuosity of porous ZrO2 synthesized by two different colloid- aggregation processes. The pore structure of column- packing materials plays a significant role in high- performance liquid chromatography (HPLC) and will be particularly importance for the separation of macromolecules. In this studied, spherical, porous zirconia particles 5 -10 μm in diameter were synthesized by the controlled aggregation of 700 Å colloids. Two different aggregation methods were used: oil emulsion processing and polymerization induced colloid aggregation (PICA). The pore structures of the resulting materials were characterized by electron microscopy, nitrogen adsorption/ desorption, mercury (Hg) intrusion/ extrusion, pulsed field gradient spin- echo NMR self diffusion measurements and NMR spin- lattice relaxation measurements. The tortuosity and hydraulic diameter resulting from the two aggregation methods are compared. PICA generated sample is less porous but shows a more well- connected pore structure. These results show the need to restore high porosity while retaining the beneficial pore structure and the high degree of control of aggregate size that are characteristics of the PICA process.

Chien-To Hsieh and H. Teng (2000) proposed the influence of the pore size distribution of activated carbon on the adsorption of phenol from aqueous solutions was explored. Activated carbons with different porous structures were prepared by gasifying a bituminous coal char to different extents of burn- off. The results of adsorption experiments show that the phenol capacity of these carbons does not proportionally increase with their BET surface area. This reflects the heterogeneity of the carbon surface for adsorption. The pore size distributions of these carbons, determined according to the Dubinin- Stoeckli equation, were found to vary with the burn- off level. By incorporating the distribution with the Dubinin- Radushkevich equation using an inverse proportionality between the micropore size and the adsorption energy, the isotherms the adsorption of phenol onto these carbons can be well predicted. The present study has demonstrated that the heterogeneity of carbon surface for the phenol adsorption can be attributed to the different energies required for adsorption in different- size micropores.

G.M. Walker and L.R. Weatherley (2001) presented the adsorption of dyes from aqueous solution- the effect of adsorbent pore size distribution and dye aggregation. The removal of acid dyes, Tectilon Blue 4R, Tectilon Red2B and Tectilon Orange 3G, from single component solution by adsorption on activated carbon and bone char has been investigated in isotherm experiments. Results from these experiments were successfully modeled using Langmuir and Freundlich isotherm analyses. Nitrogen adsorption analysis was also undertaken and indicated that the activated carbon had a much higher specific surface than the bone char. Calculations involving the pore size distribution data indicate that only 14% of the total specific surface of the activated carbon is available for adsorption due to the high

molecular area and aggregation of the dye. The equilibrium data indicated that dye aggregation takes places in the solid phase of both adsorbents with higher solid phase aggregation numbers found using the bone char, which is indicative of multilayer adsorption.

L. Li, P.A. Quinlivan and R.U. Knappe (2002) presented the effects of activated carbon surface chemistry and pore structure on the adsorption of organic contaminants from aqueous solution. The objective of this research was to develop activated carbon selection criteria that assure the effective removal of trace organic contaminants from aqueous solution and to base the selection criteria on physical and chemical adsorbent characteristics. To systematically evaluate pore structure and surface chemistry effects, a matrix of activated carbon fibers with three activation levels and four surface chemistry levels was prepared and characterized. In addition, three granular activated carbons were studied. Two common drinking water contaminants, relatively polar methyl tertiary- butyl ether (MTBE) and relatively nonpolar trichloroethane (TCE), served as adsorbate probes. TCE adsorbed primarily in micropores in the 7- 10 Å width range while MTBE adsorbed primarily in micropores in the 8- 11 Å width range. These results suggest that effective adsorbents should exhibit a large volume of micropores with widths that are about 1.3 to 1.8 times larger than the kinetic diameter of the target adsorbate. Hydrophobic adsorbents more effectively removed both TCE and MTBE from aqueous solution than hydrophilic adsorbents, a result that was explained by enhanced water adsorption on hydrophilic surfaces.

2.3 Adsorption kinetics

G.M. Walker and L.R. Weatherley (1998) presented the treatment of simulated industrial waste water containing acid dye- stuffs with granular activated carbon adsorption selected as the treatment method. Predicting the rate at which adsorption takes place for a given system is probably the single most important factor for adsorber design, with adsorbate residence time and ultimately the reactor dimensions controlled by the system's kinetics.

Y. Onganer, and C. Temur (1998) presented a granular activated carbon was utilized as adsorbent for the removal of Fe (III) ions from aqueous solutions at different temperatures and fixed pH. The batch adsorption kinetics has been described by the Lagergren equation which is a pheudo- first- order rate expression; the surface mass transfer coefficients and diffusion coefficients have been calculated at different temperatures. The intraparticle transport of Fe(III) within the pores of activated carbon was found to be the rate- limiting step, while the process of uptake obeyed the Langmuir model of adsorption.

C. Pelekani, and V. L. Snoeyink (2001) studied on a kinetic and equilibrium study of competitive adsorption between atrazine and Congo red dye on activated carbon: the importance of pore size distribution. A series of phenolic resin- based microporous activated carbon fibers (ACF) with different micropore size distributions were used to assess the role of pore size distribution (PSD) in the mechanism of competitive adsorption between the organic micropollutant, atrazine, and a compound larger in size, Cong red dye (CR). Batch kinetic and equilibrium experiments with the CR/atrzine system consisted of single- solute, simultaneous adsorption, CR

preloading followed by atrazine contact, and atrazine preloading followed by CR contact. Based on the previous pore characterization studies and the PSD, two type of pore structures were proposed: telescopic pores, and branched pores. With the telescopic pore structure, evidence is presented to support a transition from surface pore blockage to pore constriction (without loss of atrazine capacity) to direct competition for adsorption sites, with increasing average micropore size. With the branched pore structure (micropore branching off from mesopore), direct competition for adsorption sites in the fraction of large micropores, and pore constriction, and pore blockage of smaller micropores were found to be important. The kinetics of adsorption was found to be important in determining the impact of simultaneous adsorption, while CR surface coverage and preloading time were the key factors controlling the impact of preloading on atrazine adsorption.

C.W. Cheung, C.K. Chan, J.F. Porter and G. McKay (2001) proposed the film- pore diffusion control for the batch sorption of cadmium ions from effluent onto bone char. Equilibrium isotherms for the sorption system were correlated by Langmuir and bi- Langmuir equations. The application of bi- Langmuir equation was developed because the mechanistic analysis in this research indicated that cadmium removal occurs ion exchange and physical adsorption onto different surface sites. The bi- Langmuir equation provides a better fit to the experimental data. In addition, the removal rates of cadmium ions based on the Langmuir models have been investigated. The effective diffusivity was calculated using the effects of initial metal ion concentration and bone char mass. Two mass- transport models based on film-pore diffusion control have been applied to analyze the concentration decay curves. The film and pore diffusion coefficients using and analytical equation are equal to

1.26 x 10-3 cm/s and 5.06 x 10-7 cm2/s, respectively. A sensitivity analysis showed that the film- pore diffusion model and constant effective diffusivity could be used to describe the mass- transport mechanism of the sorption system with a high degree of correction.

J.L. Sotelo, G. Ovejero, J.A. Delgado and I. Martinez (2002) presented the comparison of adsorption equilibrium and kinetics of four chlorinated organics from water onto GAC. This study deals with the adsorption of four chlorinated pollutants onto GAC (F-400) ; two pesticides (lindine and alachor) and two PCB congeners: 2-PCB (MPCB) and 2,2',5,5'-PCB (TPCB). Equilibrium and kinetic parameters have been obtained for the adsorption of alachor and each PCB, whereas the kinetic results for lindane presented elsewhere are reanalyzed in this work. A model assuming a bidisperse structure (macro- and micropores), each region having a different adsorption isotherm, is used to study the adsorption kinetics in batch system in the period dominated by macropore diffusion. Both the saturation capacity and the rate of internal transport of TPCB are much lower than those of the other solutes. This difference is attributed to a chemisorption mechanism for this compound, which is favored by its very low solubility.

J.R. Evans, W.G. Davids, J. D. MacRae and A. Amirbahman (2002) presented kinetics of cadmium uptake by chitosan- based crab shells. Batch experiments were performed to study the uptake equilibrium and kinetics of cadmium by chitosan. Adsorption equilibrium followed a Freundlich relation ship and was found to be independent of particle size indicating that adsorption rate suggesting intrapartcle diffusion as the rate- limiting step. The cadmium uptake data were

successfully modeled using pore diffusion model incorporating nonlinear adsorption. The effect of boundary layer resistance was modeled through inclusion of a mass transfer expression at the outside boundary.

Q. Sun and L.Yang (2003) studied in the adsorption of basic dyes from aqueous solution on modified peat- resin particle. Modified peat was prepared by mixing thoroughly raw peat with sulfuric acid and modified peat- resin particle was obtained, by mixing modified peat with solutions of polyvinylalcohol (PVA) and formaldehyde. The adsorption of Basic Magenta and Basic Brilliant Green onto modified peat- resin particle was examined. The adsorption isotherm showed that the adsorption of basic dyes on modified peat- resin particle deviated from Langmuir and Freundlich equations. The pseudo- first- order, pseudo- second- order and intraparticle diffusion models were used to fit the experimental data. By comparing the standard deviation, it was found that the intraparticle diffusion model could be used to describe the adsorption of two basic dyes on modified peat- resin particle. According to the change of intraparticle diffusion parameter, the adsorption processes could be divided into different stages. The kinetics experiment also indicated that initial dye concentrations, particle dose and particle size could affect the adsorption processes of basic dyes.

K.H. Choy, J.F. Porter and G. McKay (2004) proposed the film- pore diffusion models- analytical and numerical solutions. The sorption of acid dyes from aqueous effluents onto activated carbon has been studied. The effects of initial dye concentration and activated carbon mass on the rate of Acid Blue 80 and Acid Yellow 117 removal have been investigated. Three mass transport models based on film and

pore diffusion control have been applied to model the experimental concentration decay curves. The models are compared on the basis of the solid- phase loading capacity using various assumptions since the assignment of an appropriate solid-phase loading has been the subject of several papers on this topic and no comparisons have been provided on the effectiveness of each approach.

Z. Aksu and E. Kabasakal (2004) studied in adsorption equilibrium, kinetics in batch system adsorption of 2,4- dichlorophenoxy- acetic- acid (2,4-D) from aqueous solution by granular activated carbon with respect to pH, temperature and initial concentration. At 600 mgl^{-1} initial 2,4-D concentration activated carbon exhibited the highest 2,4-D uptake capacity of 518 mgg^{-1} at 45 ^{o}C and at an initial pH value of 2. Freundlich, Langmuir, Redlich- Peterson and Koble- Corrigan isotherm models were applied to experimental equilibrium data of 2,4-D depending on temperature. Equilibrium data fitted very well to the Freundlich and Koble- Corrigan equilibrium models in the studied concentration range of 2,4-D at all the temperatures studied. Some simple mass transfer and kinetic models were applied to the experimental data to examine the mechanisms of adsorption and potential rate controlling steps such as external mass transfer, intraparticle diffusion and adsorption process. It was found that both the boundary layer and intraparticle diffusion played important roles in the adsorption mechanisms of 2,4-D and adsorption kinetics followed a pseudo- first- order kinetic model rather than pseudo- second- order and saturation type kinetic models for all temperatures studied. The activation energy of adsorption was determined as 8.46 $kJmol^{-1}$ using the Arrhenius equation. Using the thermodynamic equilibrium coefficients obtained at different temperatures, the

thermodynamic equilibrium coefficients obtained at different temperatures, the thermodynamic constants of adsorption were also evaluated.

CHAPTER III

FUNDAMENTAL THEORY

3.1 Adsorption

Adsorption is brought about by the interactions between the solid and the molecules in the fluid phase. Two kinds of forces are involved, which give rise to physical adsorption (physisorption) or chemisorption. Physisorption forces are the same as those responsible for the condensation of vapors and the deviations from ideal gas behavior, whereas chemisorption interactions are essentially those responsible for the formation of chemical compounds.

The most important distinguishing features may be summarized as follows:

1. Physisorption is general phenomenon with a relatively low degree of specificity, whereas chemisorption is dependent on the reactivity of the adsorbent and adsorptive.

2. Chemisorbed molecules are linked to reactive parts of the surface and the adsorption is necessarily confined to a monolayer. At high relative pressures, physisorption generally occurs as a monolayer.

3. A physisorbed molecule keeps its identity and on desorption returns to the fluid phase in its original form. If a chemisorbed molecule undergoes reaction or dissociation, it loses its identity and cannot be recovered by desorption.

4. The energy of chemisorption is the same order of magnitude as the energy change in a comparable chemical reaction. Physisorption is always exothermic, but the energy involved is generally not much larger than the energy of condensation of the adsorptive. However, it is appreciably enhanced when physisorption takes place in very narrow pores.

5. The activation energy is often involved in chemisorption and at low temperature the system may not have sufficient thermal energy to attain thermodynamic equilibrium. Physisorption systems generally attain equilibrium fairly rapidly, but equilibration may be slow if the transport process is rate-determining (D.M. Ruthven [1]).

3.2 Single Adsorption Equilibrium

The simplest and by far the most widely used expression for physical adsorption (or even chemisorption) from either gas or liquid solutions is the Langmuir equation. Although the Langmuir equation can be derived several ways, this expression is commonly derived through a kinetic approach; in other words, from the assume rate expressions of both adsorption and desorption and considering adsorption equilibrium as a state of dynamic equilibrium when both the adsorption and desorption rates are the same. The assumptions used for deriving the expressions are as follows:

1. Adsorption of adsorbate molecules take place at well- defined localized states.
2. All the adsorption sites are identical (energetically), and each site accommodates one adsorbate molecule only.
3. There are no lateral interactions (i.e., interactions between neighboring adsorbed adsorbate molecules).

The adsorption and desorption rates are assumed to be

Rate of adsorption $k_a p(1-\theta)$

Rate of desorption $k_d\theta$

where θ is the coverage or for pure- component gas adsorption

$$\theta = \frac{q}{q_m} \qquad (3.1)$$

where

q = moles of adsorbate adsorbed per unit mass of adsorbent (or the adsorbed phase concentration)

q_m = the maximum adsorbed phase concentration where all the adsorption sites are occupied

At equilibrium, one has

$$k_a p(1-\theta) = k_d \theta \qquad (3.2)$$

which, upon rearrangement, becomes

$$\theta = \frac{q}{q_m} = \frac{bp}{1+bp} \qquad (3.3)$$

where

$$b = \frac{k_a}{k_d} \qquad (3.4)$$

The Langmuir expression shows the correct asymptotic behavior for monolayer adsorption since as $p \rightarrow \infty$, $q \rightarrow q_\infty$, while as $p \rightarrow 0$, Henrry's law is obeyed,

$$\lim_{p \to 0}\left(\frac{q}{p}\right) = bq_m = K \qquad (3.5)$$

The Langmuir equation is a two- parameter expression that represents adsorption equilibrium data of type I behavior. Although the Langmuir parameters have their physical significance, the Langmuir constants obtain from data fitting, unless the data are extensive, would be better regarded as empirical constants.

Eq. (3.3) may be rearranged to give

$$\frac{1}{q} = \frac{1}{q} + \frac{1}{bq_m}\frac{1}{p} \qquad (3.6)$$

In other words, the Langmuir equation displays a linear behavior between $1/q$ versus $1/p$, which provides the procedure commonly used for evaluating q_m and b from experimental data. In this regard, it should be note that a best fit of $1/q$ versus $1/p$ is not equivalent to a best fit between q and p. The Langmuir parameters can be easily obtained from experimental data by using several standard parameter- search procedures without resorting to using the linearity of $1/q$ versus $1/p$.

3.2.1 Extension of the Langmuir Expression to heterogeneous Surfaces

A heterogeneous surface may be considered to be a composite surface composed of many homogeneous patches. If the Langmuir equation is assumed to apply to the individual patches, then the overall isotherm expression may be written as

$$q = \frac{(q_m)_1 b_1 p}{1 + b_1 p} + \frac{(q_m)_2 b_2 p}{1 + b_2 p} + \ldots = \sum \frac{(p)(q_m)_i}{b_1^{'} - p} \quad (3.7)$$

where $(q_m)_i$ and b_i are the values of q_m and b for ith patch,

$$q_m = \sum_i (q_m)_i \quad (3.8)$$

and

$$b_1^{'} = \frac{1}{b_i} \quad (3.9)$$

Each patch (or, more appropriately, the adsorption site on each patch) is characterized by its adsorption energy [namely, -ΔH]. If the distribution of the patch is not discrete but continuous, then Eq. (3.7) may be rewritten as

$$q = \int_0^{\infty} \frac{p}{b^{'} + p} a(b^{'}) db^{'} \quad (3.10)$$

where $a(b^{'})$ = probability density function of the site distribution

$a(b')db'$ = fraction of adsorption sites with Langmuir constant between b' and $b' + db'$

It is obvious that the isotherm equation depends on the probability density function of the site distribution. Zeldowitsch (1935) showed that if $a(b')$ is assumed to be

$$a(b') = A(b')^{(1/n)-1} \qquad (3.11)$$

then the resulting expression from (10) may be approximated as

$$q = Ap^{1/n} \qquad (3.12)$$

which is commonly known as the Freundlich isotherm expression. The Freundlich equation, in many ways, is the simplest equation for data representation. It does have a serious defect, namely, it fails to observe Herry's law behavior in the limiting situation of p→ 0.

3.2.2 Modified Langmuir Expressions

The Langmuir expression can be modified in several ways to improve its fit which experiments. The so-called Langmuir- Freundlich expression combines the Langmuir and Freundlich equation and is given as

$$\frac{q}{q_m} = \frac{bp^{1/n}}{1 + bp^{1/n}} \qquad (3.13)$$

The Langmuir- Freundlich equation contains tree parameter q_m, b and n. There are, of course, many other three- parameter isotherm expressions, among them the Toth equation, which has been used extensively to correlate gas- adsorption isotherm data when the Langmuir equation alone fails.

3.3 Multicomponent Adsorption Equilibrium

Like pure- component adsorption isotherms, adsorption equilibrium data of gas mixtures and solutions with several species of adsorbable solutes can be determined experimentally. However, as the number of components increases, the required experimental efforts becomes more demanding and may even reach the point of impracticality if the number becomes large. Of equal importance is the fact that it also become more difficult to correlate and interpret adsorption equilibrium data of systems with a large number of adsorbate species. The existence relatively few multicomponent isotherm data reflects this fact.

As a practical matter, it is rather obvious that we need to develop theories or procedures capable of predicting or estimating adsorption equilibrium data of gas mixtures or solution containing several adsorbates from pure- component isotherm data of the individual adsorbates. In fact, developing such as a theory has been the goal of many investigators during the past 20 years. Although this objective has not yet been realized, some promising progress has been made in recent years.

3.3.1 Extended Langmuir Equation

Expressions of adsorbed- phase concentration

The most obvious approach for obtaining a general expression of the adsorption isotherm of gas mixtures is by generalizing the Langmuir theory. First the Langmuir equation may be written to give

$$q_0^i = \frac{a_i p_i^0}{1 + b_i p_i^0} \qquad (3.14)$$

where the superscript 0 denotes the pure- component adsorption state. Analogous to the procedure used by Markham and Benton (1931), who extended Eq. (3.14) to binary gas mixtures, the equivalent expression of q_i for a gas mixture with N adsorbates and partial pressures $p_1, p_2, \ldots, p_N$ can be found to be

$$q_i = \frac{a_i p_i}{1 + \sum_{j=1}^{N} b_j p_j} \qquad (3.15)$$

Thus, by knowing the Langmuir constants, a_i and b_i, of the individual adsorbates, we can readily estimate the equilibrium concentrations from Eq. (3.15)

Similarly, for liquid solutions with N adsorbates, the adsorbed- phase concentration, $q_i = 1, 2, \ldots, N$ is given as

$$q_i = \frac{a_i c_i}{1 + \sum_{j=1}^{N} b_j c_j} \qquad (3.16)$$

where

c_i = concentration of the ith adsorbate in the solution

a_i and b_i = as before, single- component liquid- phase adsorption isotherm parameters of the ith adsorbate

3.3.2 Extended Langmuir- Freundlich Equation

Expressions of adsorbed- phase concentration

As in the previous case, the mixed Langmuir- Freunlich equation for the pure-component adsorption isotherm may be extended to multicomponent cases as follows:

$$q_i = \frac{a_i p_i^{1/n_i}}{1 + \sum_{j=1}^{N} b_j p_j^{1/n_i}} \quad \text{for gas adsorption} \quad (3.17)$$

and

$$q_i = \frac{a_i c_i^{1/n_i}}{1 + \sum_{j=1}^{N} b_j c_j^{1/n_i}} \quad \text{for liquid adsorption} \quad (3.18)$$

3.3.3 Ideal Adsorbed Solution Theory

The ideal adsorbed solution (IAS) theory was first proposed by Myers and Prausnitz (1965) for the adsorption of gas mixtures and was subsequently extended to multicomponent liquid- phase adsorption by Radke and Prausnitz (1972). It is general theory capable for predicting multicomponent adsorption equilibrium from the pure component adsorption isotherm data of the individual adsorbate without specifying the functional forms of the pure- component isotherms. Consequently, adsorption equilibrium is represented not by a specific equation, but by a system of equations.

Equations describing the equilibrium between the adsorbed and solution phases

For adsorption of gas mixtures, Myers and Prausnitz (1965) assumed that the various fundamental thermodynamic equations of liquid are applicable to the adsorbed phase. Assuming that the solution in the adsorbed phase is ideal (such that Raoult's law is valid) and applying the criterion of equilibrium between the gas and adsorbed phase (namely, at constant temperature and spreading pressure, the chemical potential of any adsorbate in the two phases is the same), one has

$$Py_i = p_i^0(\pi_i, T)x_i, \qquad i = 1, 2, \ldots, N \qquad (3.19)$$

where

P = total pressure of gas phase

x_i and y_i = mole fraction of the ith adsorbate in the adsorbed- phase and the gas phase, respectively

p_i^0 = hypothetical pressure of the ith adsorbate in its pure- component adsorption that yields a spreading pressure, π

π_i = spreading pressure equal to that of the multicomponent adsorption case (and, therefore, ($\pi_i = \pi_j = \pi, i \neq j$)

the relationship between p_i^0 and π_i is

$$\frac{\pi_i A}{RT} = \int_0^{p_i^0} \frac{q_i^0}{p_i^0} dp_i^0 \qquad (3.20)$$

where

superscript 0 = as before, pure- component adsorption state

q_i^0 and p_i^0 = equilibrium adsorbed- phase concentration and pressure of gas phase in the pure- component adsorption of the ith adsorbate

A = adsorption surface area per unit mass of adsorbent

A consequence of the ideal solution assumption for the adsorbed phase is that is no change in the specific adsorption area (adsorption area per mole of adsoebate) upon mixing the various adsorbates. Since the specific adsorption area is inversely proportional to q, the adsorbed phase concentration, one has

$$q_t = \left[\sum_{j=1}^{N} \frac{x_i}{q_j^0} \right]^{-1} \qquad (3.21)$$

The amount of adsorption of the i[th] adsorbate, q_i, is given as

$$q_i = q_t x_i \qquad (3.22)$$

Eqs.(3.18) through (3.22), together with the requirement

$$\sum_{j=1}^{N} x_i = 1$$

constitute the system of equations describing the multicomponent adsorption equilibrium between the gas phase and adsorbed phase.

The equations describing the liquid- phase adsorption equilibrium are similar to those given previously with c_i replacing (P, y_i). The equations derived by Radke and Prausnitz are

$$c_i = c_i^0(\pi, T) x_i \qquad (3.23)$$

$$\frac{\pi_i A}{RT} = \int_0^{c_i^0} \frac{q_i^0}{c_i^0} dc_i^0 \qquad (3.24)$$

$$q_t = \left[\sum_{j=1}^{N} \frac{x_i}{q_j^0} \right]^{-1} \qquad (3.25)$$

$$\sum_{j=1}^{N} x_i = 1 \qquad (3.26)$$

As shown previously, predicting multicomponent adsorption equilibrium from IAS theory requires pure- component adsorption isotherm data for each adsorbate down to zero pressure (or concentration). It is also clear that the calculations necessarily involve a trial- and- error procedure.

3.4 Adsorption Kinetics

For the transport of adsorbates from the bulk of the fluid phase to the interior of a pellet before adsorption take place, the following mass- transfer processes may be present: interpellet mass transfer, inter phase mass transfer and intrapellet mass transfer. Interpellet mass transfer may become significant in cases in which an adsorption- treated solution is contacted with adsorbent pellets in relative motion, as in the case of fixed- bed, moving- bed, or fluidized- bed operations. Interpellet mass transfer refers to the diffusion and mixing of adsorbates in fluid occupying the spaces between the pellets. Interphase mass transfer is the transfer of adsorbate across the fluid pellet interface. Intraparticle mass transfer refers to the diffusion of adsorbates (either dissolved or adsorbed) within the pellet. Intraparticle mass transfer often takes place simultaneously with adsorption.

In physical adsorption, adsorption of adsorbate from the solution phase onto the adsorption site occurs because of the difference between the adsorbate's chemical potential in the solution and adsorbed phases. In most cases, it occurs much faster than the various transport steps and can therefore be ignored when formulating the overall rate expression.

3.4.1 Interpellet Mass Transfer

In fixed- bed (or moving- as well as fluidized- bed) adsorption, diffusion and mixing of adsorbates in fluid occur as a result of the adsorbate concentration gradients and the nonuniformity of fluid flow. This effect gives rise to the dispersion of adsorbates, which takes place along both the direction of main fluid flow (axial dispersion) and the direction transverse to the main flow direction (radial dispersion). Although the effect of axial dispersion is undesirable, since it reduces the separation efficiency, radial dispersion is usually considered helpful. Radial dispersion tends to equalize the differences in the concentration of small fluid elements at the same axial location; consequently, the undesired axial dispersion effect may be reduced.

3.4.2 Interphase Mass Transfer

The transport of the adsorbable species from the bulk of the fluid phase to the external surface of adsorbent pellets constitutes an important step in the overall uptake process. For single- species adsorption with spherical pellets, the interphase mass-transfer rate may be expressed as

$$\frac{\partial \bar{q}}{t} = k_f a(c_b - c_s)$$

$$= \frac{3k_f}{a_p p_p}(c_b - c_s) \qquad (3.27)$$

where

$\bar{q}$ = average adsorbed- phase concentration (on mass basis)

c_b and c_s = adsorbate concentration in the bulk of fluid and that at the fluid- pellet interface

a = specific surface area (area per unit mass of adsorbent)

k_f = interphase (or external) mass transfer coefficient

The magnitude of k_f, of course, depends upon the flow condition around the pellet. Correlations useful for estimating k_f are summarized as follows.

3.4.3 Intrapellet Mass Transfer

Concerning the mechanisms by which intrapellet mass transfer is effected, since pellets are microporous and their void (pore space) is occupied by the fluid to be treated by adsorption, adsorbate may diffuse through the pore fluid because of the presence of the radial concentration gradient. The presence of concentration gradient implies the existence of a similar concentration gradient in the adsorbed phase, which, in turn, causes the diffusion of the adsorbed molecules. Both types of diffusion may be operative simultaneously or individually. These two different mechanisms are discussed separately as follows.

3.4.3.1 Pore diffusion

Pore diffusion operates if the intrapellet mass transfer is due only to the diffusion of adsorbate molecules through the pore fluid. For the simple case of single-species adsorption assuming that Fick's law applies, the macroscopic conservation equation is given as

$$\varepsilon_p \frac{\partial c}{\partial t} + \rho_p \frac{\partial q}{\partial t} = \frac{1}{r^2} \frac{\partial}{\partial r}\left[D_p r^2 \frac{\partial c}{\partial r} \right], 0 \le r \le a_p \qquad (3.28)$$

where c and q are the adsorbate concentrations in the pore fluid and of the adsorbed phase corresponding to any given point within the pellet. Note that the solution of Eq.(3.28) requires that one specify appropriate initial and boundary conditions as well as an additional relationship between c and q. For the time being, it suffices to note that the parameter characterizing the pore diffusion is the pore diffusivity, Dp.

3.4.3.2 Surface diffusion

In the case in which the intrapellet mass transfer is affected through the diffusion of the adsorbed molecules, for single- species adsorption with spherical pellets and assuming that Fick's law applies, the intrapellet mass transfer is described by the following equation:

$$\left(\frac{\varepsilon_p}{\rho_p}\right)\frac{\partial c}{\partial t}+\frac{\partial q}{\partial t}=\frac{1}{r^2}\frac{\partial}{\partial r}\left[D_s r^2\frac{\partial c}{\partial r}\right] \qquad (3.29)$$

Since the term $(\varepsilon_p/\rho_p)(\partial c/\partial t)$ is much less than $\partial q/\partial t$, Eq.(3.29) can be readily solved with appropriate initial and boundary conditions (C. Tien [2]).

CHAPTER IV

EXPERIMENTAL PROCEDURE

4.1 Preparation of activated carbon

Activated carbon was produced in three distinct steps. First of all is the carbonization step. About 6 g of pulverized waste tire rubber was set in a quartz tube reactor and electrically heated in N_2 atmosphere from room temperature to 500 ^{0}C at a constant heating rate of 5 ^{0}C/min. The sample was then held at this temperature for 1 hr, and subsequently left to naturally cool down. Next 2-3 g of the char obtained from the carbonization process was immersed in 200 cm^3 of 1 M HCl at room temperature for 24 hours. After the acid treatment the char was thoroughly rinsed with distilled water and dried in an oven at 110 ^{0}C. Finally, 10 g of the HCl –treated char was gathered and activated with steam in the quartz tube reactor by heating the sample from room temperature to 850 ^{0}C at a constant heating rate of 20 ^{0}C/min, and held at this temperature for 4 and a half hr. The steam used for the activation process was generated with a heated pot at a constant rate of 0.5 g/min, and was introduced into the reactor along with a 200 cm^3/min flow of N_2. The partial pressure of steam was 46 kPa.

4.2 Characterization of porous properties of the produced activated carbon

The pore size distribution, BET surface area S_{BET}, mesopore volume V_{meso}, and micropore volume V_{micro} of the activated carbon were determined from N_2 adsorption and desorption isotherms measured at 77 K using an adsorption apparatus (ASAP 2000 V3.03, Micromeritics Instrument Corporation or AUTOSORB-1-C,

Quantachrome Corporation, USA). The pore size distribution and V_{meso} were evaluated by applying the Dollimore - Heal method to the desorption isotherm, whereas the t - plot method was used to estimate V_{micro}. As for particle size distribution, it was evaluated with a particle size analyzer (Mastersizer S long bed Ver. 2.11, Malvern Instruments Ltd., Malvern, UK).

4.3 Adsorption equilibrium and kinetics

4.3.1 Materials

4.3.1.1 Adsorbents

The activated carbon produced from waste tires and commercial activated carbons obtained from Thai - Oil Company were used as adsorbent to investigate their adsorption characteristics and compare their competitive adsorption kinetics of the binary system.

4.3.1.2 Adsorbates

Widely used as a solvent in the textile industry, phenol (Fisher Scientific Ltd., UK) was selected here to represent a less bulky adsorbate. More bulky in size than phenol, red31 (Asia Dyestuff Industries, Thailand), a reactive dye, was selected as competing adsorbate. Their molecular sizes and structures, which were estimated using the WINMOPAC program, are shown in Figure 4.3.1

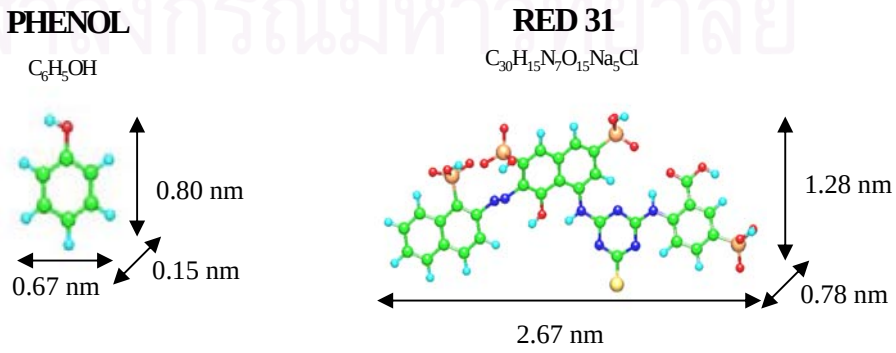

Figure 4.3.1 Molecular dimensions and structures of adsorbates

4.3.2 Single- component adsorption isotherm

Aqueous solutions of various initial concentrations were prepared by diluting the adsorbates with distilled water. 250-500 mg of the activated carbon was put in contact with each of the prepared solutions. To maintain well-mixed condition, the solid- liquid suspensions were put in either a gyratory air bath or shaking water bath kept at 30 ºC. Typically adsorption equilibrium was achieved after 10-15 days. Then the solutions were filtered to remove the activated carbon powder and the residual concentrations of the adsorbates were measured. The amounts adsorbed at equilibrium on the activated carbons were calculated from the initial and final concentrations and the adsorption isotherms were obtained.

4.3.3 Single - component adsorption kinetics tests

A jar test apparatus (equipped with a six - paddle stirrer) and a square jar were used to assess the adsorption kinetics over a period of 10 days for phenol and 15 days for red31. Aqueous solutions of various initial adsorabate concentrations ranging from 100-500 mg/l were prepared by diluting the adsorbates with distilled water. 1000 mg of the activated carbon samples were soaked overnight in 1.5 liter of distilled water to ensure complete wetting. UV- Visible spectrophotometer (UV-20000, Shimadzu Corporation, Japan or UV- 6405, Jenway, England) was used to determine the residual concentration in the liquid versus time. The maximum wavelengths of 270 and 540 nm for phenol and red31 solution, respectively, were used for the detection.

4.3.4 Estimation of single - component adsorption parameters

4.3.4.1 Adsorption equilibrium

The quantity of either phenol or red31 adsorbed individually at equilibrium was calculated from

$$q_{eq} = \frac{(C_0 - C_{eq})V}{M} \qquad (4.3.1)$$

where C_0 = the initial adsorbate concentration in the solution (mg/cm^3)

C_{eq} = the residual adsorbate concentration at equilibrium (mg/cm^3)

V = the volume of the solution (cm^3)

M = the amount of adsorbent (g)

4.3.4.2 Analytical solution of kinetic parameters

The mathematical model adopts the following assumptions:

1. Equilibrium occurs between the pore liquid and particle interior − that is, the solution flow to the pores is much faster than the solute uptake at sorption sites.
2. Mass transfer in the pores is solely by molecular diffusion, i.e. it follows Fick's first law and is measured by the effective pore diffusion coefficient, D_{eff} .
3. Solute concentration in the pore liquid is very small compared to that in the adsorbed phase and can therefore be neglected.
4. The solute concentration in the adsorbed phase is independent of that in the pore liquid; therefore, adsorption is irreversible and q_t can be

substituted by hypothetical equilibrium concentration, q_h, which is constant for all $C_{e,t}$ values in the analytical method.

The adsorbate concentration profile around and inside the carbon particle based on the film- pore diffusion model is shown in Fig. 4.3.2. The concentration of the adsorbate decreases from the value of C_t at bulk to $C_{e,t}$ at the particle surface due to the external film resistance measured by external mass transfer coefficient, k_f. Then, the value of $C_{e,t}$ drops further to zero at the radius r in the particle interior due to the internal resistance measured by D_{eff}. The reaction zone moves inwards in a well- defined concentration front with a variable velocity and at all times there is an unreacted core shrinking in size. Therefore, k_f, D_{eff} and q_h are the main parameters that describe the profile of a concentration decay curve.

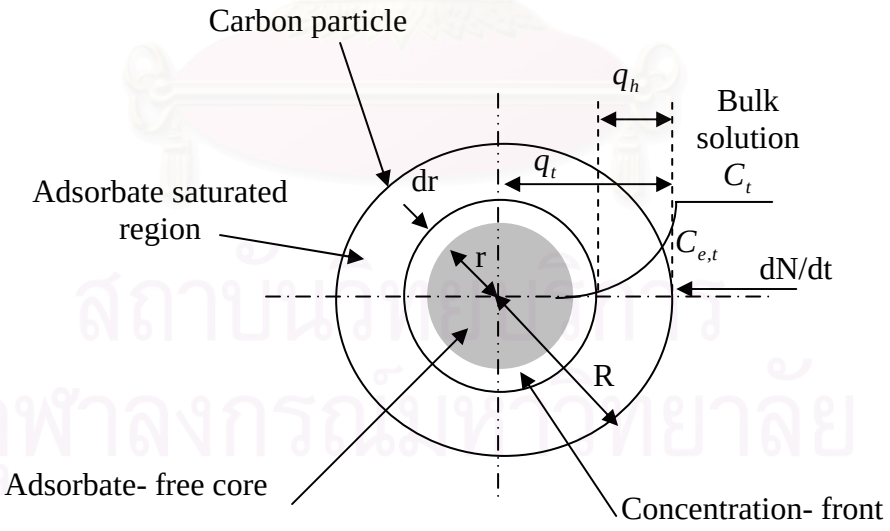

Figure 4.3.2 Mass transport of adsorbate and concentration profile of adsorbent

1. The mass transfer from the external phase, dN/dt (mg/s), is

$$\frac{dN}{dt} = k_f 4\pi R^2 \left(C_t - C_{e,t}\right) \qquad (4.3.2)$$

where k_f = the film mass transfer coefficient (cm/s)

R = the outer radius of the adsorbent (nm)

2. The diffusion in the pore according to Fick's law is

$$\frac{dN}{dt} = \frac{4\pi D_{eff} C_{e,t}}{1/r - 1/R} \qquad (4.3.3)$$

where r = the radius (cm) of virgin adsorbent at time t

D_{eff} = the effective diffusion coefficient (cm^2/s)

3. The velocity of the concentration front is obtained from the mass balance on a spherical element,

$$\frac{dN}{dt} = -4\pi r^2 q_h \rho_s \frac{dr}{dt} \qquad (4.3.4)$$

where q_h = hypothetical equilibrium solid- phase concentration (mg/g)

ρ_s = particle density (g/cm^3)

4. The average concentration in the adsorbent is given by

$$q_t = q_h \left[1 - \left(\frac{r}{R}\right)^3\right] \qquad (4.3.5)$$

By considering these conditions and introducing dimensionless parameters, the adsorption rate for a single particle can be expressed as a function of the adsorbate

concentration ξ in the water phase, the adsorbate concentration η in the adsorbent phase, and the Biot number Bi. The adsorption rate is represented by

$$\frac{d\eta}{d\tau} = \frac{3(1-C_h\eta)(1-\eta)^{1/3}}{1-(1-1/Bi)(1-\eta)^{1/3}} \tag{4.3.6}$$

where the dimensionless parameters are defined as

$$\tau = \frac{C_0}{\rho_s q_h}\frac{D_{eff}\, t}{R^2} \tag{4.3.7}$$

$$\eta = \frac{q_t}{q_h} \tag{4.3.8}$$

$$\xi = \frac{C_t}{C_0} \tag{4.3.9}$$

$$Bi = \frac{k_f R}{D_{eff}} \tag{4.3.10}$$

Then, Eq.(4.3.6) can be integrated to give

$$\tau = \frac{1}{6C_h}\left\{\ln\left|\frac{X^3+a^3}{1+a^3}\right|^{2(1-1/Bi)-1/a} + \ln\left|\frac{X+a}{1+a}\right|^{3/a}\right\} + \frac{1}{\sqrt{3}aC_h}\left\{\arctan\left(\frac{2-a}{\sqrt{3}a}\right) - \arctan\left(\frac{2X-a}{\sqrt{3}a}\right)\right\} \tag{4.3.11}$$

where
$$X = (1-\eta)^{1/3} \tag{4.3.12}$$

$$a = \left(\frac{1-C_h}{C_h}\right)^{1/3} \tag{4.3.13}$$

$$C_h = \frac{q_h M}{C_0 V} \tag{4.3.14}$$

The limits for Eq. (4.3.11) are

At τ = 0, η = 0, and X = 1

At τ = τ, η = η, and X = X

Therefore by converting the dimensionless time τ into real time t it is possible to compare the experimental and theoretical concentration decay curves.

4.3.5 Adsorption isotherm of binary system

Initial concentrations of phenol ranging from 100 – 500 mg/l were prepared from solution of constant red31 concentration at 500 mg/l. Similarly, initial concentrations of red31 ranging from 100 – 500 mg/l were prepared from solution of constant phenol concentration at 500 mg/l. Then 250-500 mg of activated carbon was put in contact with each of the prepared solutions. To maintain well-mixed condition, the solid - liquid suspensions were put in either a gyratory air bath or shaking water bath kept at 30 ºC. Typically adsorption equilibrium was achieved after 15 days. Then the solutions were filtered to remove the activated carbon powder and the residual concentration of each of the adsorbates was measured. The amounts adsorbed at equilibrium on the activated carbons were calculated from the initial and final concentrations and the adsorption isotherms were obtained.

4.3.6 Batch binary adsorption kinetics tests

Three scenarios of the competitive adsorption process were investigated:

- phenol adsorption followed by red31 adsorption
- red31adsorption followed by phenol adsorption
- simultaneous adsorption of phenol and red31 adsorption

A jar test apparatus (equipped with a six - paddle stirrer) and a square jar were used to assess the competitive adsorption kinetics over a period of 10 days for phenol adsorption and 15 days for red31 adsorption in various competitive adsorption kinetics modes. 1000 g of the activated carbon samples were soaked overnight in 1.5 liter of distilled water to ensure complete wetting. The aqueous concentration of the

adsorbate versus time was determined at the maximum wavelengths of 270 and 540 nm for phenol and red31 solution, respectively.

4.3.6.1Procedure of phenol adsorption followed by red31 adsorption

Phenol solution was contacted with the completely wetted adsorbent. The phenol concentration versus time was determined until 10 days, then the phenol − loaded adsorbent was filtered and contacted with single – solute red31 solution for another 15 days.

4.3.6.2 Procedure of red31 adsorption followed by phenol adsorption

Red31solution was contacted with the completely wetted adsorbent. The red31 concentration versus time was determined until 15 days, then the red31 − loaded adsorbent was filtered and contacted with single – solute phenol solution for another 10 days.

4.3.6.3 Procedure of simultaneous adsorption of phenol and red31 adsorption

Phenol - red31solution was contacted with the completely wetted adsorbent. The aqueous concentrations of both adsorbates versus time were determined until 15 days.

CHAPTER V

RESULTS AND DISCUSSION

The present study is concerned with the adsorption equilibrium and kinetics of phenol and reactive dyes on both the activated carbon produced from waste tires and a commercial activated carbon. Preparation of the activated carbon produced from waste tires was carried out under the following conditions as shown in Table 5.1.

Table 5.1 Conditions of activated carbon preparation

	***Carbonization**	**HCl − Treatment**	***Steam Activation**
Temperature (ºC)	500	Room temperature	850
Heating rate (ºC/min)	5	-	20
Holding time (hr)	1.5	24	4.5

*Under N_2 atmosphere

Furthermore, the single and binary adsorption kinetics were investigated under the conditions that the amount of adsorbents and the agitation speed are constant. Moreover, investigation of the binary adsorption kinetics consists of three scenarios of the competitive adsorption process:

- phenol adsorption kinetics followed by red31 adsorption
- red31 adsorption kinetics followed by phenol adsorption
- simultaneous adsorption kinetics of phenol and red31 adsorption

5.1 Physical characterization of the adsorbents

Porous properties of the produced activated carbon, and commercial activated carbon are evaluated by nitrogen adsorption method. Adsorption and desorption isotherms of N_2 on the activated carbons were measured at 77 K by the adsorption apparatus. BET surface area S_{BET} is determined by BET method. Moreover, micropore volume V_{mic} is evaluated from the adsorption isotherm by the t - plot method. In addition, mesopore volume V_{mes} is estimated by applying the Dollimore − Heal method to the desorption isotherms.

Figs. 5.1.1 − 5.1.2 show the typical N_2 adsorption - desorption isotherm of the activated carbon produced from waste tires (AC_Tire) and commercial activated carbon (AC_COM), respectively. It is found that fairly mesoporous activated carbons with V_{meso} and S_{BET} values up to 0.41 cm^3/g and 540 m^2/g, respectively, can be obtained from waste tires. Nevertheless, the commercial activated carbon shows microporous characteristic with V_{micro} and S_{BET} value to 0.40 cm^3/g and 1080 m^2/g, respectively.

Fig. 5.1.3 compares the pore size distributions of the commercial activated carbon and activated carbon prepared from waste tires where R_p and V_p are the pore radius, and pore volume, respectively. .

It is confirmed that the activated carbon produced from waste tires has larger mesopore volume than the commercial activated carbon; on the other hand, it has less micropore volume and BET surface area. The micropore volume, mesopore volume, and BET surface area of both activated carbons are summarized in Table 5.1.1.

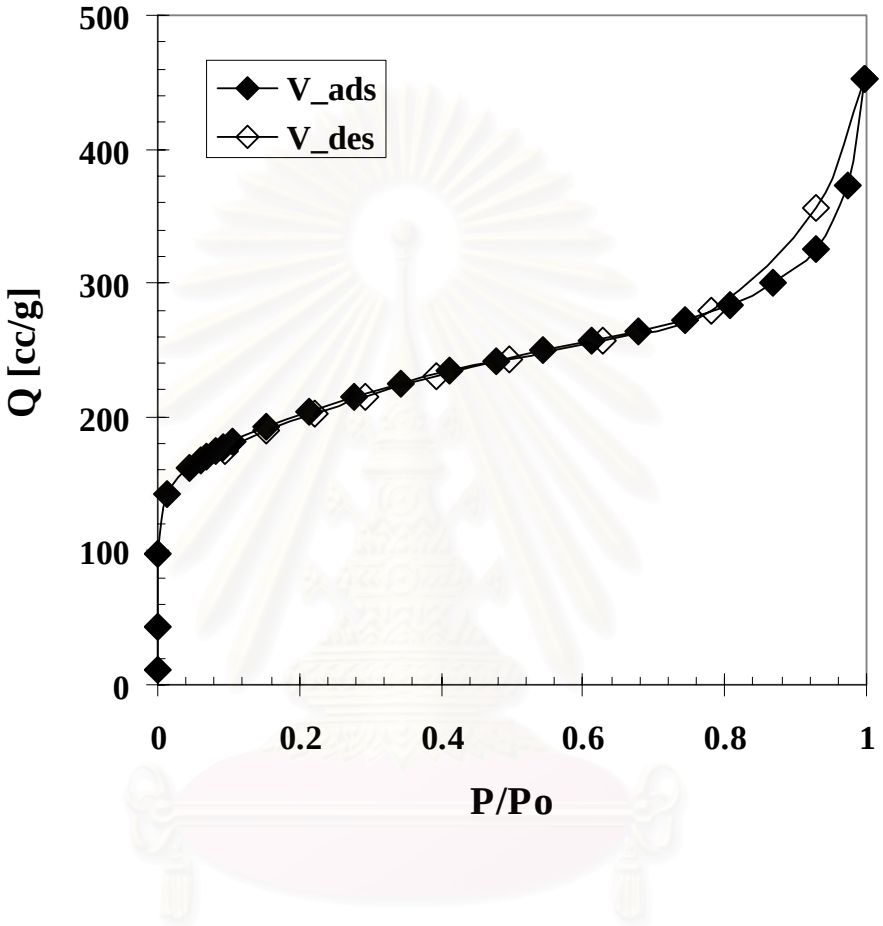

Figure 5.1.1 N_2 adsorption − desorption isotherm of activated carbon prepared from waste tires

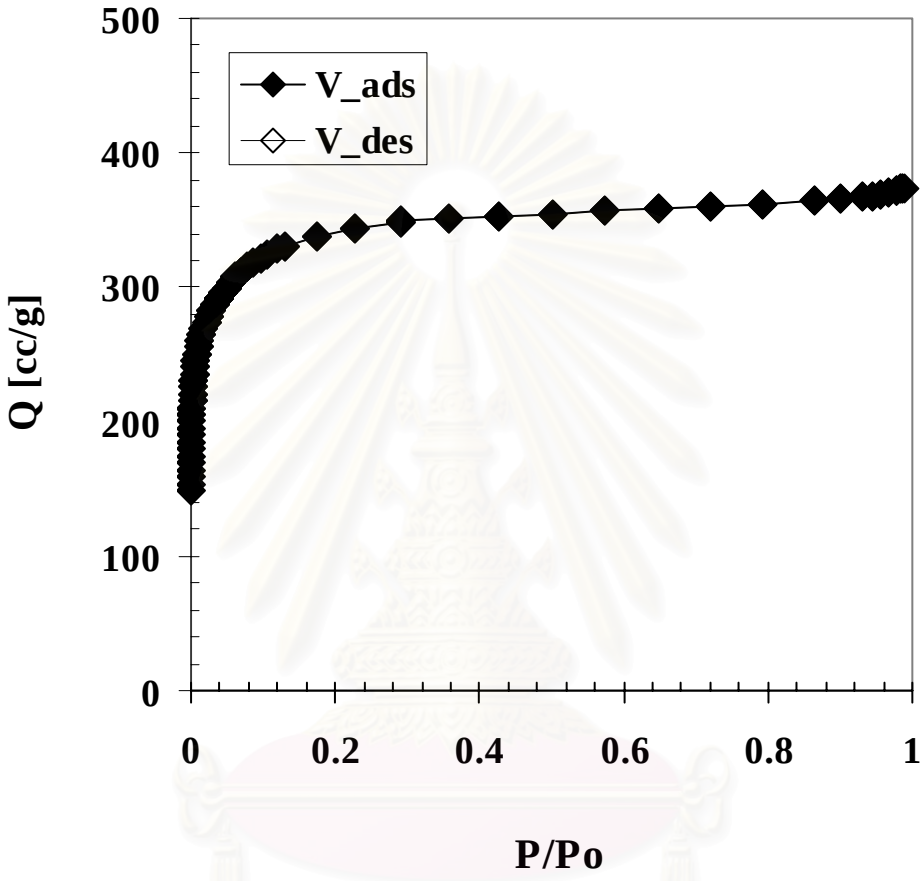

Figure 5.1.2 N_2 adsorption − desorption isotherm of commercial activated carbon

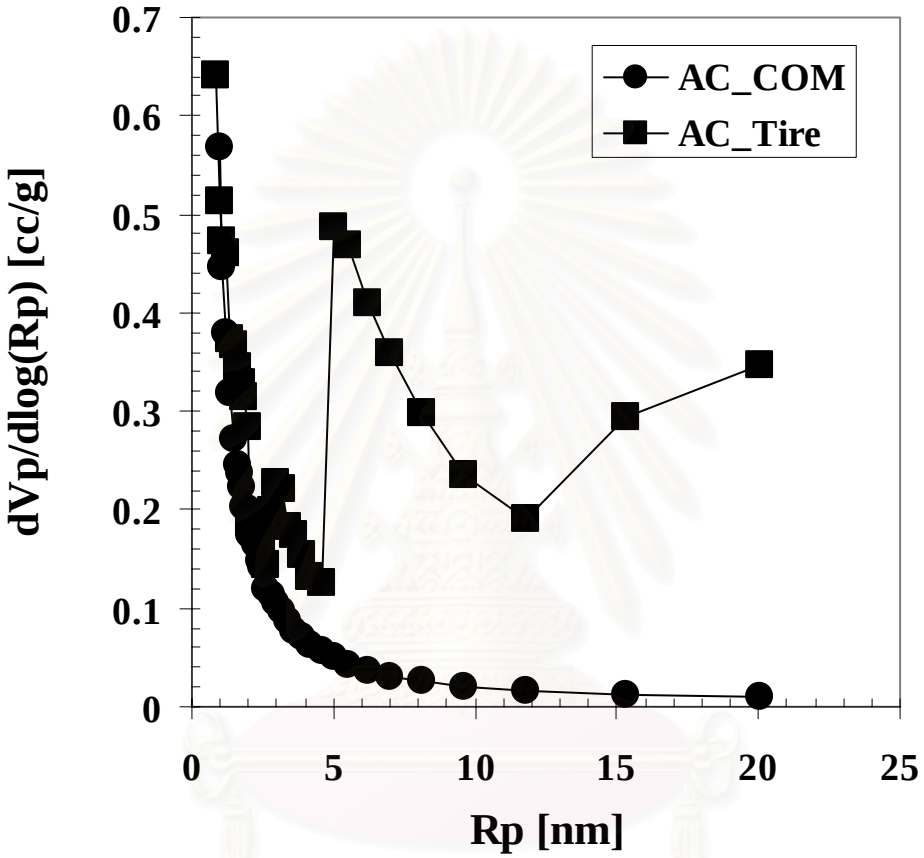

Figure 5.1.3 Pore size distribution of produced activated carbon and commercial activated carbon

Table 5.1.1 Porous properties of activated carbon prepared from waste tires and commercial activated carbon

Porous properties	AC_Tire	AC_COM
S_{BET} [m^2/g]	540	1080
V_{total} [cm^3/g]	0.70	0.52
V_{micro} [cm^3/g]	0.28	0.40
V_{meso} [cm^3/g]	0.42	0.12

5.2 Single system

5.2.1 Single − component adsorption isotherm

The adsorption isotherm of aqueous phenol adsorbed on the produced activated carbon and the commercial activated carbon are shown in Fig. 5.2.1. The q_{eq} and C_{eq} are the equilibrium amount of adsorbate and equilibrium concentration, respectively. Since the average pore size and total mesopore volume (0.41 cm^3/g) of AC_Tire are bigger compared with the average pore size and total mesopore volume (0.12 cm^3/g) of AC_COM, the phenol adsorption capacity of AC_Tire is higher than those of AC_COM.

Similarly, the adsorption isotherm of red31 adsorbed on the produced activated carbon and the commercial activated carbon are shown in Fig. 5.2.2. The q_{eq} and C_{eq} are the equilibrium amount of adsorbate and equilibrium concentration, respectively. It is observed that the red31 adsorption capacity of the AC_COM is much lower than of AC_Tire because its small mesopore volume and average pore diameter are not suitable for the molecular size of red31.

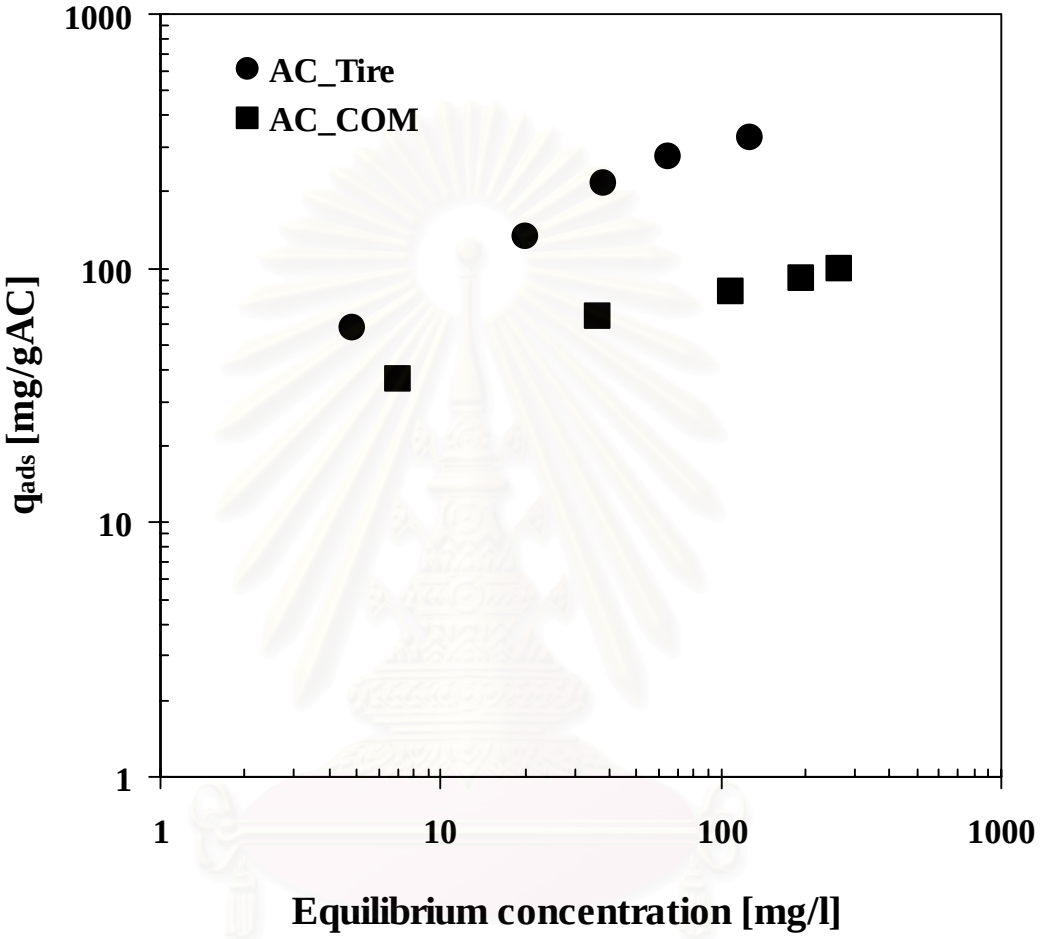

Figure 5.2.1 Phenol adsorption equilibrium of activated carbon prepared from waste tires and commercial activated carbon

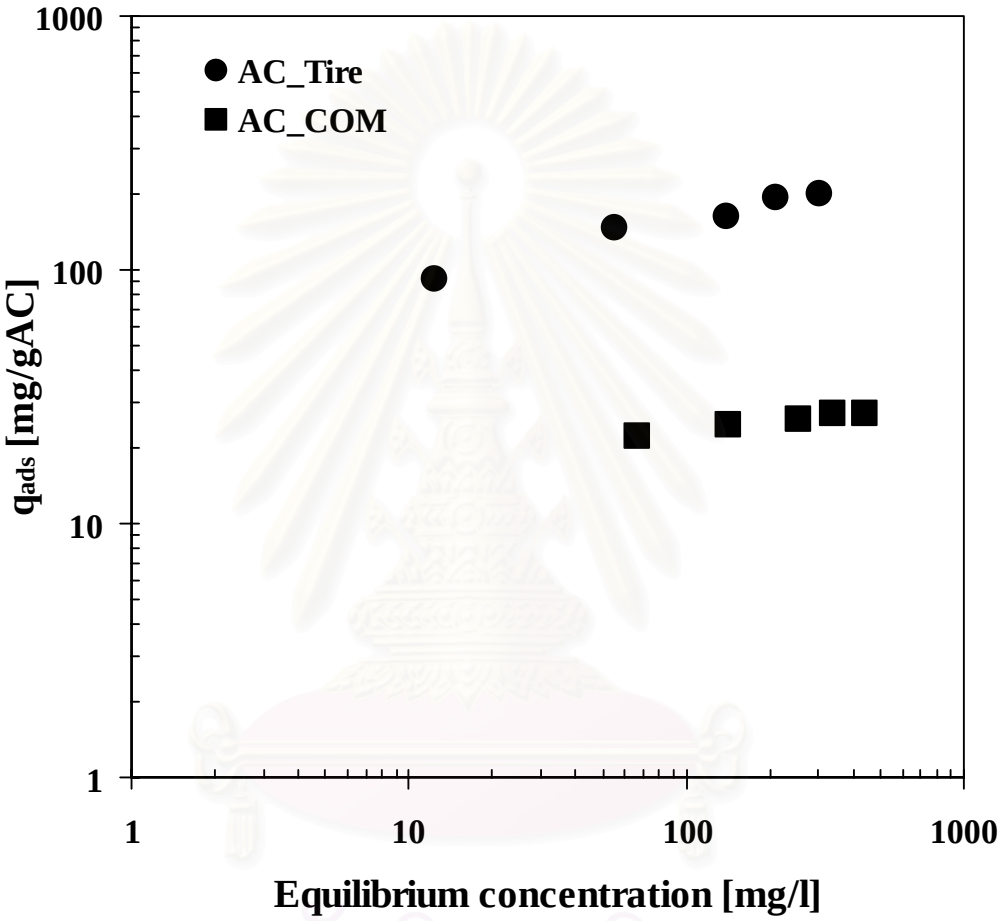

Figure 5.2.2 Red31 adsorption equilibrium of activated carbon prepared from waste tires and commercial activated carbon

Next the isotherm equilibrium data are analyzed using either Langmuir or Freundlich equilibrium equation. The Langmuir equation can be written in the following form:

$$q_{eq} = \frac{K_L C_{eq}}{1 + a_L C_{eq}} \quad (5.2.1)$$

$$\frac{1}{q_{eq}} = \frac{1}{K_L C_{eq}} + \frac{a_L}{K_L} \quad (5.2.2)$$

where K_L and a_L are the Langmuir constants. Moreover, the empirical Freundlich equation is given below by Eq. (5.2.3)

$$q_{eq} = K_F C_{eq}^{1/n} \quad (5.2.3)$$

$$\log q_{eq} = \log K_F + \frac{1}{n} \log C_{eq} \quad (5.2.4)$$

where K_F and n are the Freundlich constants characteristic of the system. K_F and n are indicators of adsorption capacity and adsorption intensity, respectively.

The linear plot of $1/q_{eq}$ versus $1/C_{eq}$ and log q_{eq} versus log C_{eq} for the Langmuir and Freundlich isotherm model are shown, respectively in Figs. 5.2.3 − 5.2.6. The Langmuir and Freundlich constants are determined from the intercept and slope of the plot and presented in Table 5.2.1 − 5.2.2.

In order to quantitatively compare the applicability of the parameters of the two models, a normalized standard deviation, Δq, are calculated

$$\Delta q(\%) = 100 \times \sqrt{\frac{\sum((q_{t\exp} - q_{tcal})/q_{t\exp})^2}{n-1}} \qquad (5.2.5)$$

where n is the number of data points; $q_{t\ exp}$ the experimental values; and $q_{t\ cal}$ the calculated values by models.

In view of the values of percentage errors in the Table 5.2.1 − 5.2.2, the Freundlich model exhibits the best fit to the adsorption equilibrium of phenol and red31 adsorbed onto AC_Tire. However, the Langmuir model seems to agree better with the adsorption equilibrium of both phenol and red31 adsorbed onto AC_COM. Again the Langmuir model presents slightly better fit than AC_Tire considering that the obtained percentage error values are lower than 1%.

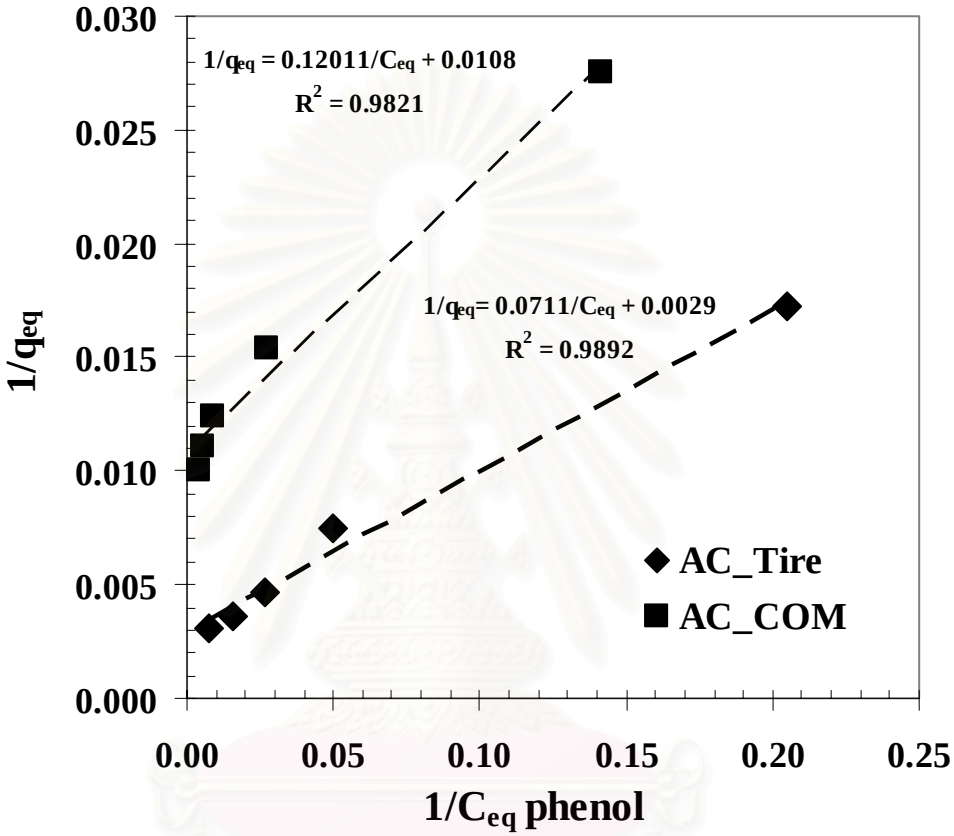

Figure 5.2.3 Comparison of the experimental adsorption equilibrium data (■♦) with Langmuir equilibrium data (- - - -) of phenol

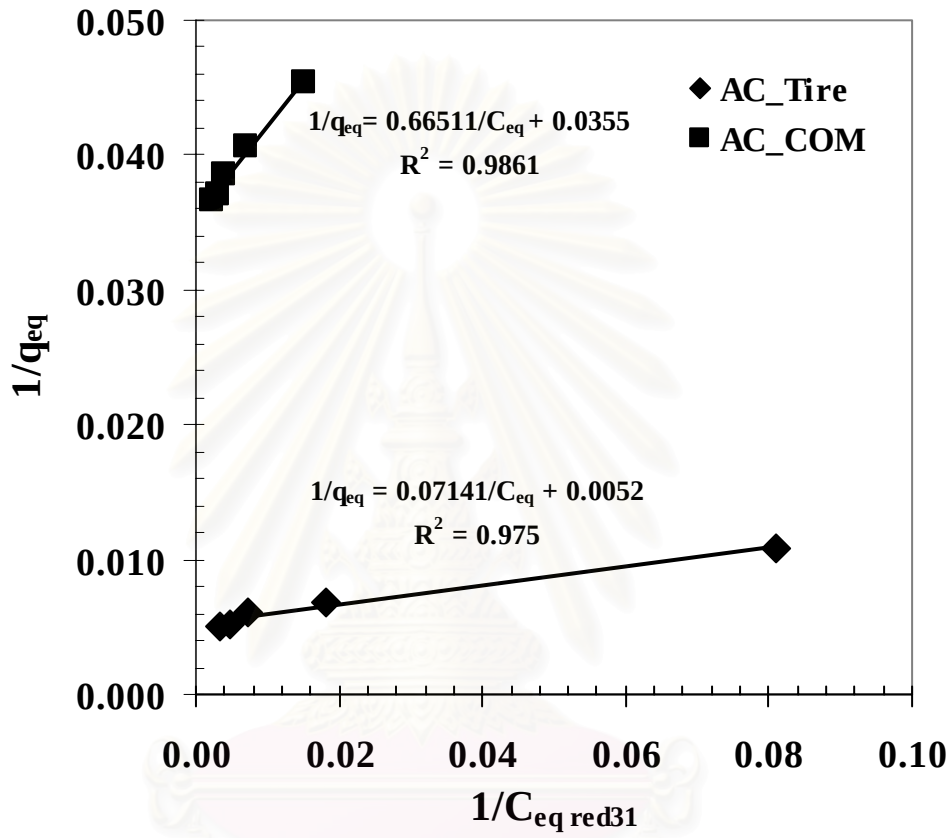

Figure 5.2.4 Comparison of the experimental adsorption equilibrium data (■♦) with Langmuir equilibrium data (– – –) of red31

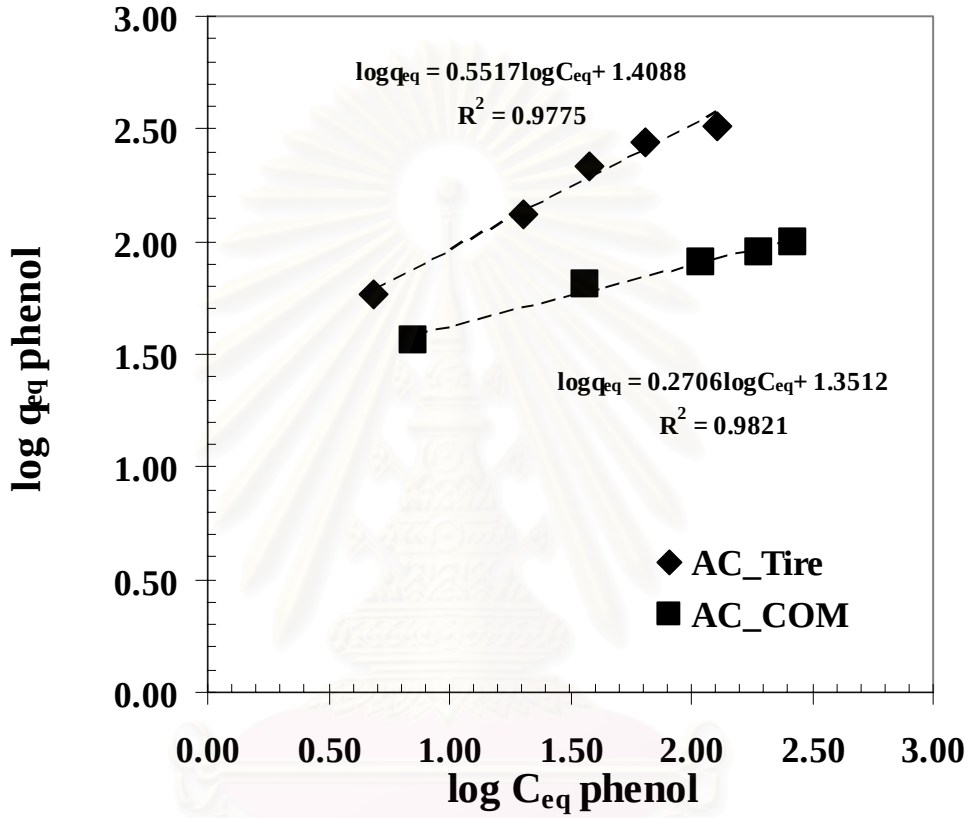

Figure 5.2.5 Comparison of the experimental adsorption equilibrium data (■♦) with Freundlich equilibrium data (– – –) of phenol

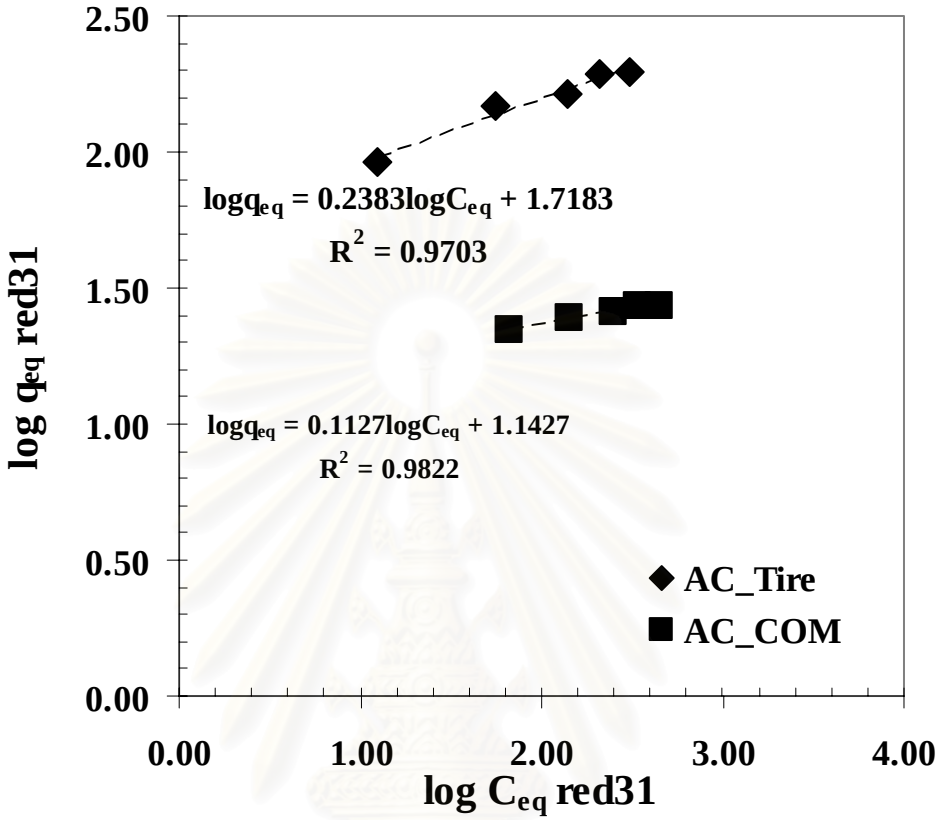

Figure 5.2.6 Comparison of the experimental adsorption equilibrium data (■♦) with theoretical equilibrium data (Freundlich model) (─ ─ ─) of red31

Table 5.2.1 Langmuir constants for AC_Tire and AC_COM

Adsorbents	Adsorbate	K_L (mg/g)	a_L (L/mg)	Δq%	r^2
AC_Tire	Phenol	14.0845	0.0408	0.9881	0.9892
	Red31	19.9600	0.1078	0.9732	0.9750
AC_COM	Phenol	8.3264	0.0899	0.4636	0.9821
	Red31	1.5035	0.0534	0.0093	0.9861

Table 5.2.2 Freundlich constants for AC_Tire and AC_COM

Adsorbents	Adsorbate	K_F (L/g)	n	Δq%	r^2
AC_Tire	Phenol	25.6330	0.5517	0.8835	0.9775
	Red31	59.7173	0.2126	0.3695	0.9808
AC_COM	Phenol	22.4492	0.2706	5.2535	0.9821
	Red31	13.8899	0.1127	0.0550	0.9822

5.2.2 Single − component adsorption kinetics

5.2.2.1 Determination of external mass transfer and effective pore diffusion coefficient

Film − pore diffusion model (C.W. Cheung, C.K. Chan, J.F. Porter and G. McKay [3]) is used to describe the kinetic rate and the aqueous solute concentration decay curves for phenol and red31 adsorbing onto the two types of activated carbons (AC_Tire and AC_COM). For easy comparison the results from the model will be expressed in terms of a plot of the experimental and modeled solute concentrations versus time and represented by the external mass transfer coefficient, k_f , and an effective pore diffusion coefficient, D_{eff} , for each particular system.

In order to optimize the parameters of the model with respect to the experimental data, the following normalized standard deviation, Δt, are calculated and minimized:

$$\Delta t(\%) = 100 \times \sqrt{\frac{\sum((t_{\exp} - t_{cal})/t_{t\exp})^2}{n-1}} \qquad (5.2.6)$$

where n is the number of data points; t_{exp} the experimental values; and t_{cal} the calculated values from the model.

The performance of this model is illustrated in Figs. 5.2.7 − 5.2.10 which show the experimental and theoretical solute concentration decay curves at various conditions. As a key assumption, the hypothetical equilibrium concentration is assumed to be equal to the equilibrium capacity ($q_{e,\infty}$) which depends on the initial concentration of each adsorbate. The model displays a good fit over the courses of the experiments although there is a slight deviation in some of the initial stages due to the preliminary estimates of the effective pore diffusion coefficient and the external mass transfer coefficient. It is found that AC_Tire has a larger external mass

transfer coefficient and effective pore diffusivity of phenol and red31 than those of AC_COM, as shown in Table 5.2.3. At the same constant agitation condition, the larger sized particles (AC_COM) generally have a thicker boundary layer around the particles than the smaller ones (N.K. Hamadi, X.D. Chen, M.M. Farid and Max G.Q. Lu [4]). This results in a decrease in the external film mass transfer and overall adsorption rate of each adsorbate. On the contrary, a decrease in the boundary layer thickness and resistance leads to an increase in the overall adsorption rate at which the adsorbate diffuses through the boundary layer (external diffusion) to the particle surface (J.R. Evans, W.G. Davids, J. D. MacRae and A. Amirbahman [5]). Table 5.2.3 summarizes the set of parameters obtained by trials and errors and the value of. C_h.

Table 5.2.3 Prediction results of the film − pore diffusion model

Adsorbent	Adsorbate	Initial concentration (mg/l)	C_h (mg/g)	k_f (cm/s)	D_{eff} (cm^2/s)	Δt (%)
AC_Tire	Phenol	85.31 200.63 559.34	0.8160 0.5095 0.7046	2.08×10^{-2}	1.50×10^{-17}	5.20
	Red31	98.84 326.32 460.14	0.00062 0.00054 0.00056	1.66×10^{-2}	1.46×10^{-18}	6.67
AC_COM	Phenol	76.32 211.93 527.19	0.5662 0.5313 0.6204	1.92×10^{-2}	1.00×10^{-17}	9.71
	Red31	108.45 314.57 504.66	0.2381 0.3820 0.3849	1.43×10^{-2}	5.71×10^{-19}	7.08

To describe the diffusion mechanism of the adsorbates inside the activated carbons, the mean free paths [6] of phenol and red31 in water are estimated to be 8.76×10^{-10} m and 7.86×10^{-11} m, respectively. Compared with the pore size distribution of AC_Tire and AC_COM shown in Fig.5.1.3, the mean free paths of phenol and red31 might be considered to be significantly smaller than the average pore diameter of both activated carbons. If this assumption is correct, then the collisions of the adsorbate molecules with other diffusing molecules should occur much more frequently than their collisions with the pore walls. Under this condition, the intermolecular collisions provide the main diffusional resistance and the mechanism is known as molecular diffusion. Therefore the diffusion mechanism of both adsorbates in these activated carbons could be considered as molecular diffusion. The molecular diffusion coefficient may then be estimated via the Wilke − Chang equation,

$$D_i = \frac{7.4\times10^{-8}\sqrt{\phi M}\,T}{\mu V_m^{\,0.6}} \qquad (\mathrm{cm^2/s}) \qquad (5.2.7)$$

where ϕ denotes an association factor (= 2.6 for water), T is in K, M is the molar mass of the solute, μ denotes solvent viscosity [cp] and V_m is the molar volume of the solute [$\mathrm{cm^3/g-mole}$] as liquid at its normal boiling point. Table 5.2.4 (a) summarizes the calculated values of the molecular diffusivity. Comparing these values with the experimentally obtained values in table 5.2.3, we may conclude that the assumption here of molecular diffusion is totally incorrect. However, in small pore and in liquid phase adsorption the collisions of molecules with pore walls may occur more frequently than collisions between diffusing molecules. Under these conditions the collisions between molecule and pore wall provide the main diffuisional resistance. This means that the actual transport mechanism inside the

activated carbon particles is Knudsen diffusion. An approximation of this diffusion coefficient may be derived from the kinetic of gases as [20]:

$$D_K = 4850 d_p \left(\frac{T}{M_i} \right)^{0.5} \text{(cm}^2\text{/s)} \qquad (5.2.8)$$

where d_p denotes mean pore diameter (m), T is in K, M_i is the molecular weight of the diffusing species. Table 5.2.4 (b) summarizes the estimated values of Knudsen diffusivity. Clearly, D_i and D_K values are greater than D_{eff} value. It might be strongly suggested that either the surface diffusion effects dominate the diffusion process or the application of the film − pore diffusion model is not suitable.

Table 5.2.4(a) Molecular diffusion coefficient

Average pore diameter (m)		**Phenol**		**Red31**	
AC_Tire	AC_COM	Mean free path (m)	D_i (cm^2/s)	Mean free path (m)	D_i (cm^2/s)
5.00×10^{-9}	1.00×10^{-9}	8.76×10^{-10}	3.32×10^{-6}	7.86×10^{-11}	2.90×10^{-7}

Table 5.2.4(b) Knudsen diffusion coefficient

Adsorbate	**Knudsen diffusion coefficient (cm^2/s)**					
	AC_Tire			AC_COM		
	Minimum d_p (m)	Average d_p (m)	Maximum d_p (m)	Minimum d_p (m)	Average d_p (m)	Maximum d_p (m)
Phenol	8.32×10^{-6}	4.35×10^{-5}	1.74×10^{-4}	7.80×10^{-6}	8.71×10^{-6}	1.33×10^{-4}
Red31	2.74×10^{-6}	1.44×10^{-5}	5.75×10^{-5}	2.57×10^{-6}	2.87×10^{-6}	4.40×10^{-4}

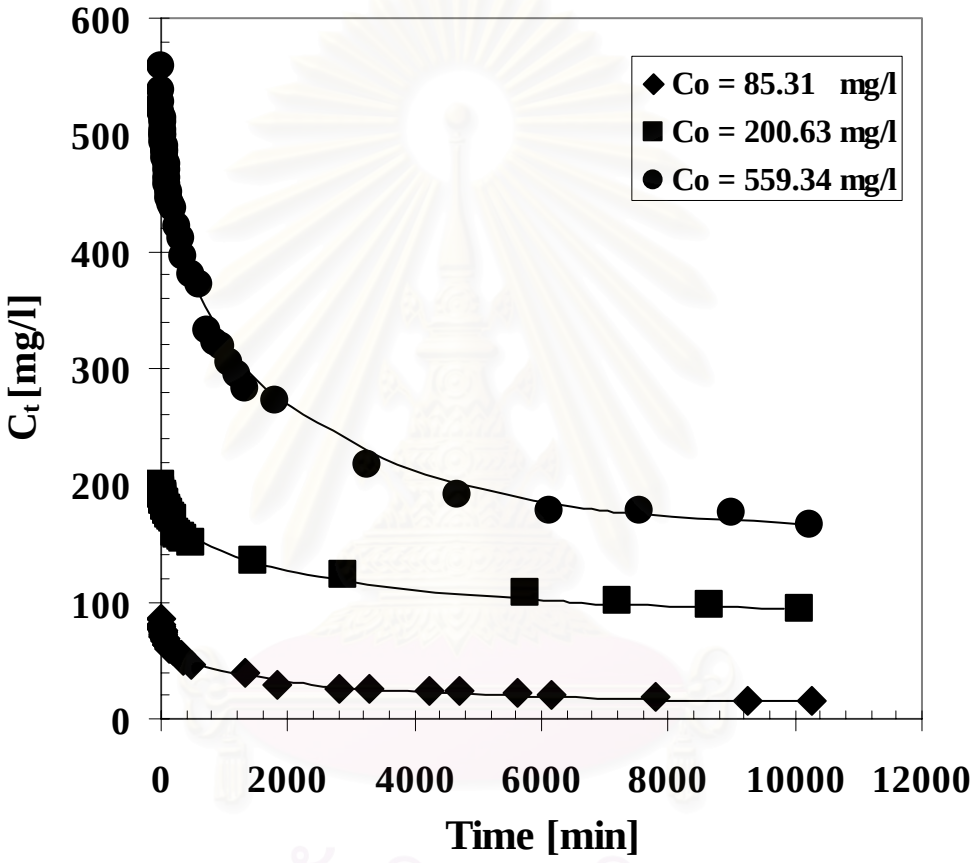

Figure 5.2.7 Phenol concentration decay curves for constant amount of activated carbon prepared from waste tires adsorbent: (◆▲●) experimental data, (——) mode: k_f = 2.08x10^{-2} (cm/s), D_{eff} = 1.50 x 10^{-17} (cm^2/s)

Particle diameter = 997.97 µm

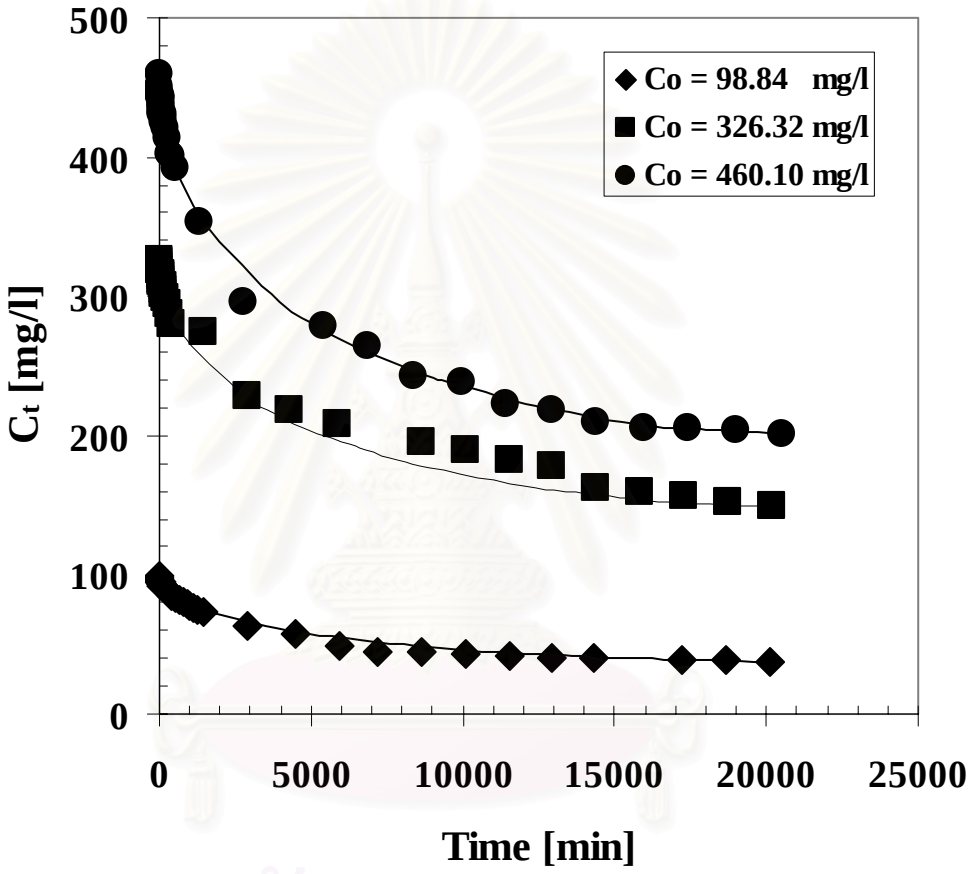

Figure 5.2.8 Red31 concentration decay curves for a constant amount of activated carbon prepared from waste tires: (◆ ▲ ●) experimental data, (——) model: k_f = 1.66x10^{-2} (cm/s), D_{eff} = 1.46 x 10^{-18} (cm^2/s)

Particle diameter = 997.97 µm

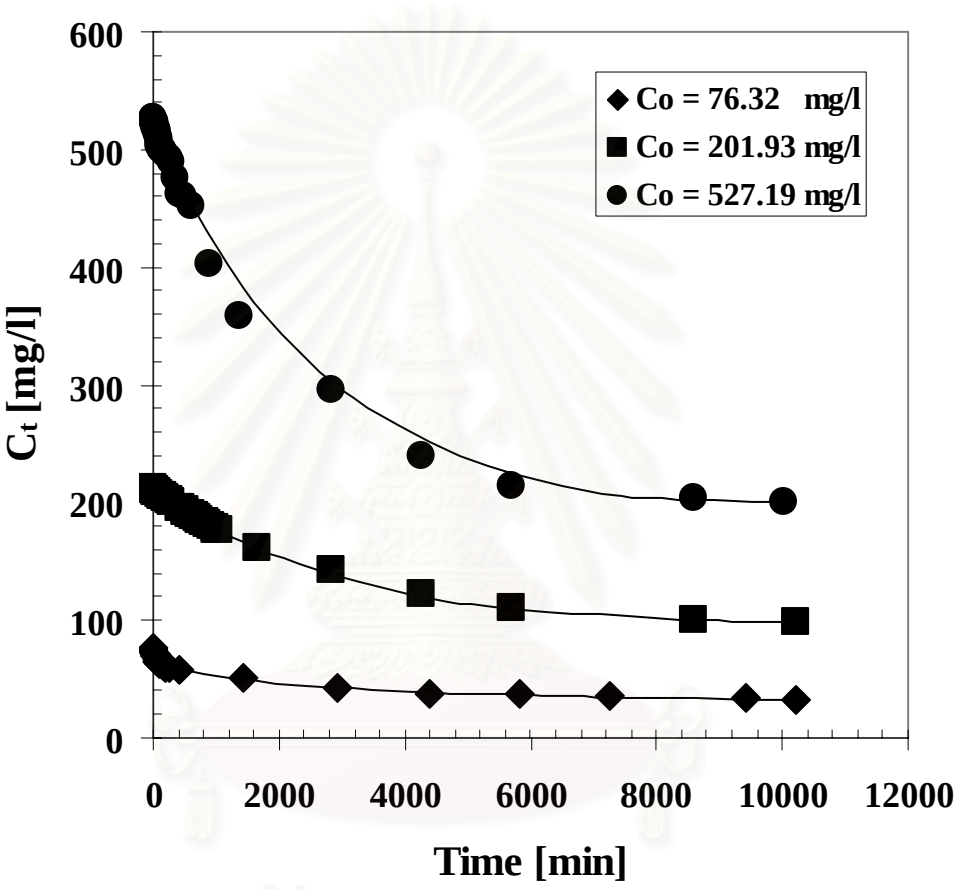

Figure 5.2.9 Phenol concentration decay curves for a constant amount of commercial activated carbon: (◆ ▲ ●) experimental data, (——) model: k_f = 1.92x10^{-2} (cm/s), D_{eff} = 1.00 x 10^{-17} (cm^2/s)

Particle diameter = 1470.81 µm

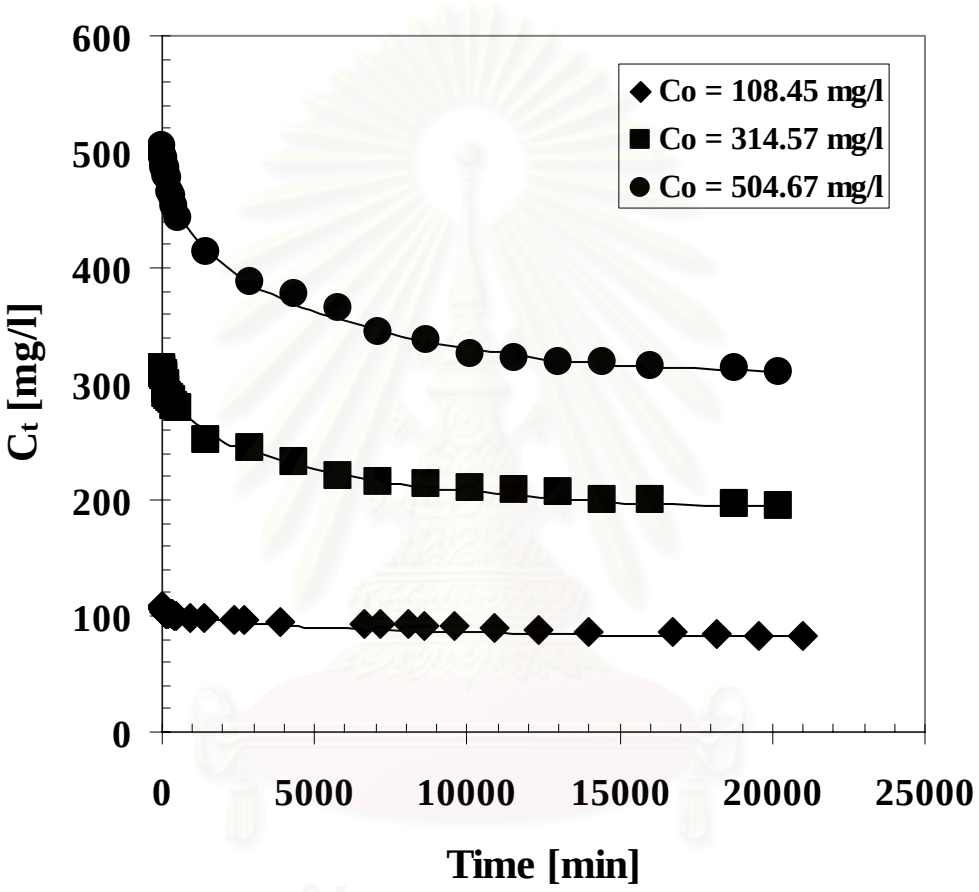

Figure 5.2.10 Red31 concentration decay curves for a constant amount of commercial activated carbon: (◆▲●) experimental data, (——) model: k_f = 1.43 x 10^{-2}(cm/s), D_p = 5.71x 10^{-19}(cm^2/s)

Particle diameter = 1470.81 µm

The experimental results in Figs. 5.2.7 – 5.2.10 are used to calculate and prepare Figs. 5.2.11 – 5.2.14, respectively. As expected, the removal of either phenol or red31 by adsorption on the activated carbon prepared from waste tires shows an increase with time and attains a maximum adsorption capacity at about 2795 min and 8640 min for phenol and red31, respectively, after which the capacity remains essentially constant. Upon changing the initial concentration of phenol from 85 to 559 mg/l, the amount adsorbed at equilibrium increases from 83 to 300 mg/gAC at 30 $^{\circ}$C as shown in Fig. 5.2.11. Similarly, when the initial concentration of red31 is varied from 98 to 460 mg/l, the amount adsorbed at equilibrium increases from 90 to 138 mg/gAC at 30 $^{\circ}$C as shown in Fig. 5.2.12.

Similarly, the individual adsorption of either phenol or red31 on the commercial activated carbon shows an increase with time and attains a maximum adsorption capacity at about 2989 min and 8660 min for phenol and red31, respectively, after which, the capacity remains essentially constant. Upon changing the initial concentration of phenol from 76 to 527 mg/l, the amount adsorbed at equilibrium increases from 68 to 310 mg/gAC at 30 $^{\circ}$C as shown in Fig. 5.2.13. Similarly, when the initial concentration of red31 is varied from 108 to 504 mg/l, the amount adsorbed at equilibrium increases from 30 to 64 mg/gAC at 30 $^{\circ}$C as shown in Fig. 5.2.14.

Evidently, the data show that an increase in the initial concentration of either adsorbate results in an increase of the initial driving force, which will increase the initial diffusion rate of the adsorbate in the pores (Q.Sun and L. Yang [7]).

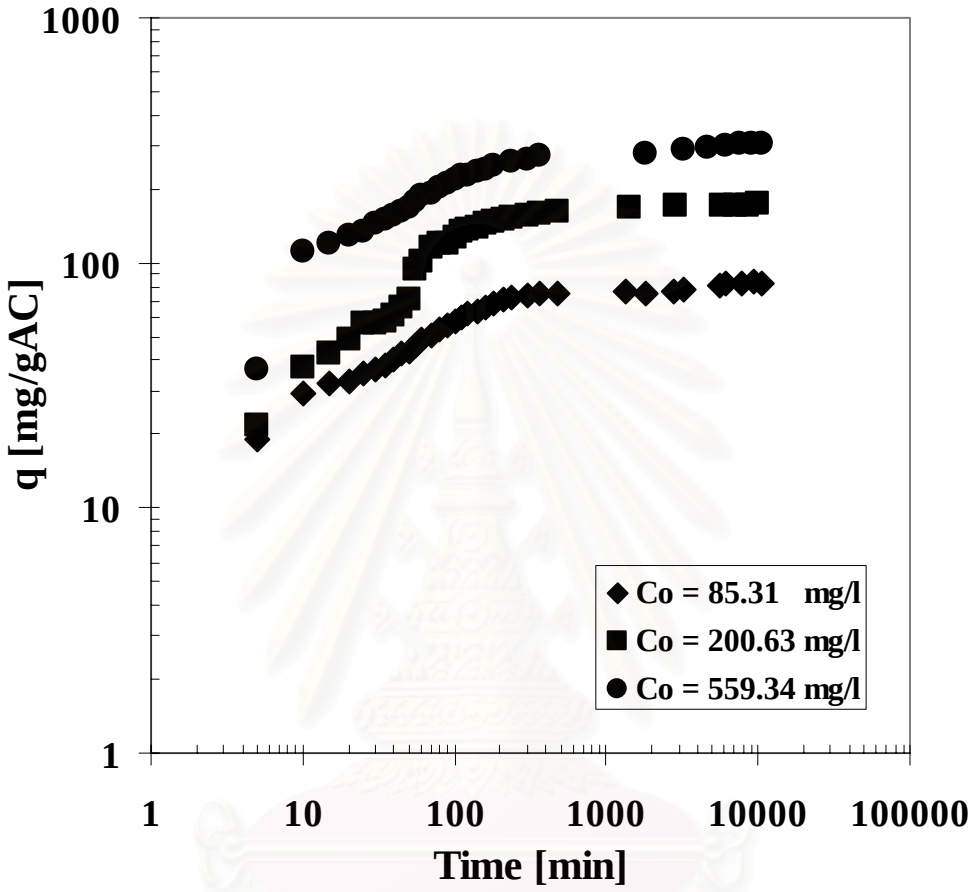

Figure 5.2.11 Phenol adsorbed onto the activated carbon prepared from waste tires versus time

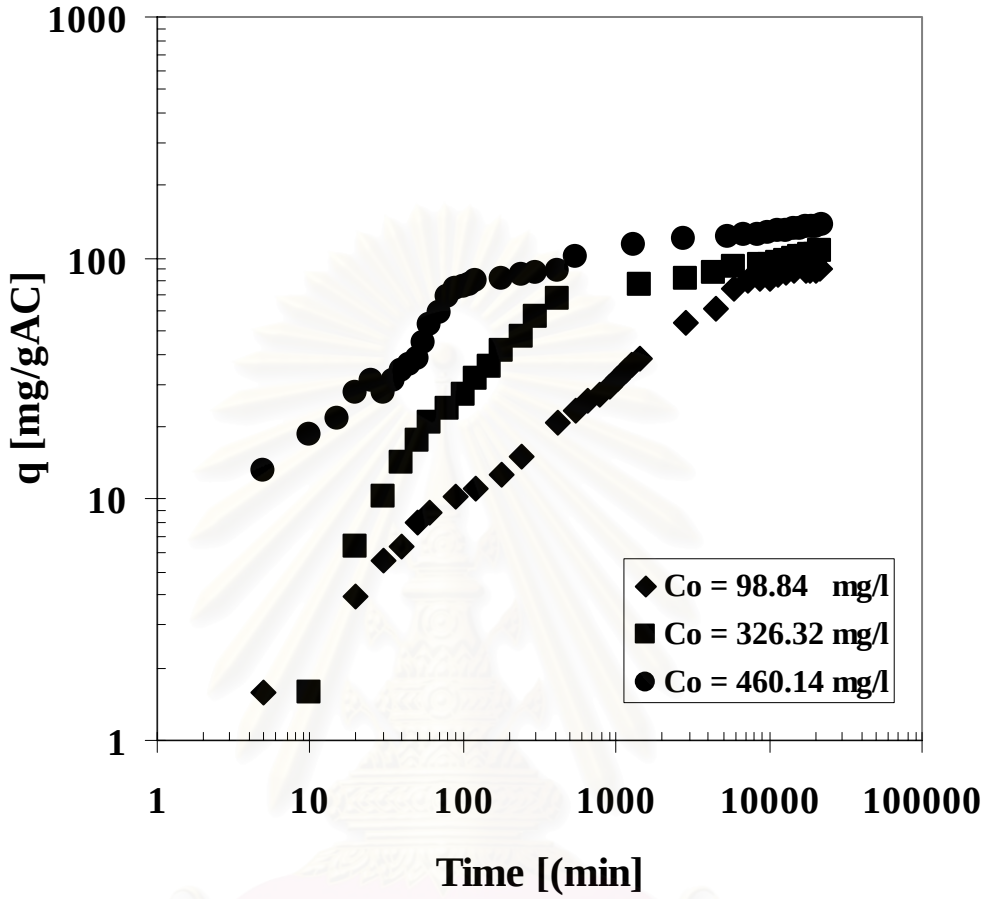

Figure 5.2.12 Red31 adsorbed onto the activated carbon prepared from waste tires versus time

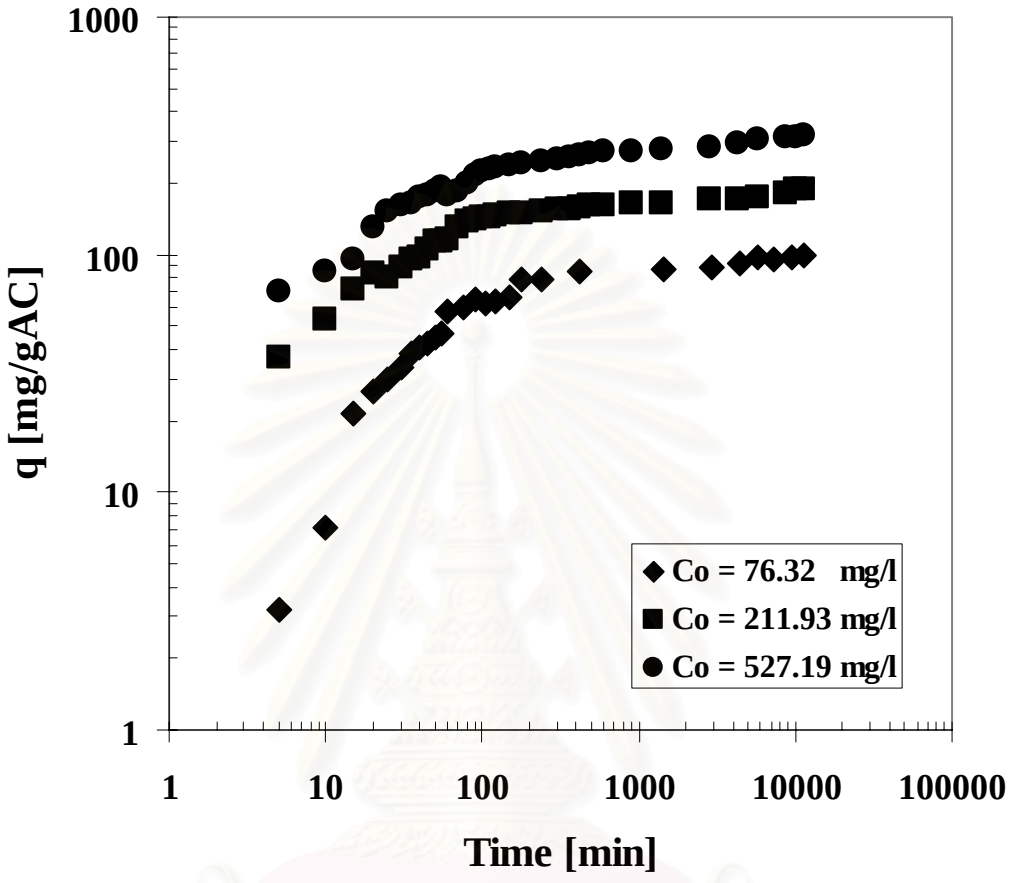

Figure 5.2.13 Phenol adsorbed onto the commercial activated carbon versus time

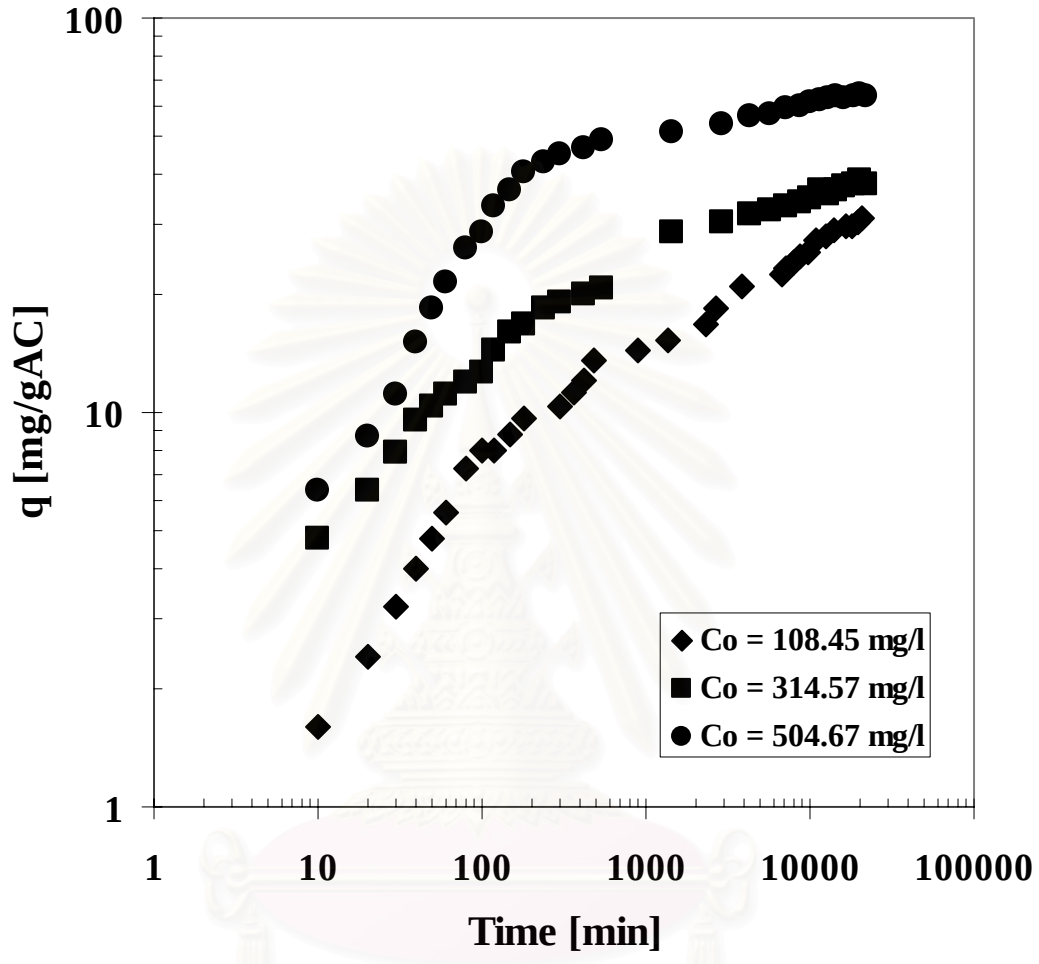

Figure 5.2.14 Red31 adsorbed onto the commercial activated carbon versus time

5.2.2.2 Determination of the rate controlling step

The adsorption of a phenol or red31 molecule onto both types of activated carbons can be divided into three consecutive stages. The following sequence of steps is logical: transport of either adsorbate from the liquid boundary film to the external surface of the adsorbent (film diffusion), transfer of the adsorbate from the external surface to the intraparticle active sites and uptake of the adsorbate by the interior active sites of the adsorbent. Generally the final step is very rapid and is not a rate − limiting step in most adsorption systems.

In our experiments, vigorous stirring of the solution takes place all the time, so the film diffusion step is relative fast. In order to investigate the adsorption mechanism of either phenol or red31 on both activated carbons, three overall kinetic rate models are tested, namely, pseudo − first − order adsorption model, pseudo − second − order adsorption model and intraparticle diffusion model.

Firstly, a simple kinetic analysis of the overall adsorption rate adopts Lagergren's equation, a pseudo − first − order adsorption model shown below:

$$\frac{dq_t}{dt} = k_f (q_e - q_t) \qquad (5.2.5)$$

where k_f is the rate constant of the pseudo − first − order adsorption model, q_e and q_t are the amounts adsorbed at equilibrium and at any time, respectively. After integration and application of the initial condition $q_t = 0$ at t = 0 and $q_t = q_t$ at t = t, the equation becomes

$$\log(q_e - q_t) = \log q_e - \frac{k_f}{2.303} t \qquad (5.2.6)$$

Eq. (5.2.6) can be plotted in a linear form. By plotting *log* $(q_e\text{-}q_t)$ against *t*, a straight line can be obtained and k_f and q_e can be estimated. The estimated value of q_e must be consistent with the experimental value.

Secondly, the pseudo − second − order overall adsorption rate model may be represented as:

$$\frac{dq_t}{dt} = k_s\left(q_e - q_t\right)^2 \qquad (5.2.7)$$

where k_s is the adsorption rate constant of pseudo − second − order model. After integrating Eq. (5.2.7) and applying the initial condition $q_t = 0$ at t = 0 and $q_t = q_t$ at t = t, the following form can be obtained:

$$\frac{t}{q_t} = \frac{1}{k_s q_e^2} + \frac{1}{q_e}t \qquad (5.2.8)$$

By plotting the term t/q_t against *t*, a straight line can be obtained and q_e and k_s may be estimated.

Finally, the intraparticle diffusion model indicates that the intraparticle diffusion is the rate controlling step as developed by Weber and Morris. In a well − agitated system, the overall adsorption rate of either adsorbate onto the particle depends on the limiting rate of the mass transport process within the activated carbon. The uptake rate in a particle which is exposed to a step change in the surface concentration of an adsorbable species is determined by the diffusional time constant. Weber and Morris [19] suggested that the fraction of solute adsorbed could be expressed in terms of the square root of time. The fractional approach to equilibrium varies according to a function of $(Dr^{-2})^{0.5}$, where r is the particle radius and D is the diffusivity of the solute within the particle. So the initial rate of intraparticular diffusion is calculated by linearization of the experimental data:

$$q = k_i t^{0.5} \qquad (5.2.9)$$

Tables 5.2.4 − 5.2.5 present the results of fitting experimental data with pseudo − first − order model, pseudo − second − order model, and intraparticle diffusion model. It is found that the decreasing order of Δq% is: pseudo − first − order > pseudo − second − order > intraparticle diffusion in all the experiments, which indicates that the intraparticle diffusion model is the best one in describing the overall adsorption kinetics mechanism of phenol and reactive dyes on the produced activated carbon.

Figs. 5.2.15 − 5.2.18 typically illustrate the comparison between the calculated and the measured results for adsorption of phenol and red31. From Fig.5.2.15, it is found that pseudo − first − order model underestimates the result at the final stage of adsorption, but pseudo − second − order model overestimates the result at the intermediate stage of adsorption. Form Fig. 5.2.16, it is found that both pseudo − first − order and pseudo − second − order models overestimate the result at the intermediate stage of adsorption. Similarly from Figs. 5.2.17 − 5.2.18, it is found that both pseudo − first − order and pseudo − second − order models overestimate the result at the intermediate stage of adsorption. The experimental results indicate that the adsorption rate is very fast at the beginning stage of adsorption.

Table 5.2.4 Kinetic parameters and normalized standard deviation for adsorption of phenol and red31 on activated carbon prepared from waste tires

Solute	C_0 (mg/l)	Pseudo − first − order		Pseudo − second − order		Intraparticle diffusion	
		k_f (cm^3/min)	Δq%	k_s (g / mg min)	Δq%	k_i (mg / (g $min^{0.5}$))	Δq%
Phenol	85.31	83.00 x10^{-3}	32.93	39.90 x10^{-5}	13.99	11.07	5.60
	200.63	10.10 x10^{-3}	27.45	7.30 x10^{-5}	13.85	24.03	12.54
	559.34	7.37 x10^{-3}	52.52	11.70 x10^{-5}	10.08	54.40	4.41
Red31	98.84	0.23 x10^{-3}	68.02	1.47 x10^{-5}	35.35	1.28	16.66
	326.32	2.30 x10^{-3}	28.47	3.33 x10^{-5}	24.07	5.37	4.61
	460.14	7.37 x10^{-3}	27.69	15.40 x10^{-5}	17.21	10.81	6.59

Table 5.2.5 Kinetic parameters and normalized standard deviation for adsorption of phenol and red31 on commercial activated carbon

Solute	C_0 (mg/l)	Pseudo − first − order		Pseudo − second − order		Intraparticle diffusion	
		k_f (cm^3/min)	Δq%	k_s (g / mg min)	Δq%	k_i (mg / (g $min^{0.5}$))	Δq%
Phenol	76.32	1.27 x10^{-3}	32.93	2.11 x10^{-5}	38.75	4.48	21.39
	211.93	1.40 x10^{-3}	27.45	2.59 x10^{-5}	6.39	21.64	6.28
	527.19	1.23 x10^{-3}	52.52	1.63 x10^{-5}	9.48	41.61	4.41
Red31	108.45	0.32 x10^{-3}	69.79	1.36 x10^{-5}	26.66	1.18	7.26
	314.57	0.28 x10^{-3}	56.47	1.41 x10^{-5}	25.93	3.48	5.30
	504.67	0.55 x10^{-3}	22.76	1.21 x10^{-5}	12.27	6.76	10.22

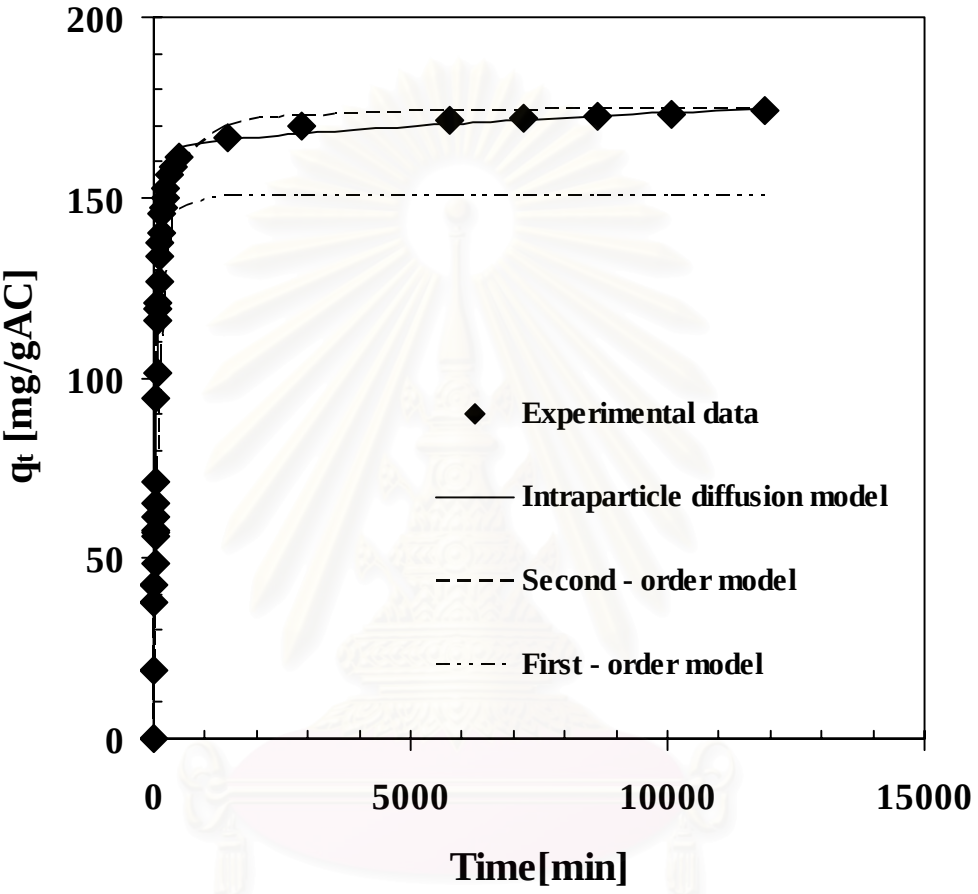

Figure 5.2.15 Plot of between the measured and modeled time profiles for adsorption of phenol on the activated carbon produced from waste tires at C_0 = 85 mg/l

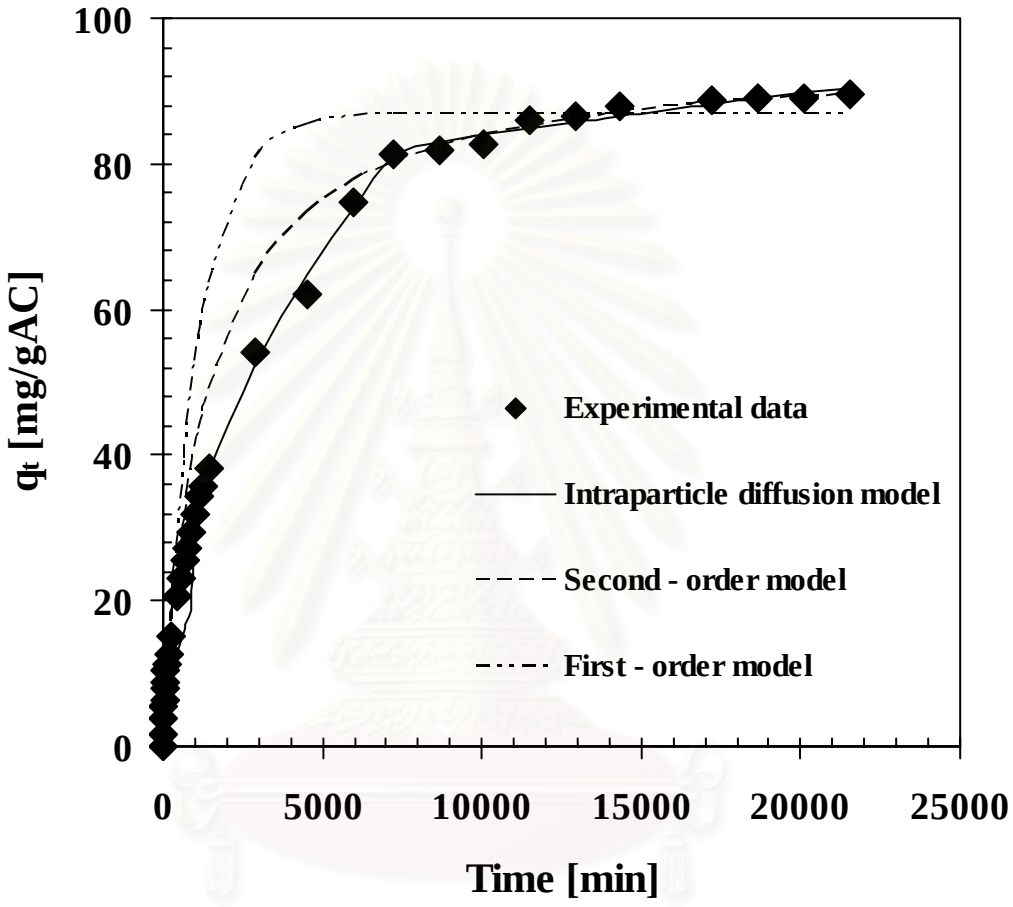

Figure 5.2.16 Plot of between the measured and modeled time profiles for adsorption of red31 on the activated carbon produced from waste tires at C_0 = 98 mg/l

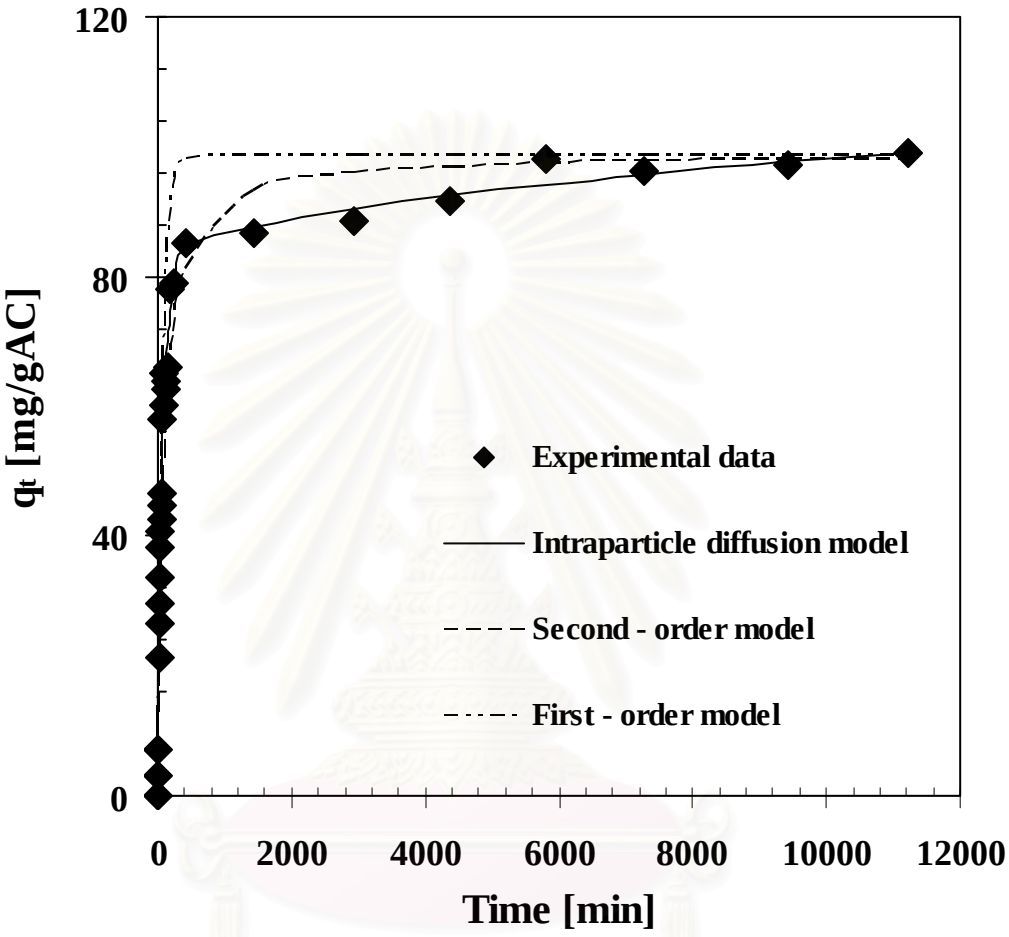

Figure 5.2.17 Plot of between the measured and modeled time profiles for adsorption of phenol on the commercial activated carbon at C_0 = 76 mg/l

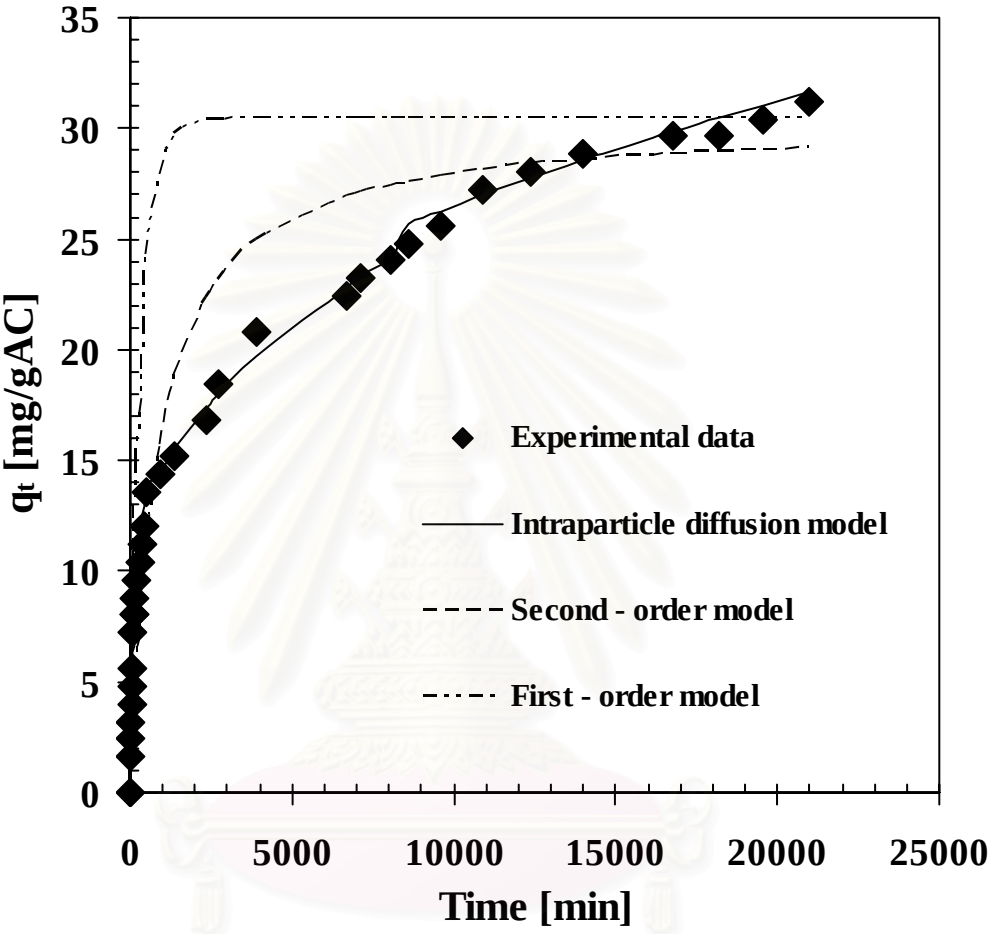

Figure 5.2.18 Plot of between the measured and modeled time profiles for adsorption of red31 on the commercial activated carbon at C_0 = 108 mg/l

Figs. 5.2.19 − 5.2.22 present a multi − linearity, implying that two adsorption steps occur. As for the physical meaning, at the beginning, phenol and red31 are adsorbed by the completely vacant surface adjacent to the outer surface of the activated carbon, so the adsorption rate is quite fast. When the adsorption on the said surface approaches saturation, the adsorbate molecules have to penetrate deep into the activated carbon particle before being adsorbed by the innermost surface. As the adsorbate molecules diffuse through the pores, its concentration decreases, the diffusion rate becomes slower and slower until the diffusion process reduces to zero at global equilibrium.

Table 5.2.6 summarizes the values of the diffusivity (D) of the solute estimated from the relevant figures based on the intraparticle diffusion model. The causes of the relatively large discrepancies between these values and those given in table 5.2.3, which shows values smaller by 1 to 2 orders of magnitude for AC_Tire and by 0 to 1 order of magnitude for AC_COM, are as follows:

- The present intraparticle diffusion model arbitrarily divide the q_t versus time curves into two stages in order to get a better fit to the measured results
- The values in table 5.2.6 are estimated using the high initial adsorption rates, thereby overestimating the diffusivity.
- AC_Tire has a large mesopore volume. In the initial stage most diffusion occurs in the mesopore and only some diffusion occurs in the micropores. Thus the resulting much higher initial rate gives a grossly overestimated value of the diffusivity. In contrast, AC_COM has only a small mesopore volume. Therefore, diffusion in the initial period

occurs mostly in the micropores, and the problem of overestimation is less severe.

Table 5.2.6 Diffusivity phenol and red31 calculated from Eq. 5.2.9

Adsorbent	Adsorbate	Initial concentration (mg/l)	D (cm^2/s)
AC_Tire	Phenol	85.31	3.52×10^{-15}
		200.63	1.44×10^{-14}
		559.34	7.40×10^{-14}
	Red31	98.84	4.12×10^{-17}
		326.32	7.22×10^{-16}
		460.14	2.92×10^{-15}
AC_COM	Phenol	76.32	2.00×10^{-17}
		211.93	4.68×10^{-16}
		527.19	1.73×10^{-15}
	Red31	108.45	1.39×10^{-18}
		314.57	1.21×10^{-17}
		504.66	4.57×10^{-17}

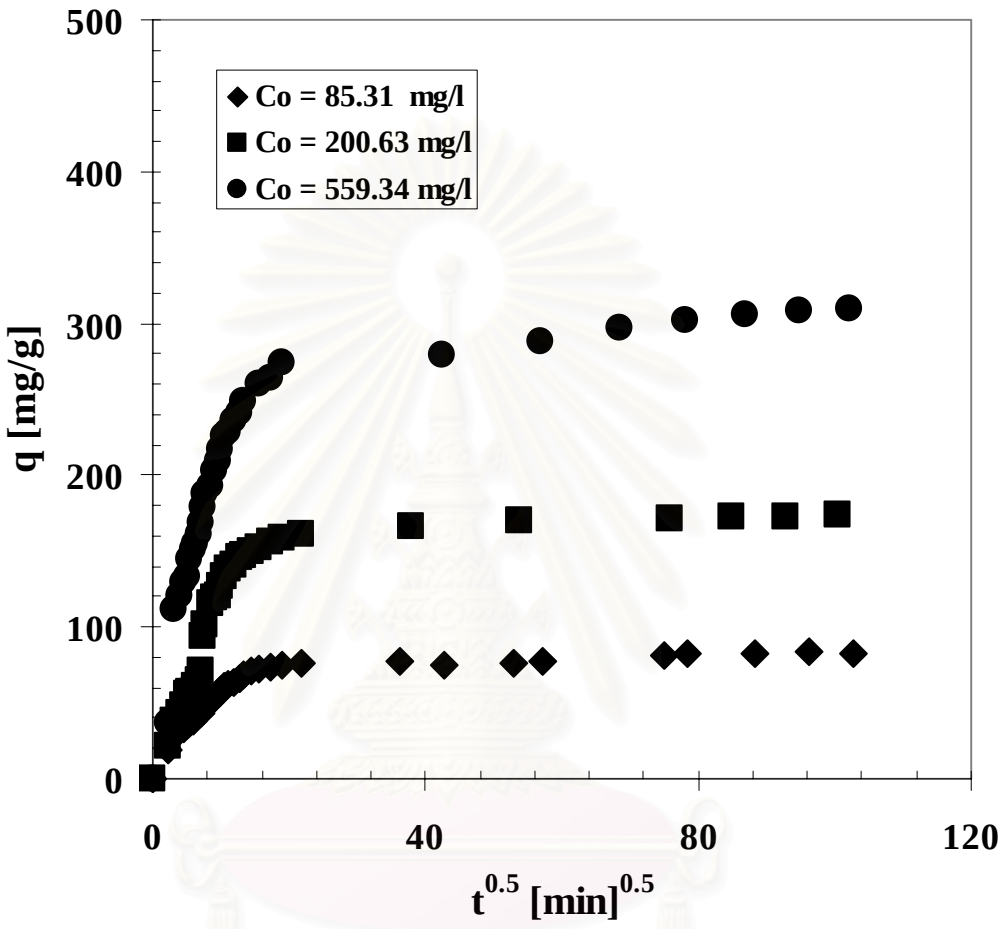

Figure 5.2.19 Plot of q vs. $t^{0.5}$ at different phenol concentration

Activated carbon prepared from waste tires

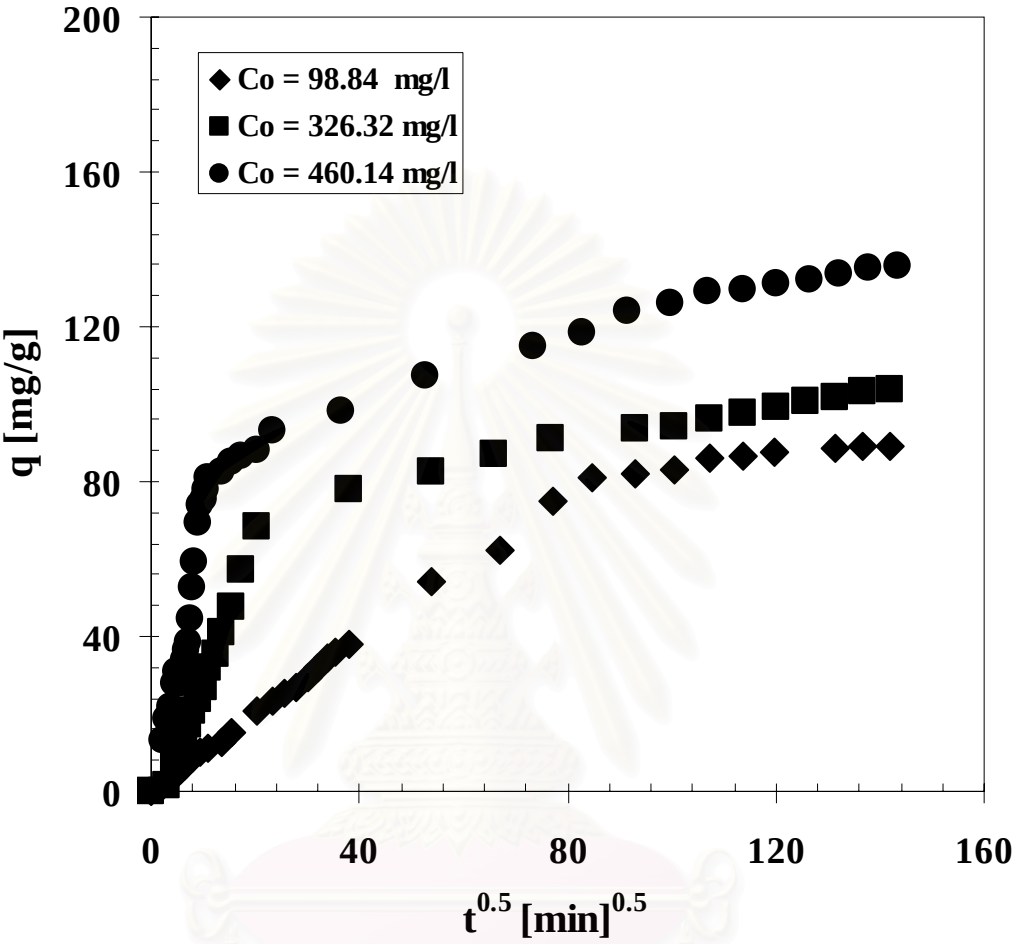

Figure 5.2.20 Plot of q vs. $t^{0.5}$ at different red31 concentration

Activated prepared from waste tires

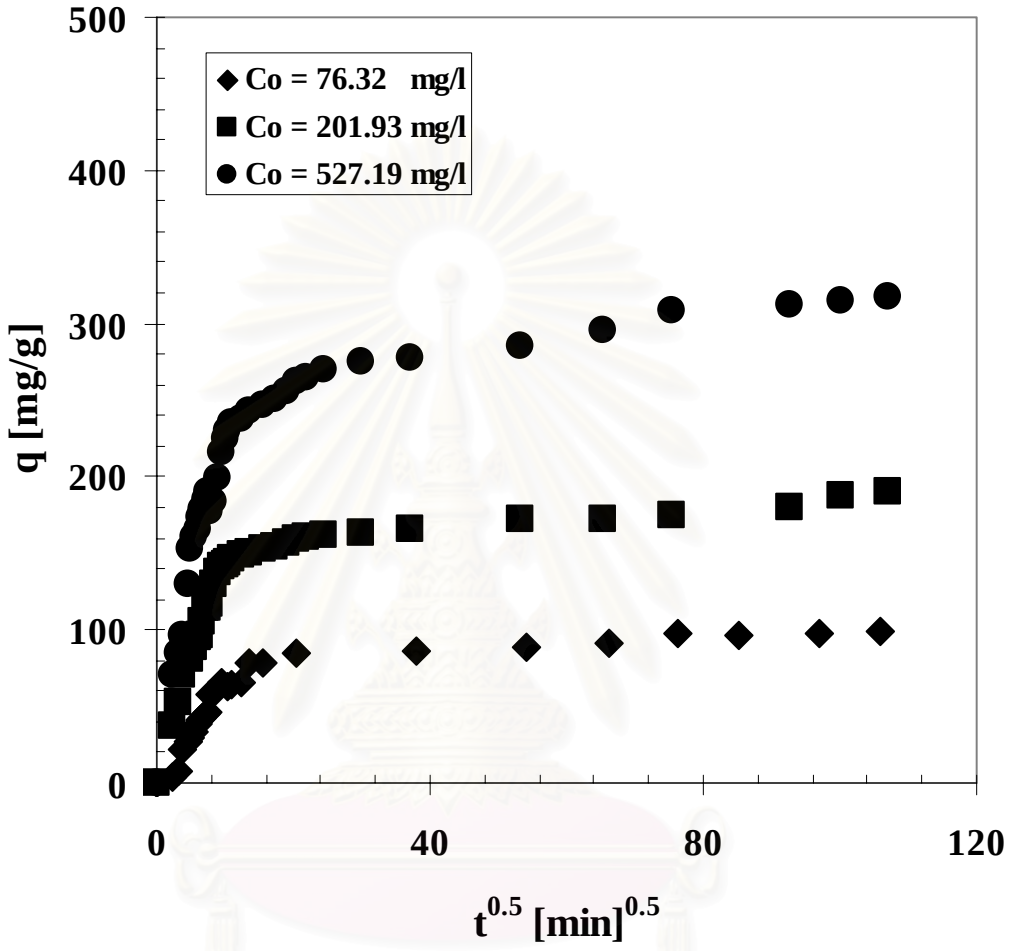

Figure 5.2.21 Plot of q vs. $t^{0.5}$ at different phenol concentration

Commercial activated carbon

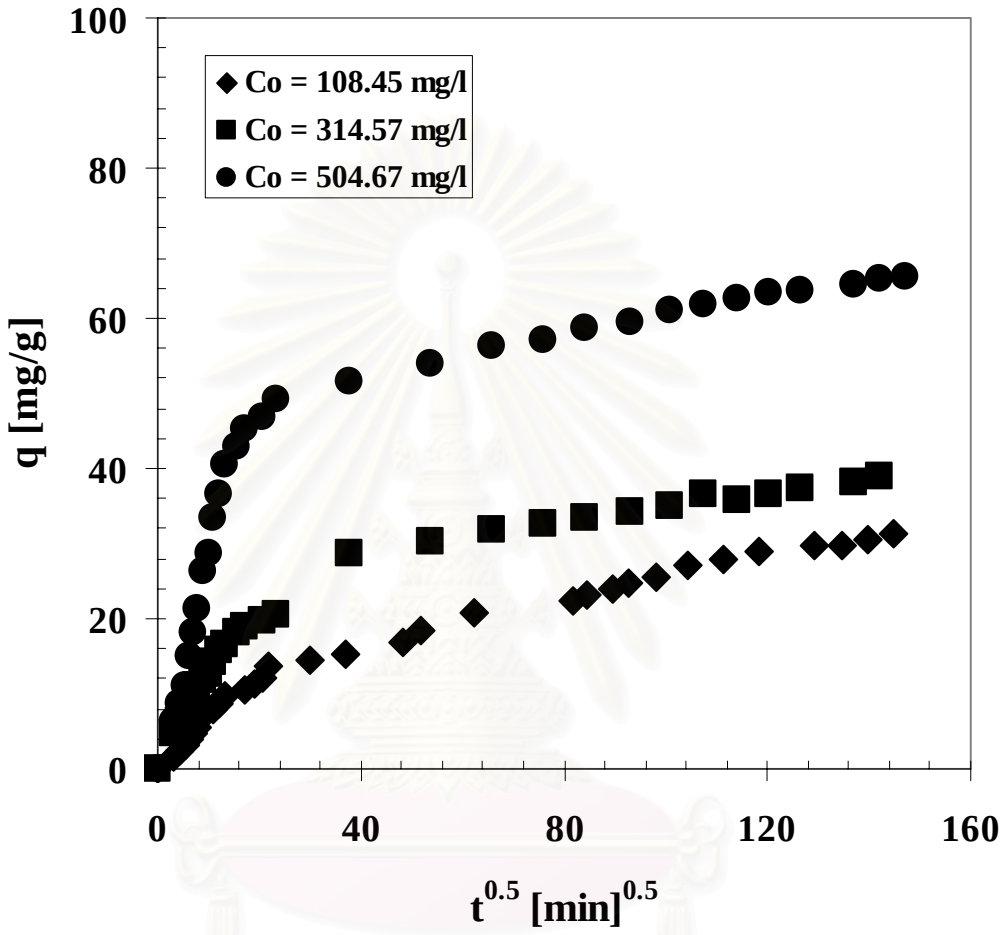

Figure 5.2.22 Plot of q vs. $t^{0.5}$ at different red31concentration

Commercial activated carbon

5.3 Competitive adsorption equilibrium and kinetics of phenol and red31

5.3.1 Competitive adsorption on mesoporous activated carbon produced from waste tires (AC_Tire)

Figs. 5.3.1 − 5.3.2 illustrate the simultaneous adsorption isotherms of phenol and red31 on the produced activated carbon (AC_Tire). Here q_1 and C_1 are the amount of phenol adsorbed and phenol equilibrium concentration, respectively. Similarly, the q_2 and C_2 are the amount of red31 adsorbed and red31 equilibrium concentration, respectively. Simultaneous adsorption equilibrium on AC_Tire shows a significant reduction in the adsorption capacity for phenol but yields a small decrease in red31 adsorption capacity. Interestingly, the experimental result from simultaneous adsorption kinetics as presented in Fig. 5.3.3 illustrates that, being the faster diffusing species, phenol is adsorbed initially to a concentration level exceeding its final equilibrium. Then phenol gradually desorbs to reach the equilibrium level as the slower diffusing species, red31 slowly penetrates and replaces some of the phenol until red31 attains its equilibrium. Fig. 5.3.4 illustrates the big reduction of phenol adsorption capacity caused by red31 preloading. Since larger and heavier red31 molecules are adsorbed on the mesopores in advance, they are difficult to be dislodged by phenol, thereby reducing the adsorption of phenol molecules.

Red31 adsorption capacity and rate are reduced because preloaded phenol molecules fill both micropores and mesopores as shown in Fig. 5.3.5. Taking account of the observed pore size distribution, and phenol − red31 adsorption characteristics, the phenol adsorption capacity reduction is considered to be due to micropore blockage, whereas the slight decrease in the rate of phenol adsorption is probably due to hindered diffusion. Since red31 is unable to dislodge and replace phenol molecules

adsorbed on both the micropore and the mesopore, this results in a decrease in its adsorption capacity and rate.

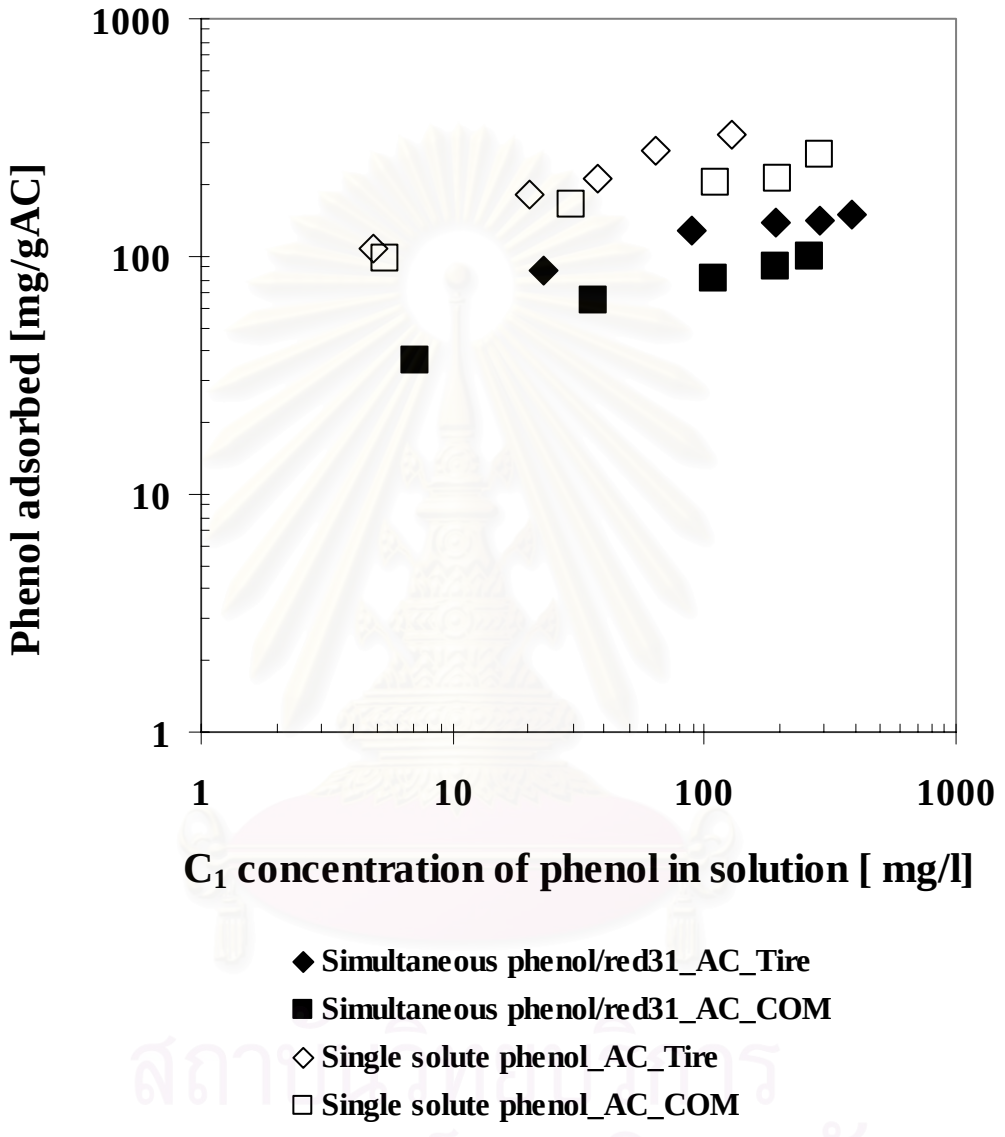

Figure 5.3.1 Effect of simultaneous adsorption on phenol adsorption capacity on activated carbon prepared from waste tires and commercial activated carbon

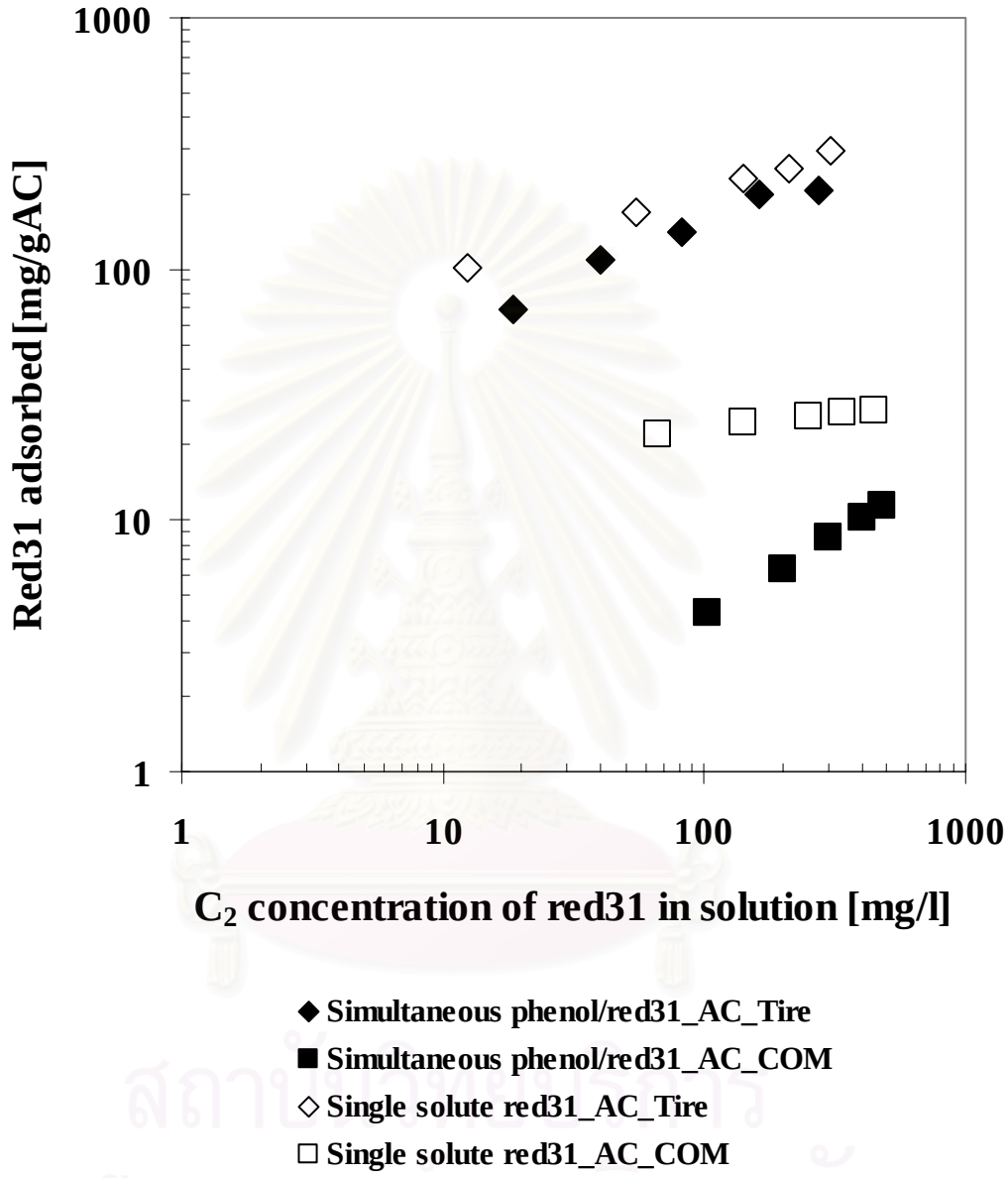

Figure 5.3.2 Effect of simultaneous adsorption on red31 adsorption capacity on activated carbon prepared from waste tires and commercial activated carbon

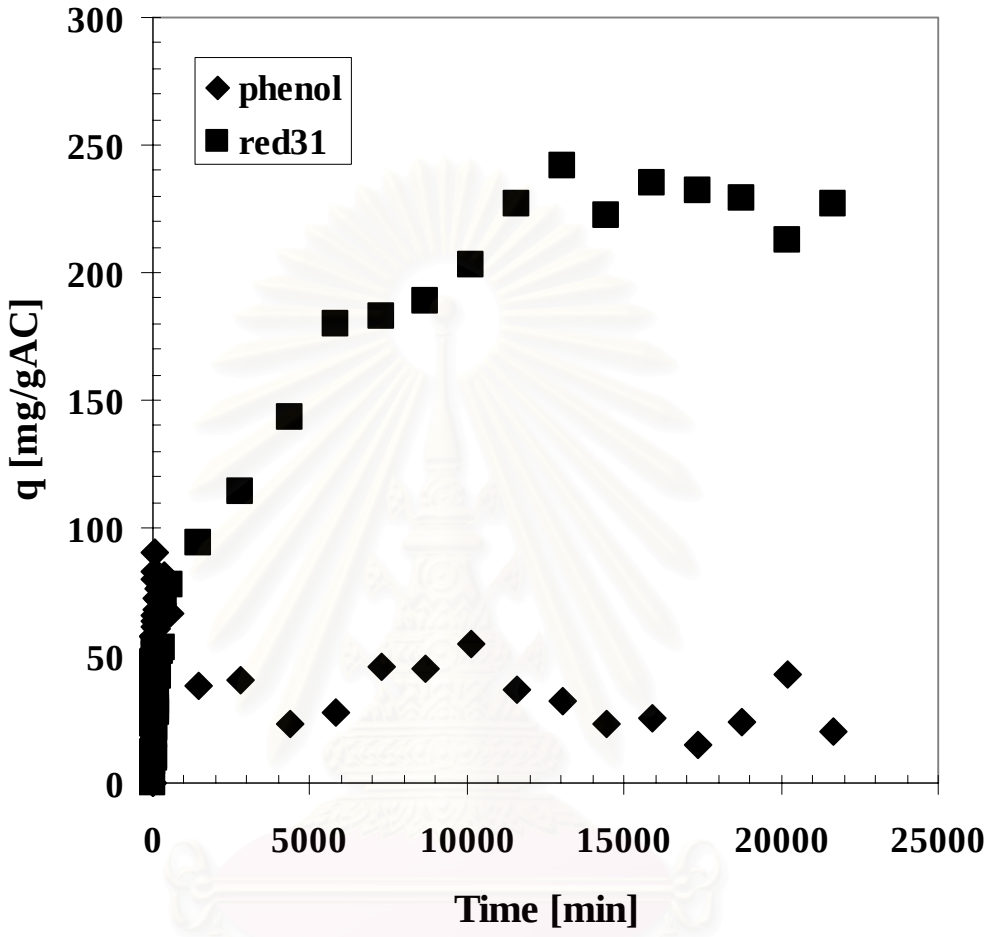

Figure 5.3.3 Simultaneous adsorption kinetics of phenol and red31 adsorbed onto activated carbon prepared from waste tires:

C_{0_phenol} = 287 mg/l, C_{0_red31} = 484 mg/l

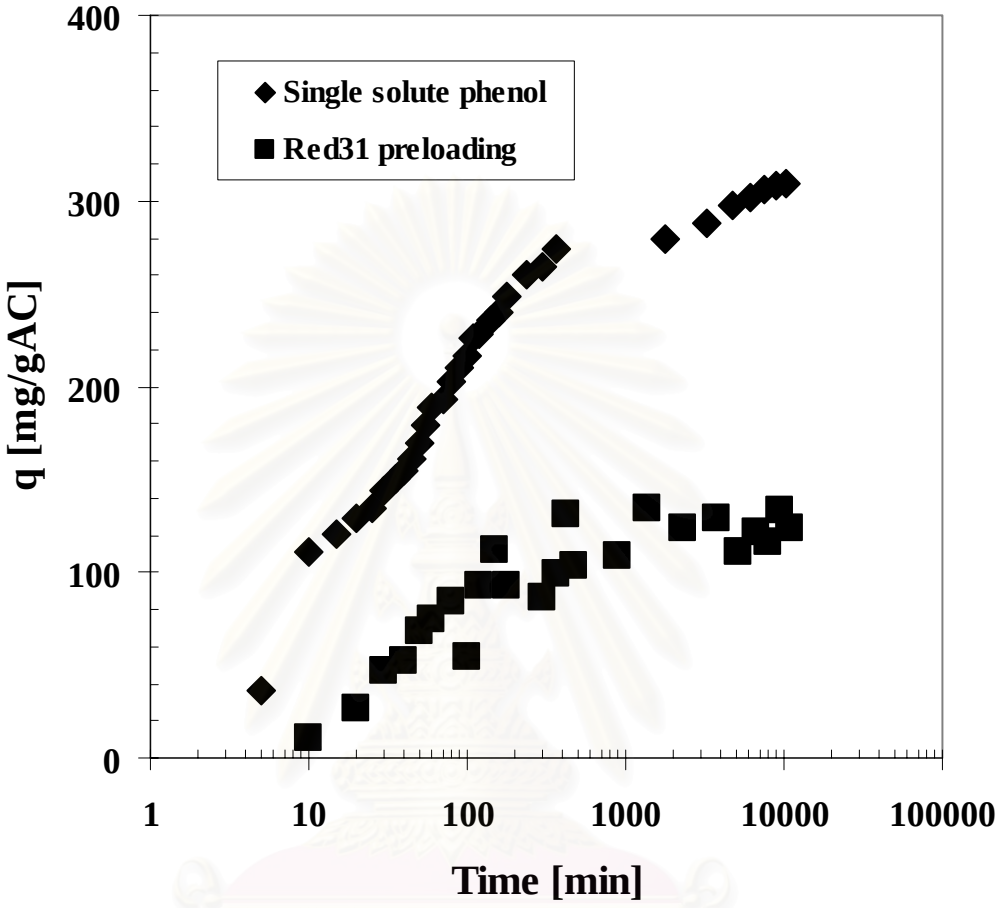

Figure 5.3.4 Comparison of adsorption kinetic of single solute phenol with adsorption kinetic of phenol with red31 preloaded onto the activated carbon produced from waste tires; C_{0_phenol} = 559 mg/l, C_{0_red31} = 518 mg/l

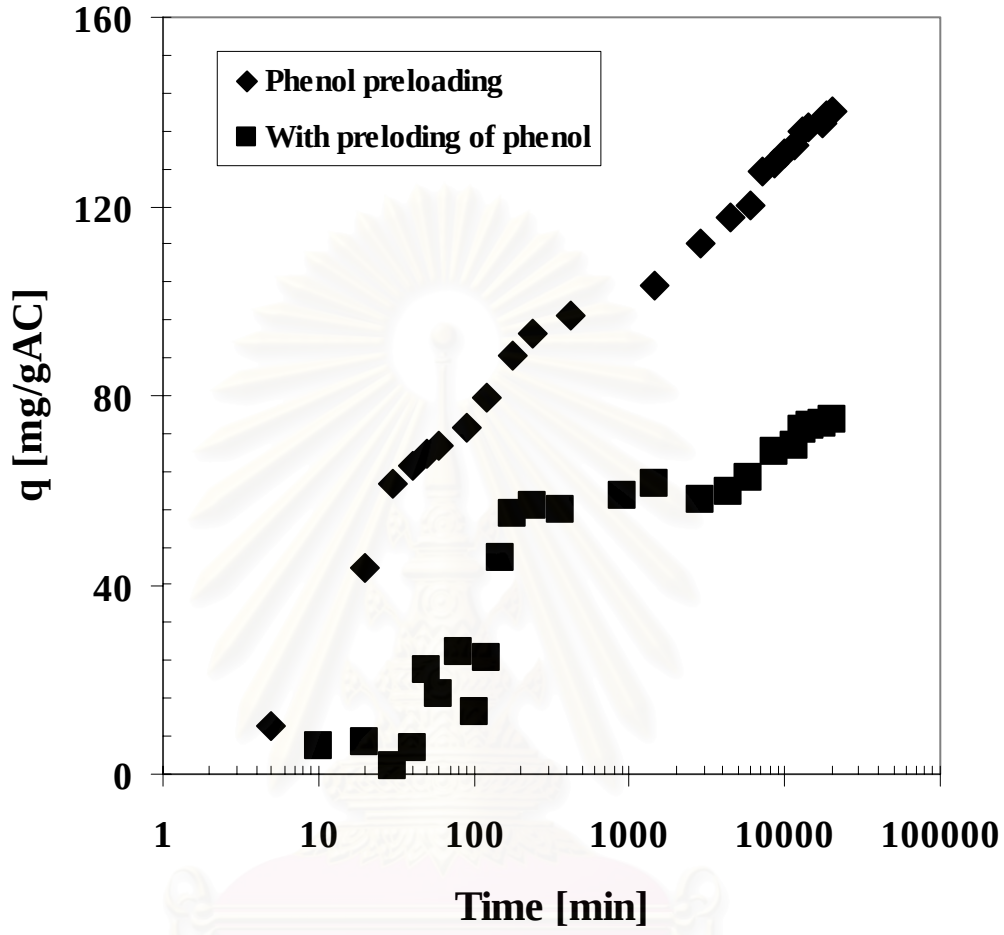

Figure 5.3.5 Comparison of adsorption kinetic of single solute red31 with adsorption kinetic of red31 with phenol preloaded onto the activated carbon produced from waste tires: C_{0_phenol} = 514 mg/l, C_{0_red31} = 505 mg/l

5.3.2 Competitive adsorption on microporous activated carbon (AC_COM)

Simultaneous adsorption equilibrium on AC_COM exhibits a great reduction in the adsorption capacity of phenol and red31 adsorption capacity as shown in Figs. 5.3.1 − 5.3.2. The simultaneous adsorption kinetic data shown in Fig. 5.3.6 is contrary to the results obtained with AC_Tire. Phenol and red31 molecules appear to adsorb separately in the micropores and mesopores, respectively, until attaining their equilibria. Red31 preloading has less significant effect on phenol adsorption rate because phenol molecules diffuse through the mesopores to the micropores faster than red31 molecules, as shown in Fig. 5.3.7. The reduction in phenol adsorption capacity is considered to be caused by coadsorption and micropore blockage. Obviously some mesopores are just large enough to admit the red31 molecules, thereby resulting in hindrance of some late − arriving phenol molecules. The reduction in red31 adsorption capacity may be attributed to the fact that parts of the available mesopores are occupied by phenol molecules as seen in Fig. 5.3.8.

In conclusion, the different results in competitive and simultaneous adsorption kinetics between AC_Tire and AC_COM may be ascribed to the distinctive difference in their pore size distributions and pore structures. The exterior surfaces of both adsorbents are characterized with scanning electron microscopy (SEM) as shown in Fig. 5.3.9 − 5.3.10. The surface of AC_Tire seems to result from the loose agglomeration of small particles. Both, macropores and mesopores can be observed in this figure. In contrast, the surface of AC_COM appears quite smooth with fewer opening of macropores and mesopores. Based upon the SEM images and binary adsorption and kinetics data, it is reasonable to consider that the pore structure of AC_Tire is a branched tree − like pore structure, with many micropores branching off from mesopores as shown in Fig. 5.3.6 (a). In contrast, the pore structure of

AC_COM may be considered to consist of many independent micropores not necessarily connected to the mesopores as shown in Fig. 5.3.6 (b).

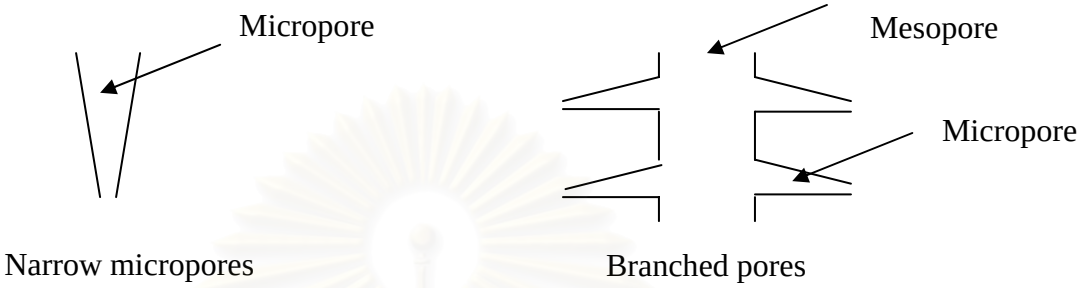

a) AC_COM **b) AC_Tire**

Figure 5.3.6 Proposed pore structure of both activated carbons

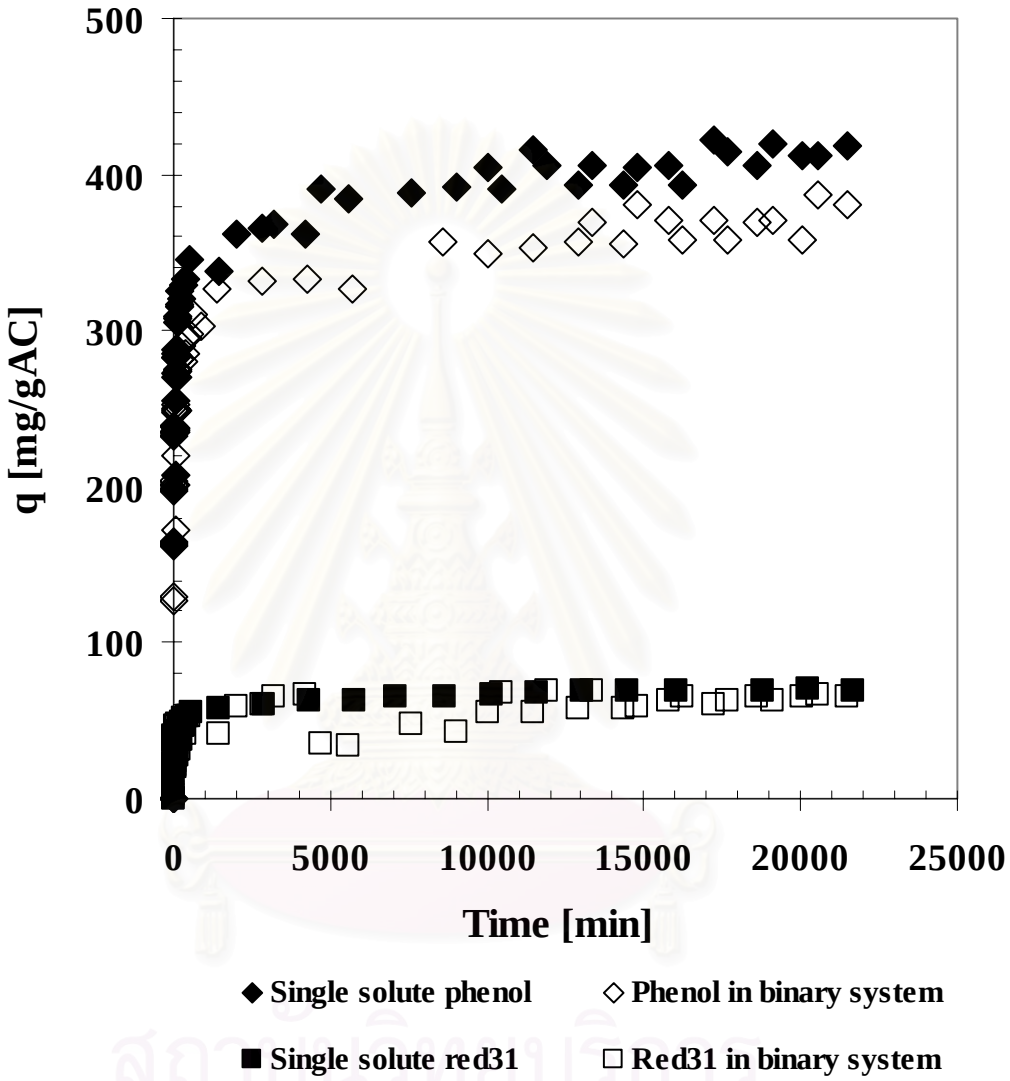

Figure 5.3.7 Simultaneous adsorption kinetics of phenol and red31 adsorbed onto commercial activated carbon

Single system: C_{0_phenol} =306 mg/l, C_{0_red31} = 504 mg/l

Simultaneous system: C_{0_phenol} =316 mg/l, C_{0_red31} = 529 mg/l

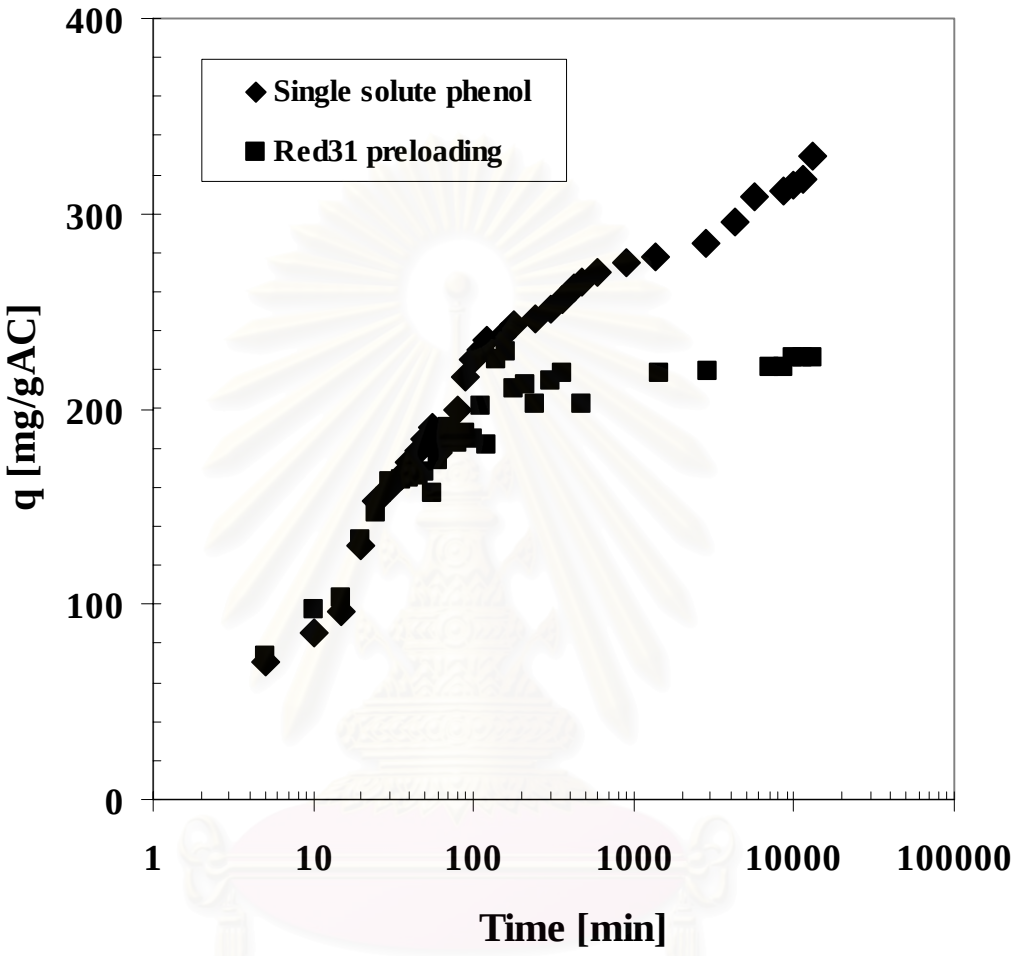

Figure 5.3.8 Comparison of adsorption kinetic of single solute phenol with adsorption kinetic phenol in red31 preloading onto commercial activated carbon: C_{0_phenol} = 527 mg/l, $C_{0\ \_red31}$ = 499 mg/l

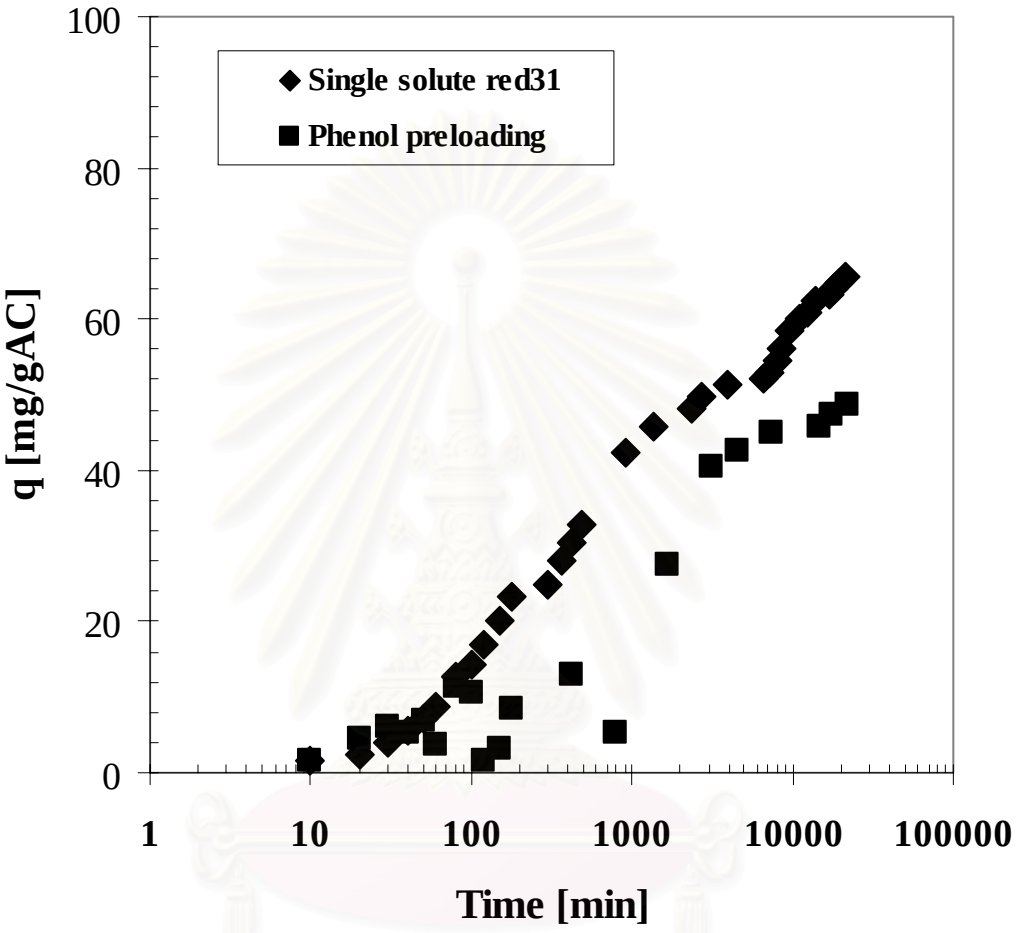

Figure 5.3.9 Comparison of adsorption kinetic of single solute red31 with adsorption kinetic of red31 in phenol preloading onto commercial activated carbon: C_{0_phenol} = 535 mg/l, $C_{0\ \_red31}$ = 505 mg/l

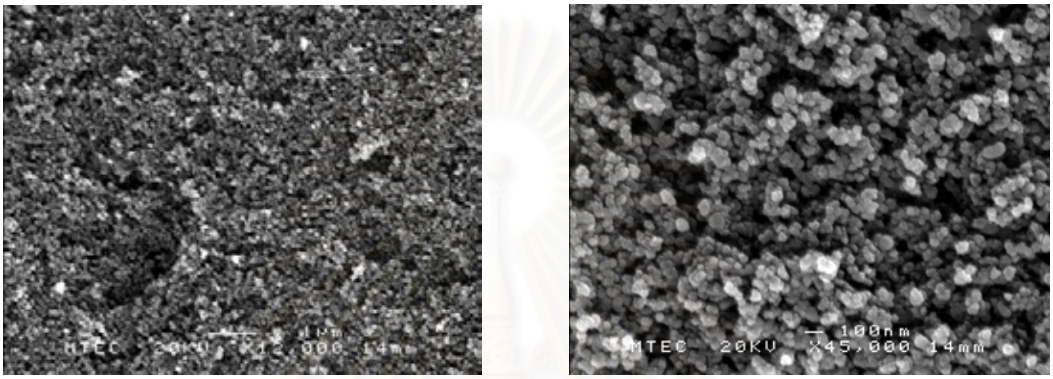

Figure 5.3.10 SEM images of the activated carbon prepared from waste tires at magnification power of 12,000 and 45,000, respectively

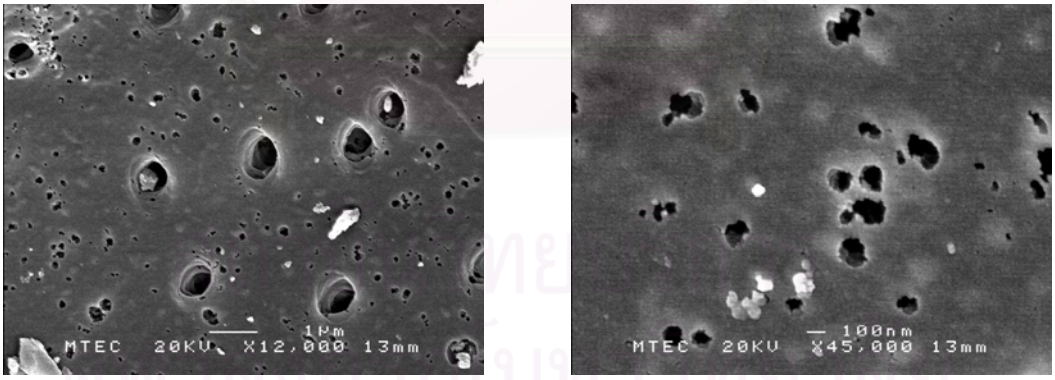

Figure 5.3.11 SEM images of the commercial activated carbon at magnification power of 12,000 and 45,000, respectively

CHAPTER VI

CONCLUSION AND FUTURE WORK

6.1 Conclusion

The adsorption equilibrium and kinetics of phenol and Red 31 adsorbed onto highly mesoporous and microporous activated carbons, namely, AC_Tire and AC_COM, respectively, are investigated in batch experimental system. The conclusions for all experimental systems are summarized as follows:

6.1.1 Single adsorption equilibrium and kinetics

Freundlich and Langmuir models exhibit the best fit to the individual adsorption equilibriums of phenol and Red 31 adsorbed onto AC_Tire and AC_COM, respectively. In addition, as the average pore size and total mesopore volume increase, there is a consistent increase in either phenol or Red 31 adsorption capacity. The film- pore diffusion model is not suitable to fit the concentration decay curves of phenol and Red 31 adsorbed onto either activated carbon. Pseudo- first order, pseudo- second order and intraparticle diffusion models are tested to find out the adsorption rate controlling step for either phenol or Red 31. The results indicate that the adsorption rate controlling step for both phenol and Red 31 can be described well by the intraparticle diffusion model, and the transport mechanism is mainly controlled by the Knudsen diffusion.

6.1.2 Binary adsorption equilibrium and kinetics

As expected, the porous structure of the activated carbons is found to have a significant effect to phenol and Red 31 adsorption capacity and kinetics in the binary

systems. Phenol adsorption capacity and adsorption rate is reduced by micropore blockage and hindered diffusion, respectively. Moreover, a reduction in Red 31 adsorption capacity and adsorption rate is caused by competing adsorption of phenol which rapidly fills both micropores and mesopores. The simultaneous adsorption kinetics of phenol and Red 31 adsorbed on AC_Tire is shown to be a co- diffusion phenomenon. On the other hand, simultaneous adsorption kinetics of phenol and Red 31 adsorbed on AC_COM take place separately on each suitable pore size.

6.2 Future work

- To study the adsorption in the column bed
- To study the desorption rate of various the adsorbates on activated carbon from waste tires
- To study the regeneration of a spent activated carbon
- To study the effect of temperature on Knudsen diffusivity

REFFERENCES

[1] D. M. Ruthven. Principles of adsorption and adsorption processes. New York: John Wiley, 1984.

[2] C. Tien. Adsorption calculations and modeling. Boston: Butterworth-Huinemann, 1994.

[3] C.W. Cheung, C.K. Chan, J.F. Porter and G. McKay. Film- pore diffusion control for the batch sorption of cadmium ions from effluent onto bone char. Journal of Colloid and Interface Science. 234 (2001): 328-336.

[4] N.K. Hamadi, X.D. Chen, M.M. Farid and Max G.Q. Lu. Adsorption kinetics for the removal of chromium (VI) from aqueous solution by adsorbents derived from used tyres and sawdust. Chemical Engineering Journal. 84 (2001): 95-105.

[5] J.R. Evans, W.G. Davids, J. D. MacRae and A. Amirbahman. Kinetics of cadmium uptake by chitosan-based crab shells. Water Research. 36 (2002): 3219-3226.

[6] G. M. Barrow. Physical chemistry. New York: McGraw – Hill, 1966, pp. 42-43.

[7] Q.Sun and L. Yang. The adsorption of basic dyes from aqueous solution on modified peat- resin particle. Water Research. 37 (2003): 1535-1544.

[8] L. Li, P.A. Quinlivan and R.U. Knappe. Effects of activated carbon surface chemistry and pore structure on the adsorption of organic contaminants from aqueous solution. Carbon. 40 (2002): 2085-2100.

[9] P. Ariyadejwanich, W. Tanthapanichakoon, K. Nakagawa, S.R. Mukai, and H. Tamon. Preparation and characterization of mesoporous activated carbon from waste tires. Carbon. 41 (2003): 157-164.

[10] B. Buczek. A. Swiatkowski, J. Goworek. Adsorption from binary liquid mixtures on commercial activated carbons. Carbon. 33 (1995): 129-134.

[11] G.M. Walker and L.R. Weatherley. Adsorption of dyes from aqueous solution- the effect of adsorbent pore size distribution and dye aggregation. Chemical Engineering Journal. 83 (2001): 201-206.

[12] Y. Onganer, and C. Temur. Adsorption dynamics of Fe (III) from aqueous solutions onto activated carbon. Journal of Colloid and Interface Science. 205 (1998): 241-244.

[13] Chien-To Hsieh and H.Teng. Liquid-Phase Adsorption of Phenol onto Activated Carbons Prepared with Different Activation Levels. Journal of Colloid and Interface Science. 230 (2000): 171-175.

[14] C. Pelekani, and V. L. Snoeyink. A kinetic and equilibrium study of competitive adsorption between atrazine and Congo red dye on activated carbon: the importance of pore size distribution. Carbon. 39 (2001): 25-37.

[15] J.L. Sotelo, G. Ovejero, J.A. Delgado and I. Martinez. Adsorption of lindane from water onto GAC: effect of carbon loading on kinetic behavior. Chemical Engineering Journal. 87 (2002): 111-120.

[16] K.H. Choy, J.F. Porter and G. McKay. Film- pore diffusion models- analytical and numerical solutions. Chemical Engineering Science. 59 (2004): 501-512.

[17] Z. Aksu and E. Kabasakal. Batch adsorption of 2,4- dichlorophenoxy- acetic- acid (2,4-D) from aqueous solution by granular activated carbon. Separation and Purification Technology. 35 (2004) 223-240.

[18] C.F. Lorenzano-Porras, M.J. Annen, M.C. Flickinger, P.W. Carr and A.V. McCormick. Pore structure and diffusion tortuosity of porous ZrO2 synthesized by two different colloid- aggregation processes. Journal of Colloid and Interface Science. 170 (1995): 299-307.

[19] V.P. Vinod and T.S. Anirudhan. Adsorption behavior of basic dyes on the humid acid immobilized pillared clay. Water, Air, and Soil Pollution. 150 (2003): 193-217.

[20] J. Seader and M. Henley. Separation Process principles. New York: Wiley, 1998.

APPENDICES

APPENDIX A

1. Single − component adsorption kinetics of black5

The removal of black 5 by adsorption on the AC_Tires and AC_COM shows an increase with time and attains a maximum adsorption capacity at about 9360 min and 11150 min, respectively, after which the capacity remains essentially constant. Upon changing the initial concentration of black 5 absorbed on AC_Tires from 103 to 503 mg/l, the amount adsorbed at equilibrium increases from 83 to 156 mg/gAC at 30 $^{\circ}$C as shown in Fig. A − 2. Similarly, when the initial concentration of black 5 adsorbed on AC_COM is varied from 99 to 515 mg/l, the amount adsorbed at equilibrium increases from 28 to 58 mg/gAC at 30 $^{\circ}$C as shown in Fig. A − 3. To determinate the adsorption mechanism of black 5 may refer to the results of red31; therefore, it might be suggested that either the surface diffusion effects dominate the diffusion process or the application of the film − pore diffusion model is not suitable. This means that the actual transport mechanism of black 5 inside the activated carbon particles is Knudsen diffusion shown in Table A − 1.

Table A − 1 Knudsen diffusion coefficient

Adsorbate	Knudsen diffusion coefficient (cm^2/s)					
	AC_Tire			AC_COM		
	Minimum d_p (m)	Average d_p (m)	Maximum d_p (m)	Minimum d_p (m)	Average d_p (m)	Maximum d_p (m)
Black 5	2.55×10^{-6}	1.34×10^{-5}	5.37×10^{-5}	2.39×10^{-6}	2.68×10^{-6}	4.11×10^{-5}

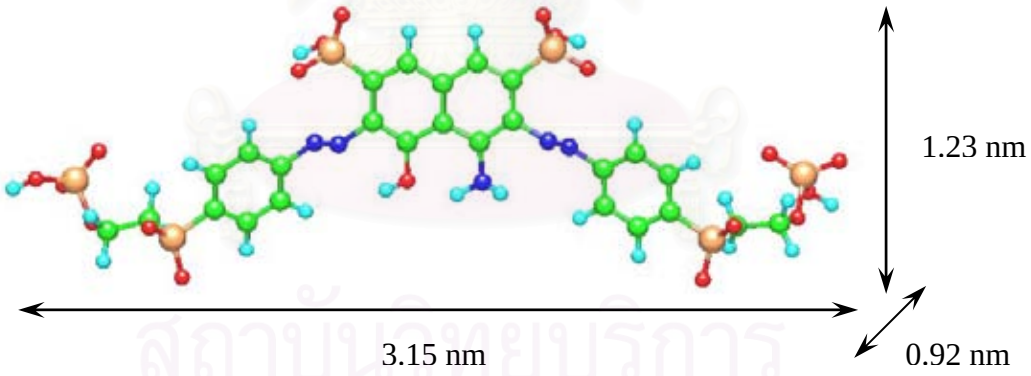

Black 5 [$C_{26}H_{21}N_5O_{19}Na_4S_6$]

Figure A − 1 Molecular dimensions and structures of Black 5

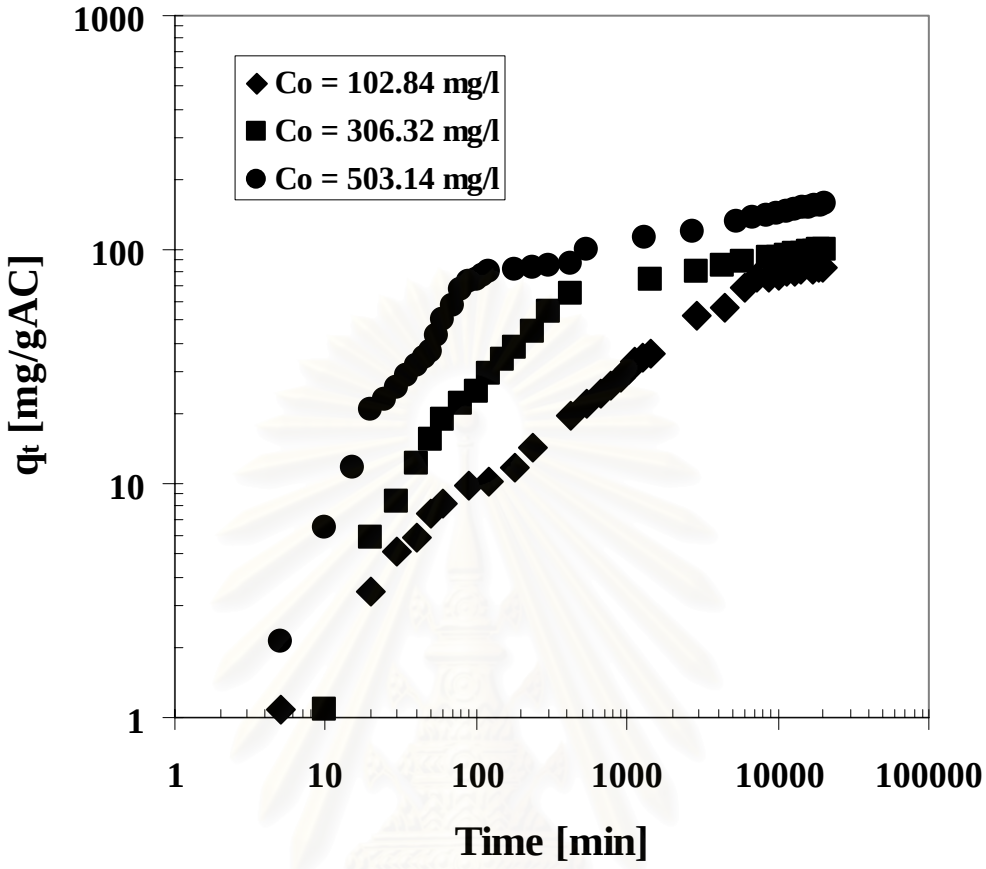

Figure A − 2 Black 5 adsorbed onto the activated carbon prepared from waste tires versus time

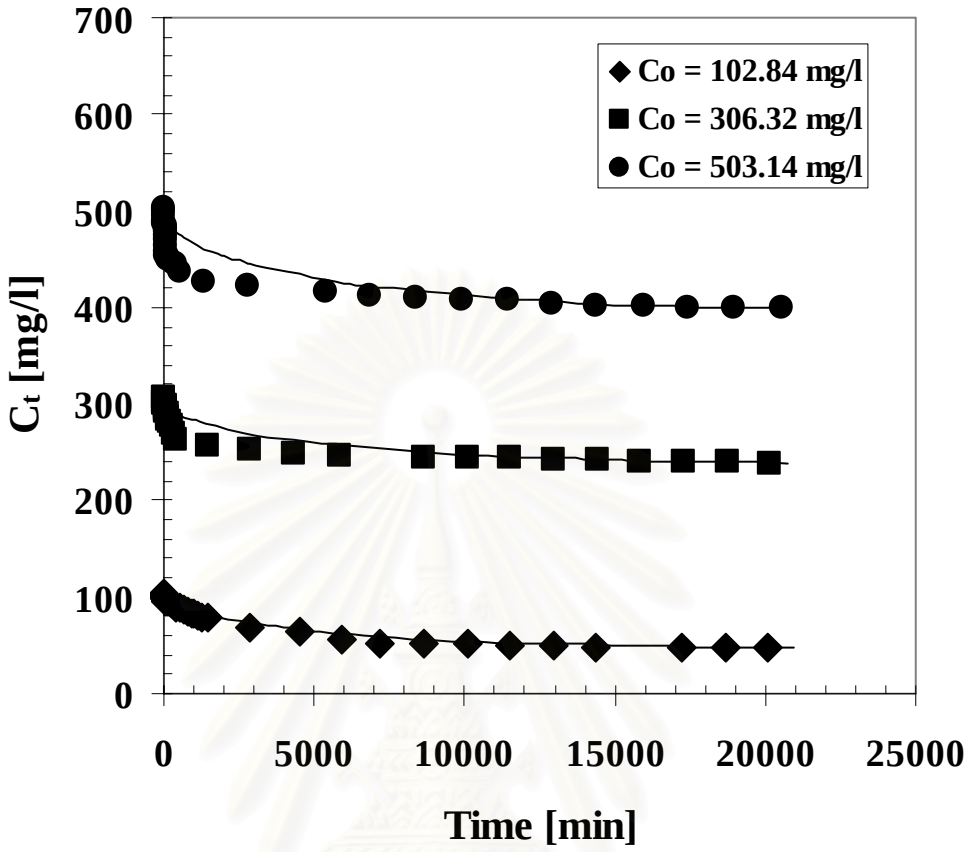

Figure A − 3 Black5 concentration decay curves for constant amount of activated carbon prepared from waste tires adsorbent: (◆▲●) experimental data, (——) model: k_f = 1.53x10^{-2} (cm/s) D_{eff} = 3.46 x 10^{-17} (cm^2/s) Particle diameter = 997.97 µm

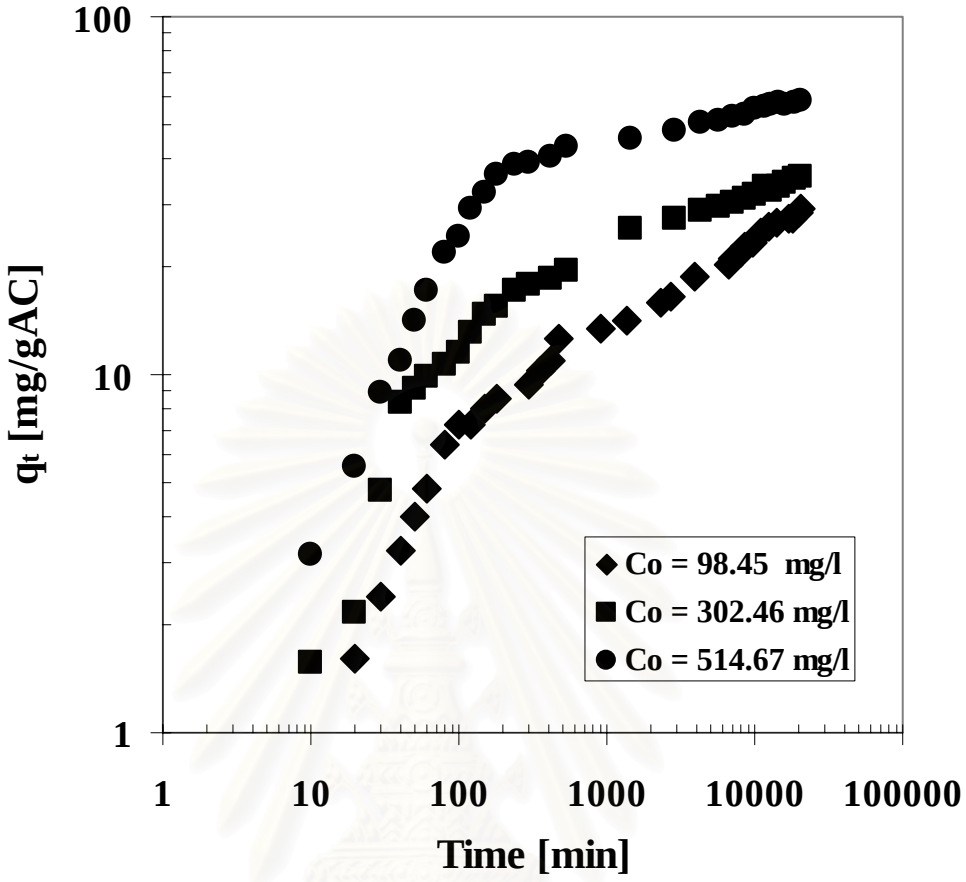

Figure A − 4 Black 5 adsorbed onto the commercial activated carbon versus time

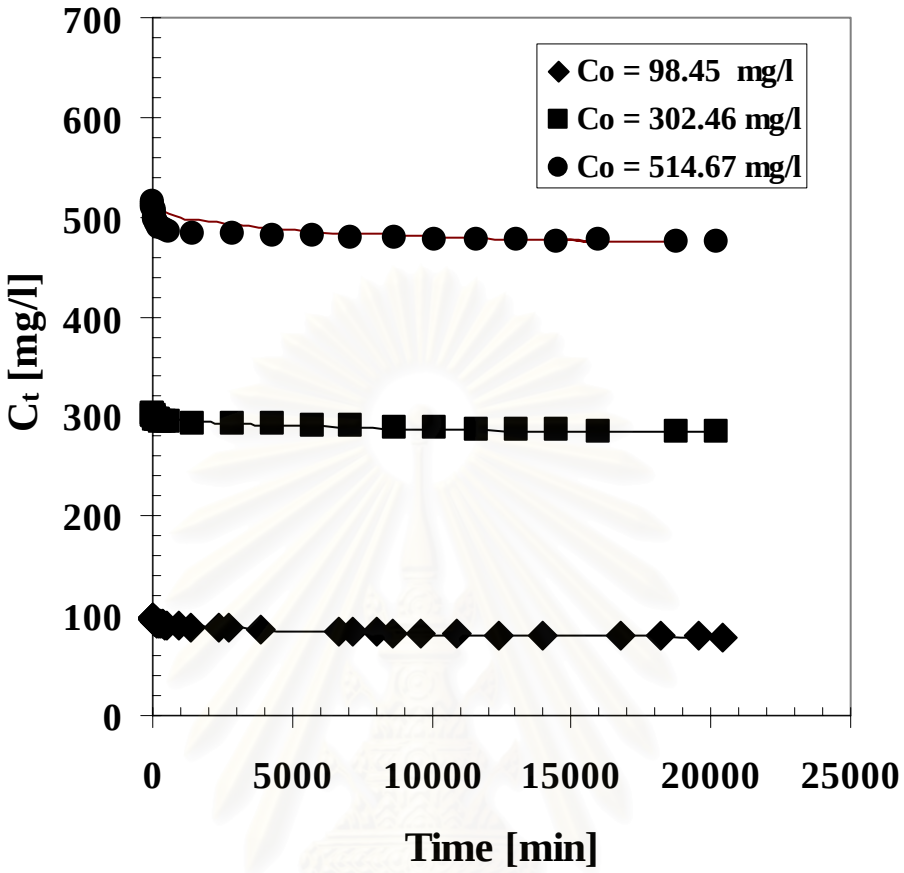

Figure A − 5 Black5 concentration decay curves for a constant amount of commercial activated carbon: (◆▲●) experimental data, (——) model : k_f = 1.40x10^{-2} (cm/s) D_p = 3.69 x 10^{-17} (cm^2/s) Particle diameter = 1470.81 µm

APPENDIX B

2. Competitive adsorption equilibrium and kinetics of phenol and black5 adsorbed on activated carbon prepared from waste tires and commercial activated carbon

Interestingly, the experimental result from simultaneous adsorption kinetics as presented in Fig. B − 1 illustrates that, being the faster diffusing species, phenol is adsorbed initially to a concentration level exceeding its final equilibrium. Then phenol gradually desorbs to reach the equilibrium level as the slower diffusing species, black5 slowly penetrates and replaces some of the phenol until red31 attains its equilibrium.

The simultaneous adsorption kinetic data shown in Fig. B − 2 is contrary to the results obtained with AC_Tire. Phenol and black5 molecules appear to adsorb separately in the micropores and mesopores, respectively, until attaining their equilibria.

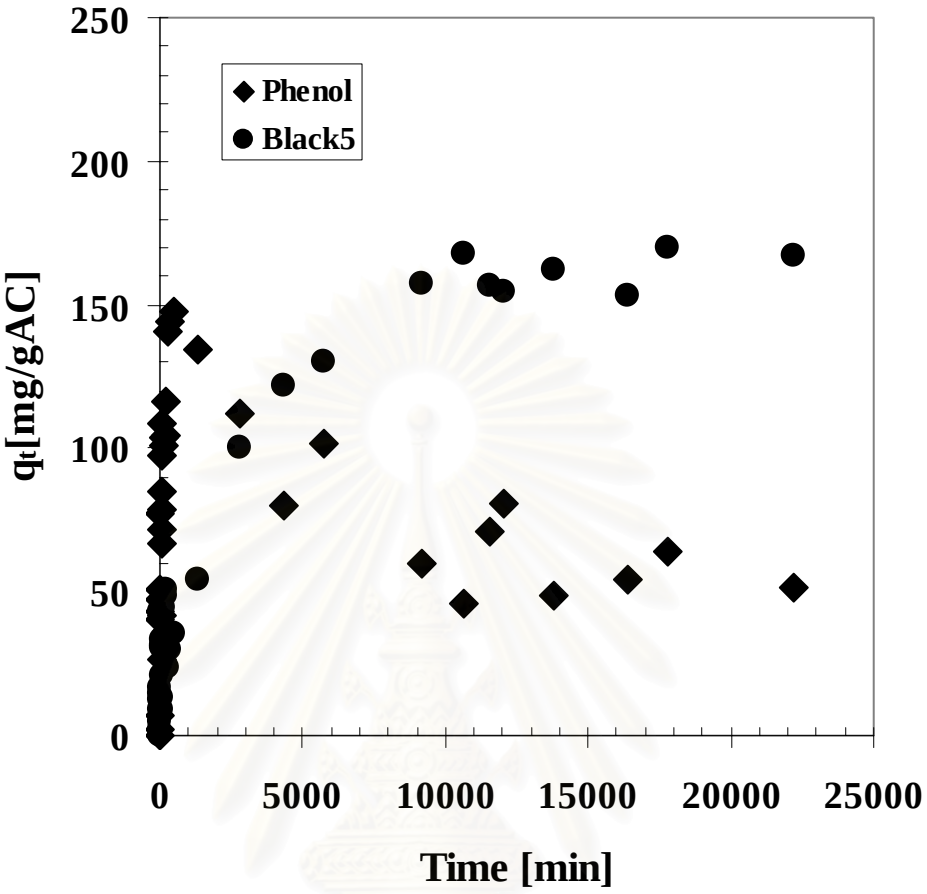

Figure B − 1 Simultaneous adsorption kinetics of phenol and black5 adsorbed onto activated carbon prepared from waste tires:

C_{0_phenol} = 318 mg/l, C_{0_red31} = 298 mg/l

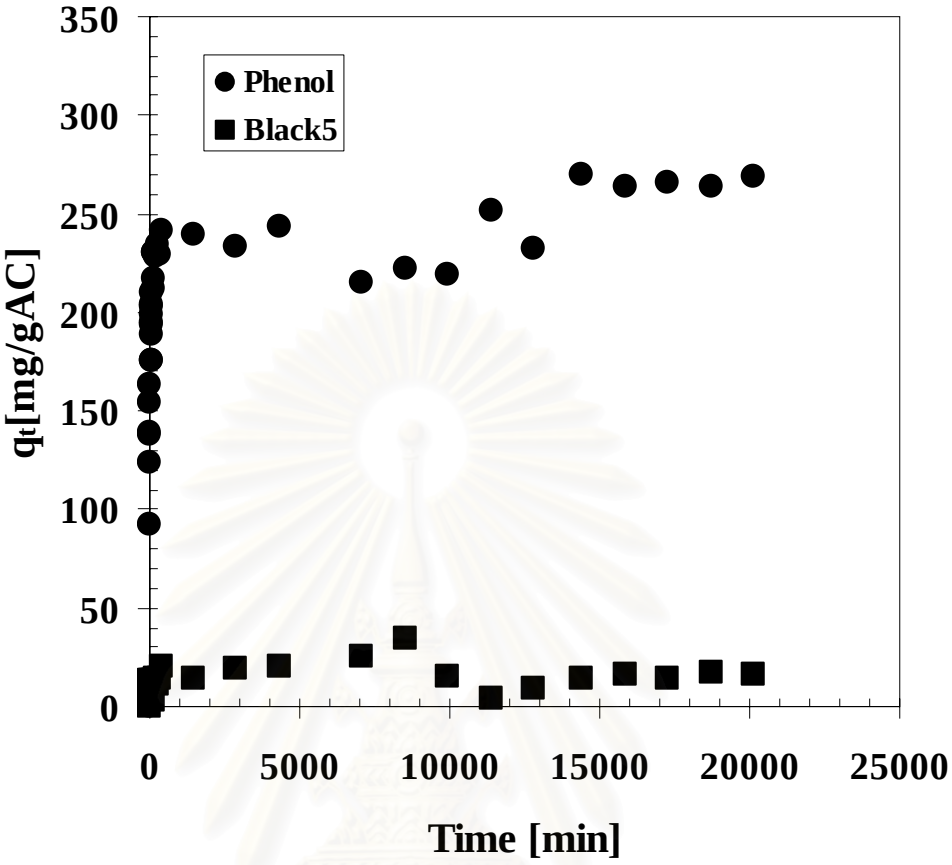

Figure B − 2 Simultaneous adsorption kinetics of phenol and black5 adsorbed onto commercial activated carbon:

C_{0_phenol} = 500 mg/l, C_{0_red31} = 293 mg/l

APPENDIX C

3. Calibration curve

Concentration of phenol and red31 at any time is calculated by converting absorbance from equation as shown in below:

- Concentration of phenol in single adsorption
  - X = (Y- 0.0162)/0.0139 at 270 nm wavelength
- Concentration of phenol in binary adsorption
  - X = (Y- 0.0118)/0.1497 at 270 nm wavelength
- Concentration of red31 in single adsorption
  - X = (Y- 0.0089)/0.0206 at 540 nm wavelength
- Concentration of red31 in binary adsorption
  - X = (Y- 0.0499)/0.0200 at 270 nm wavelength
  - X = (Y- 0.0050)/0.0213 at 540 nm wavelength

Where X = concentration (mg/l)

Y = absorbance

- Calibration curve of phenol in binary adsorption at 270 nm wavelength

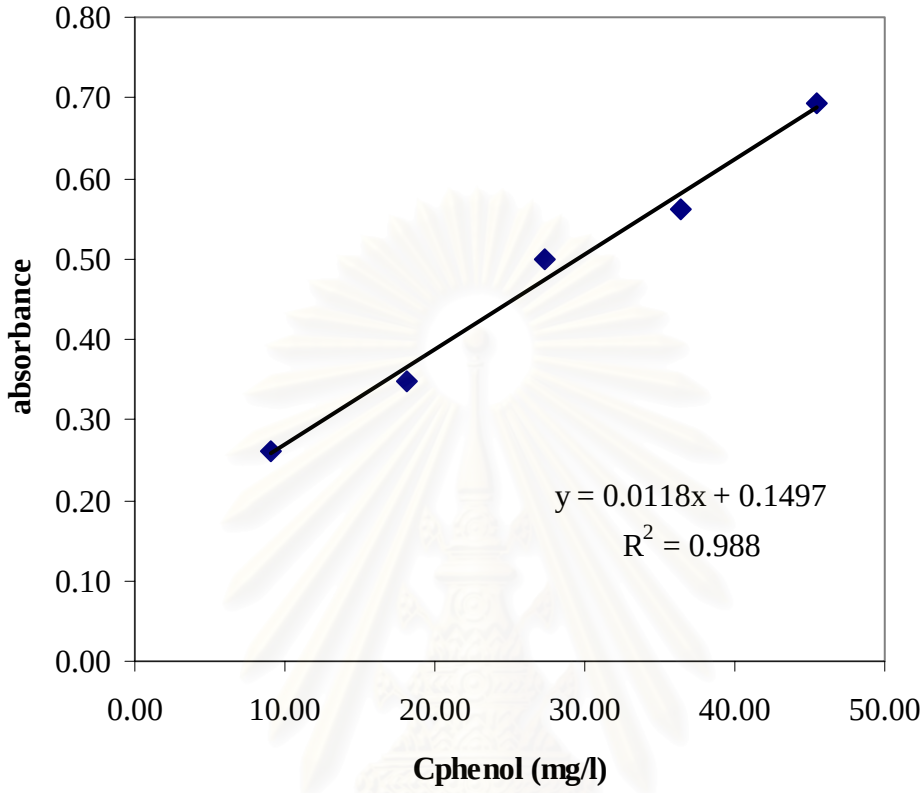

- Calibration curve of red31 in binary adsorption at 270 nm wavelength

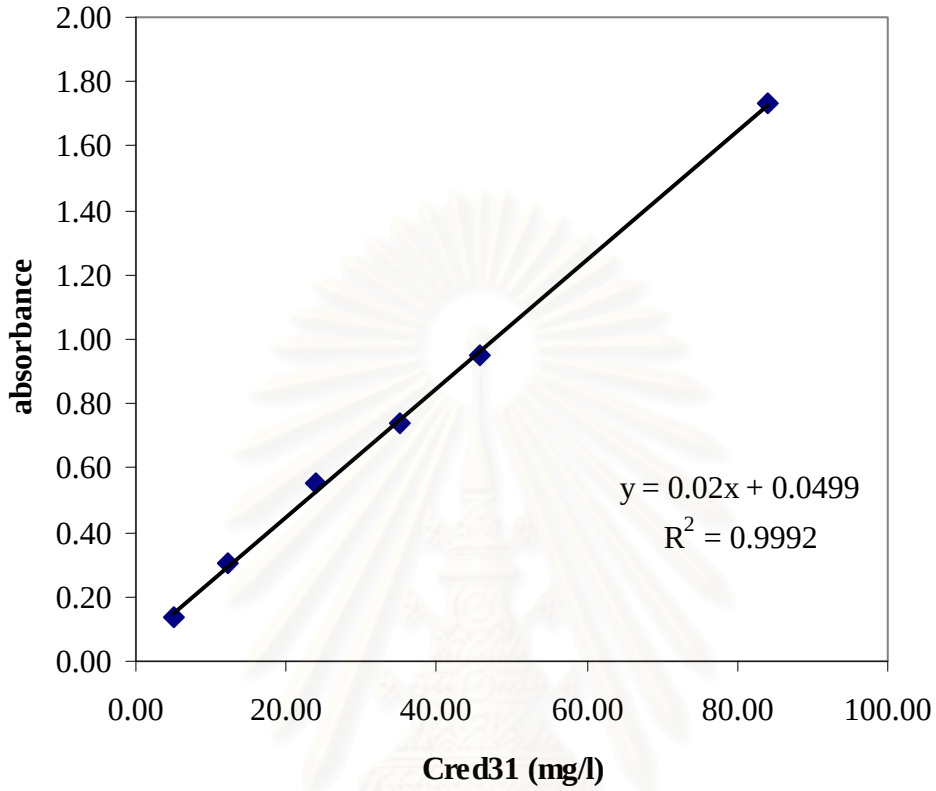

- Calibration curve of red31 in binary adsorption at 540 nm wavelength

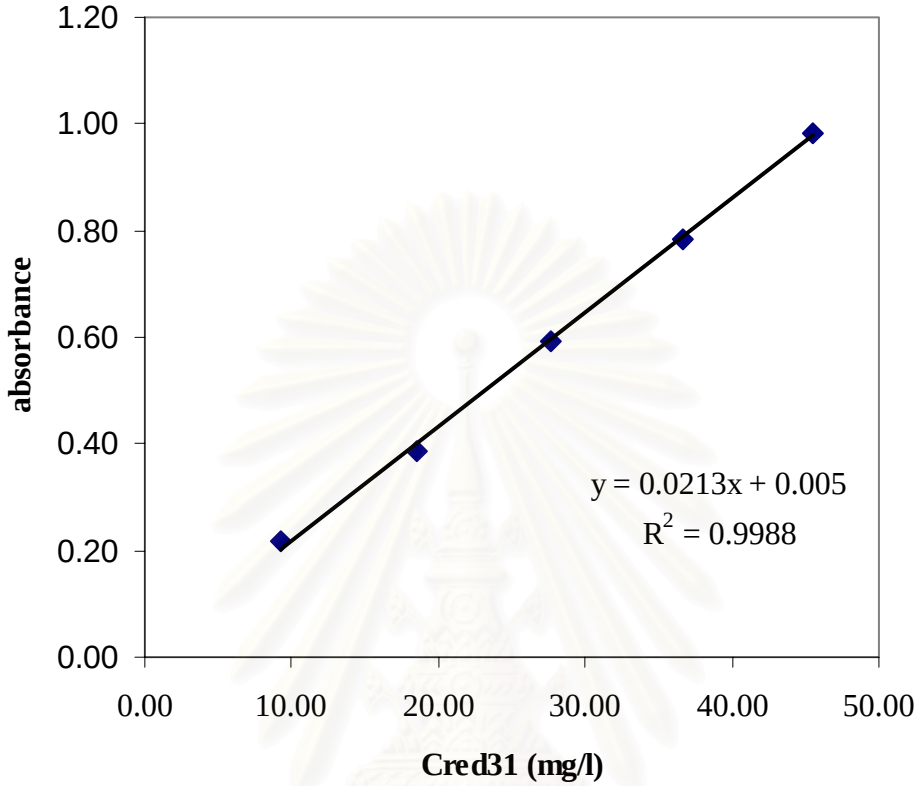

APPENDIX D

FTIR

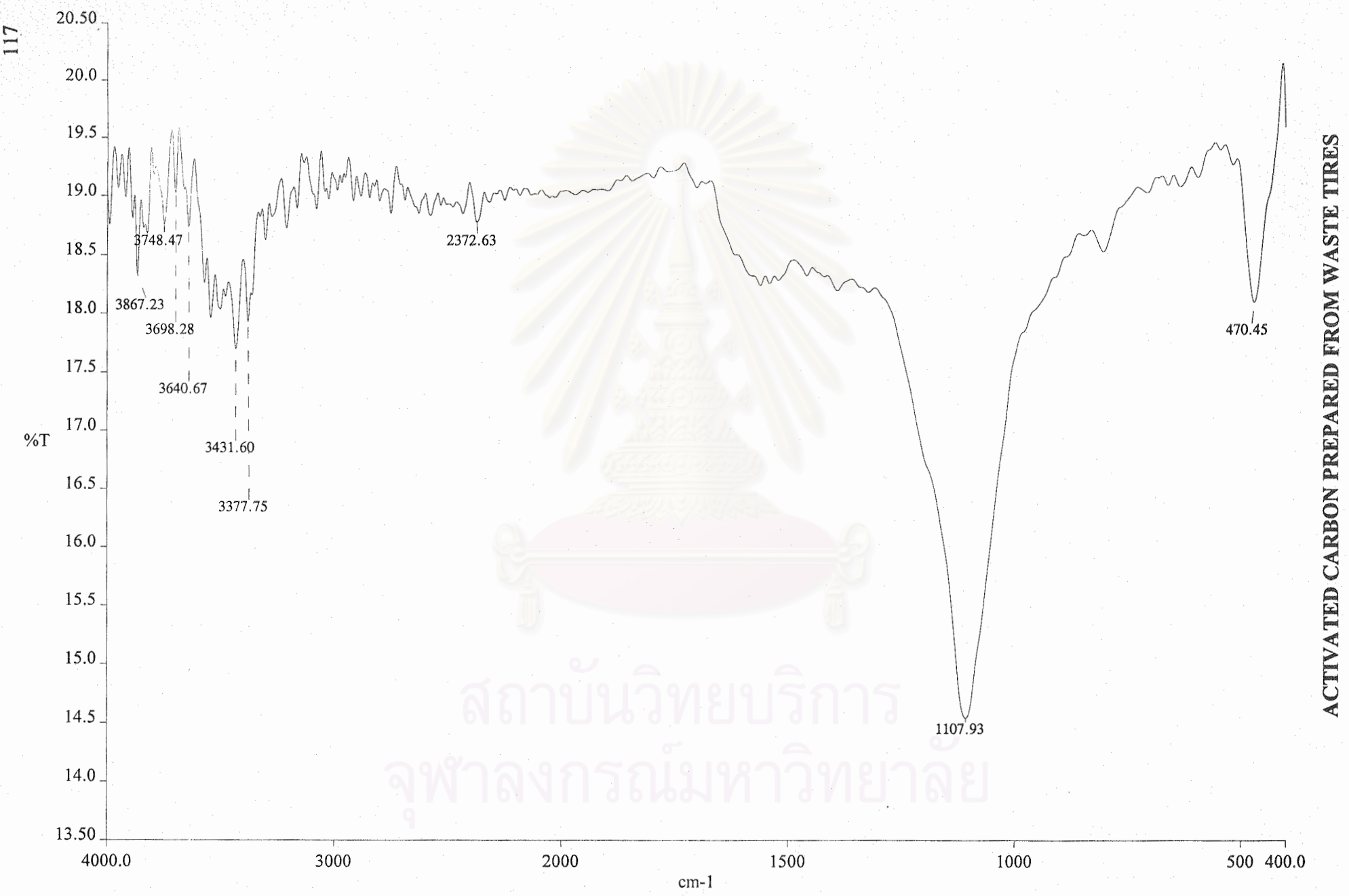

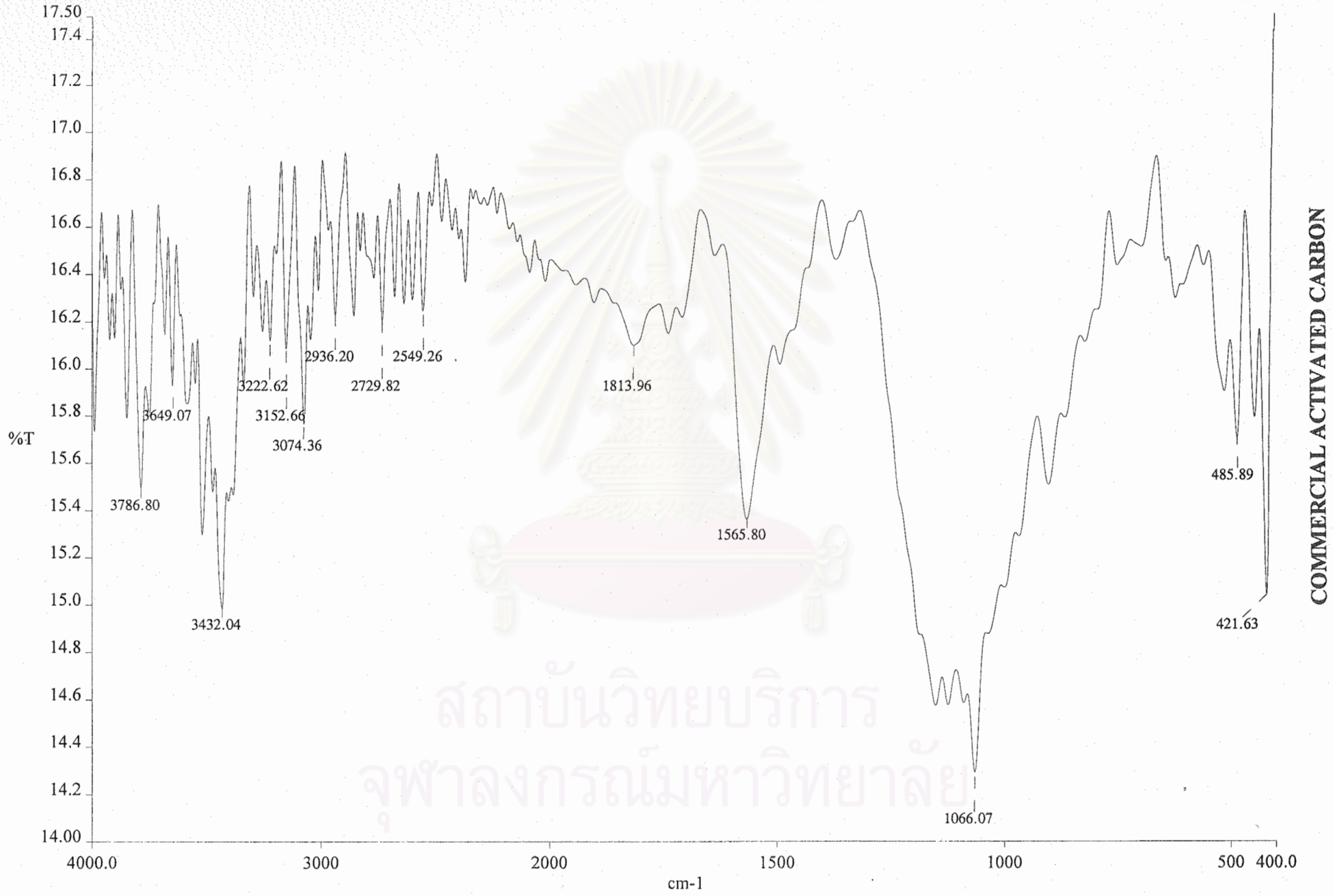

VITA

Miss Pannada Japthong was born on September 7, 1979 in Surin, Thailand. She studied in primary and secondary educations at Mueng Surin School and Sirindhorn School, respectively. In 2002, she received the Bachelor Degree of Science (Chemical Technology) from Chulalongkorn University. After that, she continued to study in Master Degree program at Chemical Engineering Department, Engineering Faculty, Chulalongkorn University with the master thesis entitled “Adsorption kinetics of aqueous binary mixtures containing phenol, red31 and/ or black5 on activated carbon produced from waste tires”.